If I chance to talk a little wild, forgive me

William Shakespeare
Henry VIII. I, iv, 26.

SPECTRAL LINE SHAPES IN ULTRADENSE PLASMAS

BY

ELIZABETH ANN MAUREEN BAKER

A Thesis Submitted for the Degree of Doctor of Philosophy of the University of London

Department of Physics, Imperial College of Science and Technology, Prince Consort Road, London, S.W.7.

May 1977

ABSTRACT

Line shape studies are reported for a dense argon plasma source suitable for investigating many of the effects predicted for high density plasmas. The source is a linear pinch producing a plasma with the special properties of a high electron density ($n_e > 10^{18}$ cm^{-3}), yet a relatively low electron temperature ($T_e \sim$ 25,000K). Under these conditions the number of particles in a Debye sphere is small ($n_{D\ min} \sim 3$) and the ratio of the mean electrostatic to the thermal energy is thus relatively high.

Precise diagnostic measurements are particularly difficult on high density plasma sources, because of problems associated with high optical opacity, high refractive index and small plasma size. Even in the very difficult plasma used in these experiments the electron density can be determined to $\pm$30% or better, and the electron temperature to $\pm$20%.

Previously, very few line shape observations have been made at electron densities greater than 10^{18} cm^{-3}, and existing observations have been confined to He II transitions. The line profile studies reported in this work substantially extend the measurements available at electron densities in excess of 10^{18} cm^{-3}.

The plasma polarization effect, first proposed by Berg (1962), is predicted to produce large wavelength shifts in dense plasmas. Observations of the resonance lines of Ar II, Ar III and N II are reported. Although under the special density and temperature conditions in this discharge, theoretical predictions would yield large shifts for these U.V. resonance lines (a few Angstroms or more), experimentally these predictions are found to be overestimates by between 3 and 6 orders of magnitude. Moreover the very small shifts that are observed

show no evidence of the strong temperature dependence predicted by theory. Experimental studies of U.V. lines of N IV set upper limits on the shifts for triply-ionized emitters at these densities, although no adequate theoretical predictions are currently available and the application of many of the current theories to non-resonance lines is questionable.

Observed asymmetries of the Ar II and Ar III U.V. resonance lines, and of the visible lines of Ar II Mult 6 are attributed to the coupling of perturbers and the transverse radiation field, first predicted by Burgess (1968).

The Stark broadened wings of H I Lyman α have been studied at high densities. Satellite features observed in both the red and blue wings are attributed to the effects of unbound states of quasi-molecular species, $H Ar^{+}$ and $H Ar^{++}$. Observations are reported of the asymmetry of Lyman α out to ± 40 Å in the wings at an electron density $\sim 2 \times 10^{18}$ cm^{-3}. This asymmetry is attributed to the effects of quadrupole interactions, predicted by Sholin (1969) for high density plasmas.

CONTENTS

			Page No.
ABSTRACT			1
CHAPTER 1 -		Introduction	11
	1.1	Some Preliminary Comments.	11
	1.1.1	The influence of high density effects on spectral line shapes.	11
	1.1.2	Present interest in high-density plasma spectroscopy.	11
	1.1.3	The absence of previous line shape studies at high densities ($n_e > 18\ cm^{-3}$)	11
	1.1.4	This experiment.	12
	1.2	The Choice of Plasma Source.	13
	1.2.1	Historical reasons for use of a linear-pinch source.	13
	1.2.2	Flexibility of plasma parameters.	13
	1.2.3	Reproducibility.	15
	1.3	The Special Properties of the Source used in this Investigation.	17
	1.4	The Choice of Diagnostic Methods.	17
	1.4.1	Thomson scattering.	20
	1.4.2	The effect of optical opacity on spectral line shape studies.	21
	1.4.3	Spatial inhomogeneity.	22
	1.4.4	Absence of electrode impurities.	22
	1.5	A Discussion of Effects Important at High Densities.	23
	1.5.1	The Plasma Polarization Effect.	23
	1.5.2	Effects of free states of unbound quasimolecular species.	24

CONTENTS (Continued)

			Page No.
	1.5.3	Plasma Satellite Features.	26
	1.5.4	Quadrupole Interaction.	26
	1.5.5	Contribution of Perturber Radiation.	28
	1.5.6	Debye Shielding.	28
	1.6	A Summary of the Work Presented in this Thesis.	29
CHAPTER II -	A Dense (i.e. $n_e > 10^{18}$ cm^{-3}) z-pinch source and its Diagnostics.		31
	2.1	Apparatus.	31
	2.2	Gross spectrum of the pinch.	34
	2.3	Difficulties in Performing Diagnostic Experiments on High Density Sources.	36
	2.4	Optical Depth Considerations.	36
	2.4.1	Ar II Profiles.	36
	2.4.2	Absorption of Off-resonance Laser Radiation.	38
	2.4.3	Conclusions from the Optical Depth Measurements.	41
	2.5	Estimation of the electron density directly from measurements of the Half Widths of Ar II lines.	42
	2.5.1	Broadening Parameter.	42
	2.5.2	This Experiment.	42
	2.5.3	Deconvolution Procedure.	43
	2.5.4	Electron Density Estimates from Ar II Profiles.	45
	2.5.5	Sources of Error in Electron Density Estimates.	45
	2.5.6	Asymmetries of Ar II Mult 6 Profiles.	47

CONTENTS (Continued)

		Page No.
2.6	Measurement of Electron Temperature.	47
2.6.1	Measurement of temperature by resonant absorption.	47
2.6.2	Assumptions Implicit in the Optical Depth calculations of Wheeler and Troughton (1969).	48
2.6.2.1	Assumptions concerned with the Line Profile.	49
2.6.2.2	The Assumption that all the Energy Levels (including the ground state) are Collisionally Dominated.	49
2.6.3	Temperature Diagnostics on this pinch.	51
2.7	Preliminary Interferometric Studies.	54
2.8	Radial Variation of Electron Density from Continuum Absorption Studies.	60
2.8.1	Method.	60
2.8.2	Abel Inversion Procedure.	60
2.8.3	Electron Density Measurements from Continuum Absorption.	63
2.9	Radial Variation of Electron Density from Interferometric Measurements.	65
2.9.1	Method.	65
2.9.2	Sensitivity of Abel inversion routine.	66
2.9.3	Results.	69
2.9.4	Density Estimates from Compression Ratio.	69
2.10	Conclusions.	69
CHAPTER III -	The Plasma Polarization Shift.	75
3.1	Introduction.	75
3.2	The Importance of the Plasma Polarization Effect.	75

CONTENTS (Continued)

		Page No.
3.3	Limitations of Previous Work on the Plasma Polarization Shift.	76
3.3.1	Experimental.	76
3.3.2	Theory.	76
3.4	Historical Background.	78
3.4.1	The Berg (1962) Experiment.	78
3.4.2	Further experiments for singly ionized emitters.	79
3.4.3	The Griem (1966) Quantum Mechanical Estimate.	80
3.4.4	The Chowdhury (1969) Experiment.	80
3.4.5	The Greig (1970) Experiment and Semiclassical Estimate.	81
3.4.6	Criticism of the Greig (1970) Estimate by Burgess and Peacock (1971).	82
3.4.7	The Experiment of Gabriel and Volonté (1973).	82
3.4.8	The Griem (1973) Semiclassical Estimate.	83
3.4.9	The Griem (1974) Quantum Mechanical Estimate.	83
3.4.10	Inclusion of a "Back Reaction" as suggested by Gabriel and Volonté (1973).	84
3.4.11	The Goto and Burgess (1974) Experiment.	85
3.4.12	The Volonté (1975) Treatment.	85
3.5	Some comments on the Time-Averaging Assumptions on which Polarization Shift Estimates are based.	86
3.6	Summary.	86
3.7	This Experiment.	87

CONTENTS (Continued)

			Page No.
CHAPTER IV	-	Ar II and Ar III U.V. Resonance Line Studies.	96
	4.1	Apparatus.	96
	4.2	Wavelength Standards.	98
	4.3	Results : Ar II Mult 1.U.V. Profiles.	100
	4.4	Results : Ar III U.V. Resonance Profiles.	103
	4.4.1	Shift Measurements.	103
	4.4.2	Asymmetries of the Ar III lines.	105
	4.5	Ar II Mult 4.U.V. Resonance Line Profiles.	105
	4.6	Conclusions.	108
CHAPTER V	-	Polarization Shifts of N II, N IV and Na I Lines.	112
	5.1	N II and N IV Lines.	112
	5.2	Studies for Neutral Emitters.	114
	5.3	Neon I Lines.	114
	5.4	Na I Lines.	114
CHAPTER VI	-	Observations of Asymmetries in the Emission Profiles of Ar II and Ar III Lines.	118
	6.1	Introduction.	118
	6.2	Analysis of the Measured Asymmetries.	118
	6.2.1	Ar II Mult 6.	122
	6.2.2	Ar II Mult 1.U.V.	122
	6.2.3	Ar III Mult 1.U.V.	122
	6.3	Trivial Causes of Asymmetry.	126
	6.3.1	Instrument Asymmetries.	126
	6.3.2	Asymmetry due to Motion of Ions along the line of sight.	126

CONTENTS (Continued)

		Page No.
6.4	Asymmetries due to overlap with neighbouring lines.	126
6.4.1	Frequency Dependence of the Asymmetry resulting from overlap with a nearby line.	127
6.4.2	Quantitative estimates of overlap asymmetries.	129
6.4.3	Some comments on the Ar II Mult 6 asymmetries with relation to overlap asymmetries.	129
6.5	Other non-pressure-broadening causes of asymmetry.	131
6.6	Ion Broadening.	131
6.7	Asymmetries due to plasma inhomogeneity.	134
6.8	Asymmetries due to contributions of perturber radiation.	136
6.8.1	Some Comments on the Nature of the Asymmetry predicted by Burgess (1968).	137
6.8.2	Conditions for Asymmetry to be large.	138
6.8.3	Inclusion of Interference Terms in the Line Shape.	139
6.8.4	Importance of Perturber Contribution Corrections to the profiles of Ar II and Ar III Studies.	140
6.8.5	Estimates of these asymmetries for the Ar II and Ar III Lines studied.	140
6.8.6	Conclusions.	142
CHAPTER VII -	An Experimental Study of Lyman α at High Electron Densities.	143
7.1	Introduction.	143
7.1.1	The influence of Quasimolecular states.	143

CONTENTS (Continued)

		Page No.
7.1.2	Plasma Satellites.	145
7.1.3	Asymmetry due to Quadrupole Interactions.	145
7.2	This Experiment.	147
7.3	Apparatus.	149
7.4	Results.	149
7.5	Possible Origins of the Satellite-like Features in the Wings of Lyman α.	151
7.5.1	Grating Ghosts.	151
7.5.2	Impurity Lines.	151
7.5.3	The Dependence of the Satellite features on the Hydrogen Concentration in the pinch.	153
7.5.4	Plasma Satellites.	155
7.5.5	Quasimolecular Features.	158
7.5.5.1	Calculation of the Ion Concentrations.	158
7.5.5.2	Scaling of the Satellite Intensities with the Lyman α Wing Intensity.	160
7.5.5.3	Scaling of the Satellite Intensities with the proton concentration.	160
7.5.5.4	Scaling of the Satellite Intensities with the Ar^{+} and Ar^{++} concentrations.	160
7.5.5.5	Conclusions.	163
7.5.5.6	Relation to Previous Work.	163
7.6	The Asymmetry of the Lyman α Profile.	163
7.6.1	The Observed Turn-Over to Smaller Asymmetry.	164
7.6.2	Errors.	164
7.6.3	Conclusions.	166

CONTENTS (Continued)

		Page No.
CHAPTER VIII -	Conclusions.	167
APPENDIX 1 -	Abel Inversion Routine.	169
APPENDIX 2 -	Radial Variation of Electron Density.	171
APPENDIX 3 -	Calculation of Electron-Impact Broadened Stark Widths and Shifts by Semiempirical Estimates.	175
	A.3.1 Width Calculations.	175
	A.3.2 Shift Calculations.	176
	A.3.3 Calculation of Stark Widths and Shifts for Ar II Mult 1.U.V., Ar III Mult 1.U.V. and N II Mult 2.U.V.	177
APPENDIX 4 -	The Cooled Cathode Discharge as a V.U.V. Wavelength Standard.	178
APPENDIX 5 -	Reprint of Paper published in J.Phys.B. 10,1977.	180
REFERENCES		182
ACKNOWLEDGEMENTS		184

CHAPTER I

Introduction

1.1 Some Preliminary Comments

1.1.1 The influence of high density effects on spectral line shapes

The validity of extending line-broadening theories, well-tested at lower densities, to increasingly high densities becomes suspect. Many effects concerned with the influence of the plasma environment on the emitter, although predicted to have negligible effect at normal densities, may at high densities be expected to become increasingly important. Such factors include the plasma polarization effect, the effects of unbound states of quasimolecular species, quadrupole interactions, the coupling of perturbers with the transverse radiation field, the generation of plasma satellites, and the effects of Debye shielding.

1.1.2 Present interest in high-density plasma spectroscopy

Recent years have seen the development of many new high density sources capable of producing emitters of high ionization stage (such as the laser-produced plasma sources where typically $n_e \sim 10^{21}$ cm^{-3}), and a growing interest in the possibilities of generating laser-compressed plasmas, and in their relevance to controlled fusion research. For these reasons, interest in high density plasma effects particularly on spectral line shapes, has ceased to be solely academic, and the need for an experimental investigation of high density effects has become increasingly important.

1.1.3 The absence of previous line shape studies at high densities ($n_e > 10^{18}$ cm^{-3})

Although the need for line shape studies at high densities has been recognised for a number of years, only a few experiments are

reported, and these are usually confined to relatively modest densities ($n_e \sim 10^{17} \longrightarrow 10^{18}$ cm^{-3}).

Almost all the observations at these densities have been concerned with He II transitions. For example, Jones, Kallne and Thomson (1977) report Stark-broadened profiles of He II 4686 Å, using a theta pinch plasma run in helium to produce electron densities 1.0 to 2.5 x 10^{18} cm^{-3}.

Fortna, Elton and Griem (1970) report observations of Stark-broadened C II and N II U.V. resonance lines at a density 3 x 10^{17} cm^{-3} and a temperature 2 eV. Their source was a T-tube run in helium with small admixtures of nitrogen and hydrogen, and methane, to produce N II and C II emission lines respectively.

The dearth of line profile studies at high densities is partly attributable to the difficulties involved in performing such experiments. As discussed in Section 1.4 below, the range of diagnostic methods for use at high densities is in any case restricted. Furthermore, the problems of high optical opacity, high refractive index and small size impose severe limitations on those techniques that are feasible, and also on the usefulness of many line profile measurements.

1.1.4 This experiment

This work has been concerned with producing a plasma source suitable for use in performing line shape studies at high density ($n_e > 10^{18}$ cm^{-3}), but at relatively low temperature ($T_e \sim 25{,}000$K).

The problems involved in diagnostic measurements at high densities are discussed, and the specialised diagnostic methods which were found to be necessary to determine the density, temperature and plasma size to within acceptable errors are described in detail.

Armed with a well-diagnosed, highly-reproducible, high-density source it was then possible to investigate many of the effects theoretically

predicted to be of possible significance to spectral line shapes in high density plasmas. The results of these experiments are discussed in detail in Chapters IV, V, VI and VII.

1.2 The Choice of Plasma Source

1.2.1 Historical reasons for use of a linear-pinch source

Previous work in this department (Burgess 1964) suggested that linear-pinch sources are capable of producing dense ($n_e \sim 10^{18}$ cm^{-3}), relatively low temperature ($T_e \sim 20{,}000$K) plasmas when run in a suitable gas, such as argon. This was the chief factor influencing the initial choice of a linear-pinch source run in argon for these experiments.

Over the last ten years, linear pinch devices have been used extensively in this laboratory, for line-shape studies. Some of the density and temperature conditions under which linear pinch devices have been operated in this group are shown in Fig.1.1. The electron densities produced range over 4 orders of magnitude (from $n_e = 10^{14}$ cm^{-3} (Mahon 1973) to $n_e \sim 3 \times 10^{18}$ cm^{-3} (present work)) and the electron temperatures produced range over 1½ orders of magnitude (from $T_e = 5{,}000$K (Cairns 1971) to 120000K (Richards, private communication).

1.2.2 Flexibility of plasma parameters

Linear pinch sources offer the important advantage that the density and temperature of the plasma can be varied over relatively large ranges of values by changing easily-

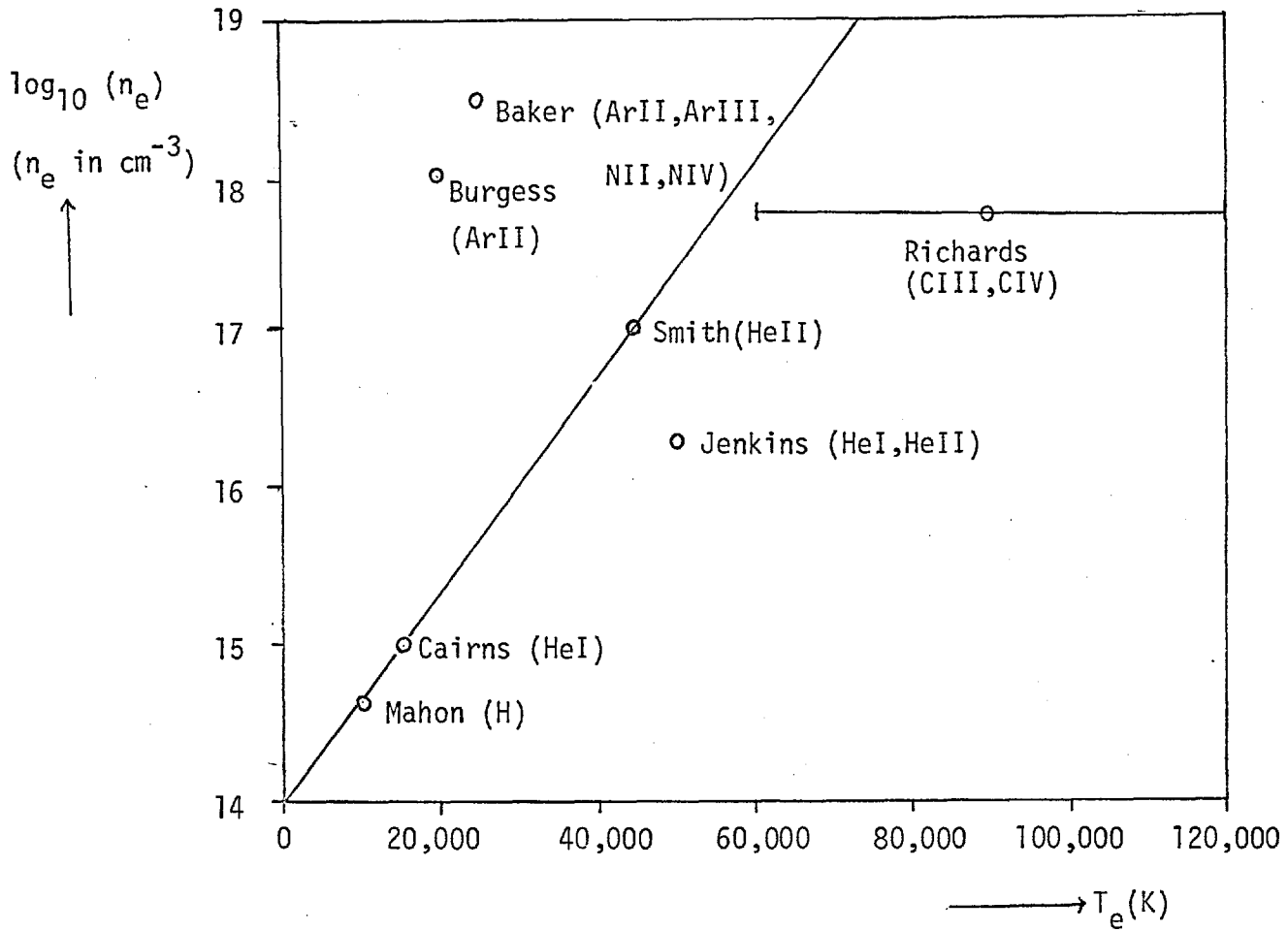

Fig 1.1 : Some density (n_e) and temperature (T_e) conditions achieved in linear pinch sources by previous workers in this department.

adjustable parameters, such as the voltage on the capacitor bank used to drive the source, and the filling pressure of gas in the pinch. The advantage of not being constrained to working at one particular density and temperature has been of enormous value in the work described in the following chapters. For example, it has been possible to test the density and temperature dependence that is theoretically predicted for the polarization shift (see Chapter IV). Moreover, the facility for varying the plasma parameters has been of great importance in discriminating between various competing effects to determine the origin of observed satellite-like features in the wings of Lyman α (see Chapter VII).

1.2.3 Reproducibility

As pointed out by Burgess (1972) an advantage of linear-pinch plasma sources is their high degree of reproducibility. This claim was found to be completely justified even in the case of the very high density source used in this experiment. Plate 1.1 shows an oscillogram of the pinch emission at line centre of Ar II Mult 6 4848 for seven different shots. The signal is reproducible to within $\pm$ 5% at peak density. Moreover, the reproducibility of the emission signal is worst at line centre. In the line wing the reproducibility is typically $\pm$ 3%.

A high degree of reproducibility is clearly very important in any scanning experiment, which entails building up line profiles from

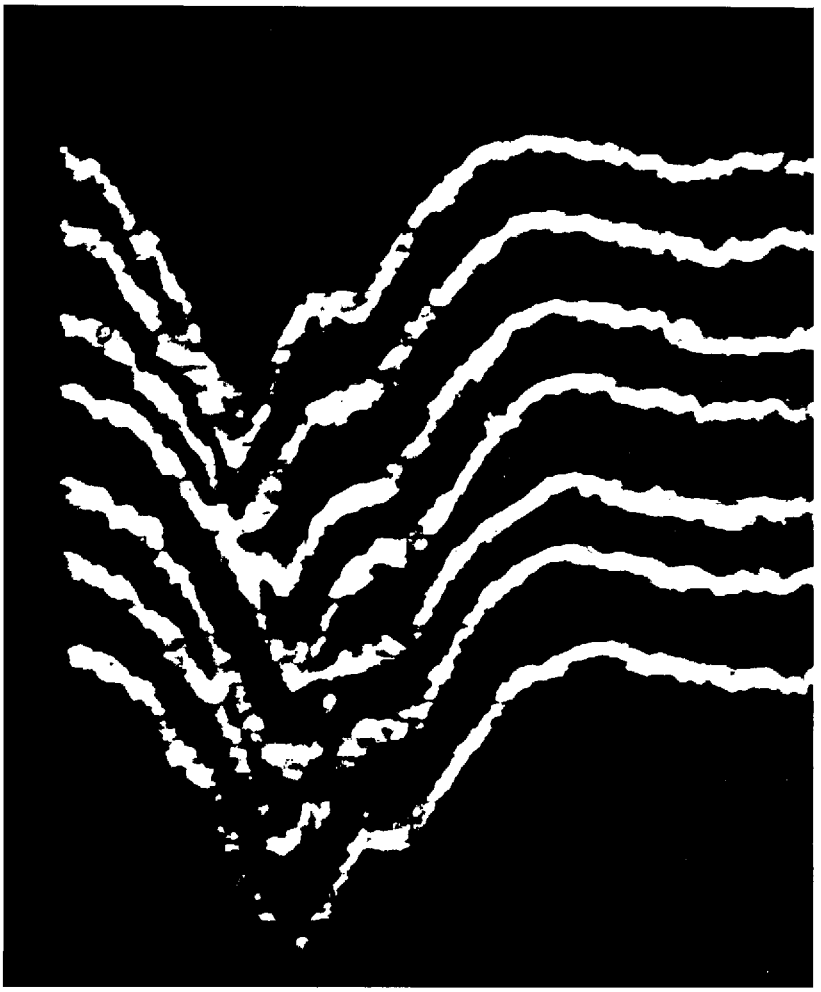

PLATE 1.1

Pinch Emission at 4848 Å

7 Shots

shot to shot, since signal reproducibility represents the fundamental limitation on the accuracy to which the line shape can be determined.

1.3 The Special Properties of the Source used in this Investigation

The diagnostic measurements discussed in Chapter II establish that the density in the linear pinch source used in the present experiments could be varied at will between $n_e = 1 \times 10^{18}$ cm^{-3} and $n_e = 3 \times 10^{18}$ cm^{-3} ($\pm$ 20%). The temperature could be varied between T_e = 22,000K and T_e = 27,000K $\pm$ 20%.

Under these circumstances, the number of particles in a Debye sphere is relatively small ($N_D \sim 4.0$) and the ratio of the inter-particle separation to the Debye length is relatively large ($\frac{R}{\lambda_D} \approx 0.62$), the typical values given being calculated from density and temperature measurements described in Chapter II.

In Fig.1.2, the ratio R/λ_D is plotted as a function of the pinch filling pressure for a bank voltage 5KV. When the Debye length approaches the interparticle spacing the ratio of the electrostatic energy E_{ES} to the thermal energy E_T in the plasma is relatively high. For the plasma used in these experiments $E_{ES}/E_T \sim 15\%$.

1.4 The Choice of Diagnostic Methods

Although the difficulties inherent in performing diagnostic measurements on dense sources are considerable, these measurements are vital to the investigation of such sources. Initially, reliable diagnostic measurements are necessary in order to establish the existence of a high density plasma zone. Furthermore, an accurate knowledge of the plasma parameters is fundamental to the quantitative interpretation of line profile studies. Some consideration is therefore given to the relative merits of various established techniques.

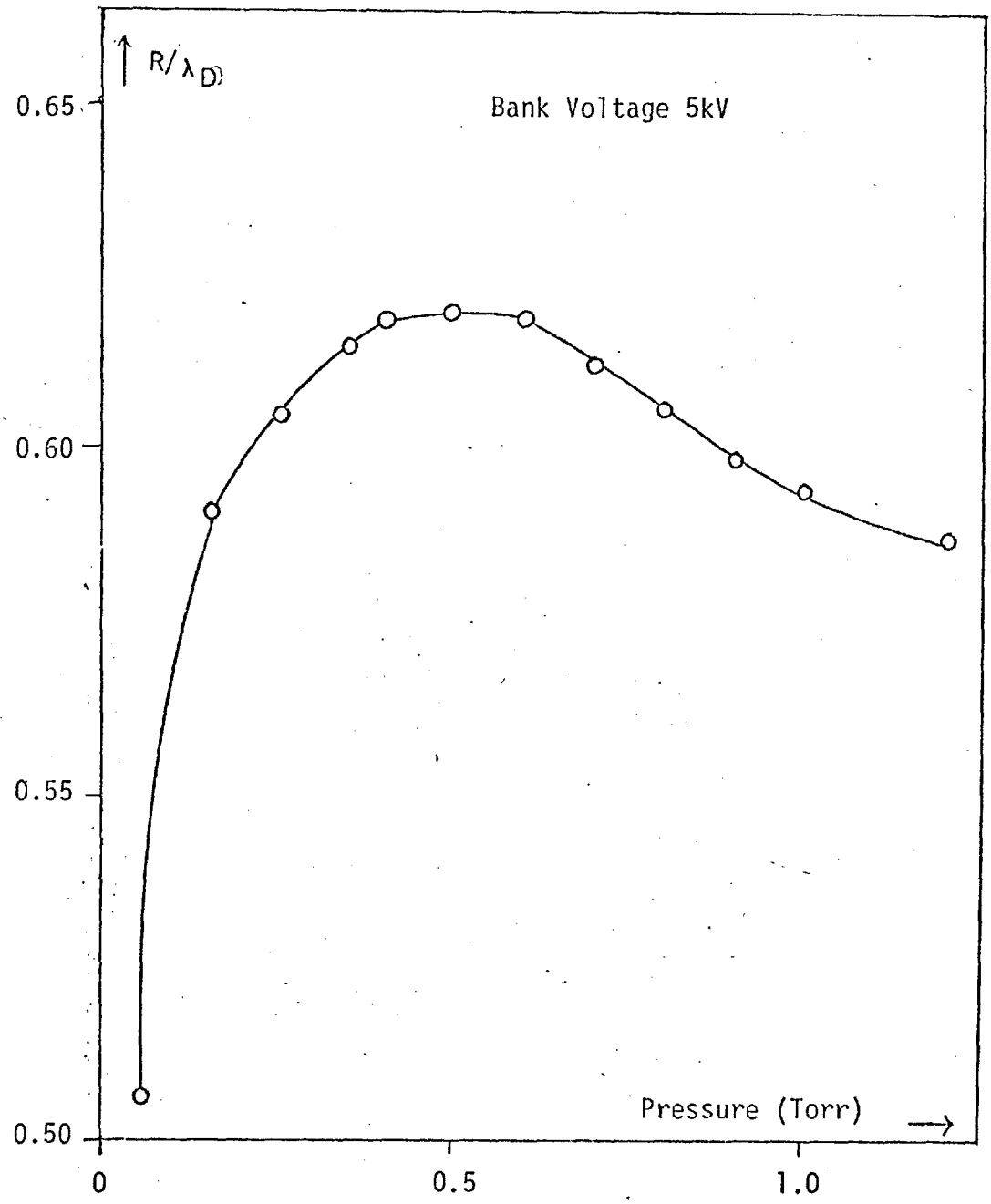

Fig 1.2 : Ratio of interparticle separation to Debye length (R/λ_D) as a function of filling pressure.

The use of interferometric techniques to determine the electron density, n_e, is restricted by the problem of counting a large number of fast fringes, frequently of reduced visibility, near to the time of peak compression (see Chapter II).

At high densities, the use of absolute and relative line intensities to determine in particular the electron temperature, T_e, will be limited by problems of optical opacity, especially for resonance lines. Moreover, measurements of spectral line intensities will be particularly sensitive to the effects of spatial inhomogeneities.

Continuum intensities will also be affected by problems of optical opacity and spatial inhomogeneity. In addition, at high densities the extended wings of pressure-broadened lines might prejudice continuum intensity measurements. Thus care must be exercised in determining n_e and T_e by the measurement of absolute continuum intensities and continuum slopes respectively.

Density determinations from line width measurements will also be affected by problems of optical opacity, at high densities. However, these problems are less serious for high-lying and therefore weak transitions. In addition, the effects of spatial inhomogeneity are more easily separated than for, say, line intensity measurements, since in low density regions the lines are negligibly broadened.

Use of Thomson scattering to determine n_e and T_e is restricted at high densities. The chief problem is the detection of a small scattered signal above a relatively high continuum.

Measurement of T_e by the absorption of resonant laser radiation is in general dependent on the accuracy to which n_e is known.

The application of these diagnostic methods to a plasma with $n_e \sim 10^{18}$ cm^{-3} is discussed in detail below and in Chapter II.

1.4.1 Thomson Scattering

Thomson scattering is perhaps the most powerful and versatile plasma diagnostic tool available. Unfortunately this method poses severe problems in the case of the dense ($n_e > 10^{18}$) plasma source of the present experiments.

In most Thomson scattering experiments, the intensity due to continuum radiation and stray light is negligible compared with the scattered laser intensity. However, because of high electron density in this source the plasma emission intensity at $\lambda = 6943$ Å due to Bremsstralung radiation is likely to be at least comparable with the scattered intensity of a ruby laser. In this case the feasibility of deducing the scattered laser intensity by subtracting the background intensity due to continuum radiation will depend on the signal reproducibility in the continuum.

Thomson scattering experiments have previously been performed on a similar high density linear pinch run in helium, in this laboratory (C.S. Smith, Ph.D. Thesis 1977). At electron densities in the region $n_e = 0.85 \times 10^{17}$ cm^{-3} to 1.65×10^{17} cm^{-3} the background continuum intensity was 400 mV compared with a scattered ruby laser intensity of 100 mV (C.S. Smith, private communication). The background intensity due to stray light was negligible.

The scattered laser intensity scales as n_e, whilst the Bremsstralung continuum intensity scales as n_e^2. Thus in the present experiment where the electron density n_e is in the region 2.8×10^{18} cm^{-3} (see Chapter II), the ratio of the scattered intensity to the continuum intensity might be expected to be of order 1.0%. Since the signal reproducibility in the continuum is of order 3.0% (Section 1.2.3), the scattered laser intensity would be of the same order as the noise on the continuum intensity.

The scale on which phenomena can be viewed in a scattering experiment is given by

$$\frac{2\pi}{k} = \frac{\lambda}{2} \frac{1}{\sin(\theta/2)} \tag{1.1}$$

For $\theta = 90^{o}$ scattering, $2\pi/k = 2.48 \times 10^{-5}$ cm for a ruby laser ($\lambda \approx 6943$ Å). By comparison, an ion in the plasma is surrounded by a shielding cloud of electrons, the size of the shielding cloud being

$$\lambda_D \approx 740 \left\{ \frac{T_e(eV)}{n_e(cm^{-3})} \right\}^{1/2} cm \tag{1.2}$$

This experiment is concerned with a plasma where $n_e \sim 3 \times 10^{18}$ cm^{-3} and $T_e \sim 2.2$ eV. From Eqn.1.2, $\lambda_D = 6.33 \times 10^{-6}$ cm. Thus the scale on which phenomena can be viewed for 90^{o} ruby laser scattering, $\frac{2\pi}{k}$ is of order $30\,\lambda_D$.

Thus in this case a ruby laser scattering experiment would be dominated by collective scattering from the ion shielding cloud, rather than scattering from individual electrons.

Because of uncertainties due to the relatively high continuum intensity, it is unlikely that a collective scattering experiment would yield density and temperature measurements to a higher degree of accuracy than the alternative diagnostic methods used. (See Chapter II).

1.4.2 The Effect of Optical Opacity on Spectral Line Shape Studies

At high densities the problem of optical depth is likely to be a serious consideration in many diagnostic measurements, as well as in subsequent line-profile studies. In practice, this problem usually results in a restriction to observations made over short path lengths

in the plasma. For a linear pinch configuration, this means that useful measurements can usually only be made observing sideways-on to the plasma column.

1.4.3 Spatial Inhomogeneity

The chief problem associated with sideways-on measurements on linear pinches is that of spatial inhomogeneity of the plasma along the line of sight. Uncertainties due to radial density gradients may be resolved by Abel-inverting the radial variation of some measurable, density-dependent plasma parameter (for example the emitted continuum intensity, Roberts 1967).

There are two main difficulties associated with making fully spatially resolved measurements on the source used in this investigation. Firstly, the optical depth of the plasma is not small enough to be neglected, even for sideways-on observations of continuum emission. This rules out the Abel inversion of emission intensities, unless inclusion is made in the Abel-inversion procedure for a further density-dependent variable, namely optical opacity.

Secondly, under typical firing conditions the plasma column is only about 5 mm in diameter at peak compression. However, using aperture-narrowed laser beams it proved possible to probe spatial regions as small as 1 mm (see Chapter II). Absolute measurements of the radial density variation were made using two independent, fully spatially resolved methods and applying an Abel inversion procedure.

1.4.4 Absence of electrode impurities in the middle plasma region

The considerable difficulties involved in working sideways-on are to some extent offset by the advantage of the facility for making observations on a plasma region free from electrode impurities. The middle of the plasma column is uncontaminated by electrode impurities

because the thermal velocities are too slow for electrode impurity ions to reach the middle plasma region from the electrode in the time taken to reach peak compression.

For example, the brass electrodes of the discharge used in this investigation might be expected to give rise to impurities Zn II and Cu II at typical pinch temperatures. However the velocities of these ions are of order 2.5×10^5 cm/sec, and at these velocities the ions would reach the middle of the plasma after $\sim 40\,\mu$sec. Since peak compression is reached after $\sim 2\mu$sec, it is reasonable to expect observations at the time of maximum density will be free from emission due to electrode impurities. This is confirmed experimentally, no electrode impurity lines being seen in all observations of the middle plasma region. In particular, in all U.V. observations in the region 700 Å - 1300 Å, none of the U.V. lines of Zn II and Cu II were observed, although in this wavelength region, many emission lines would have been observed if these emitting species had been present.

1.5 A Discussion of Effects Important at High Densities

1.5.1 The Plasma Polarization Effect

Close to an ion, the surrounding plasma will be polarized, i.e. there will exist a time-averaged excess of negative charge in the immediate vicinity of an ionized emitter. The overlap of this charge distribution with the bound electron orbits of the emitter is postulated to give rise to measurable spectral line shifts in some cases (Griem 1974). The effect is discussed more fully in Chapter III.

All the current theories of this effect predict shifts that increase linearly with the electron density. At high densities the existing estimates (for example, Greig 1970) predict large shifts for resonance lines (typically two or three orders of magnitude larger than

the ordinary Stark shifts and in some cases even larger than the wavelength of the line concerned) although such large shifts are expected to be physically unreasonable. For example, in Chapter III some estimates are given for the shifts expected for Ar II and Ar III U.V. resonance lines at electron densities $\sim 2 \times 10^{18}$ cm^{-3}. At such densities, the estimated shifts of Griem (1973) exceed the unshifted wavelength of the line concerned.

1.5.2 Effects of free states of unbound Quasi-molecular species

This effect is concerned with the influence of other ions in the immediate vicinity of an emitter, and was first suggested by Stewart, Peak and Cooper (1973). Calculations for H I Lyman$_\alpha$ by Stewart et al (1973) predicted that the effect would give rise to satellites in the wings of the transition.

When an ion approaches close to an emitter the optical electron might be expected to spend some of its time 'on' the perturbing ion, without actually becoming bound. For convenience, the emitter with its optical electron together with the perturbing ion will be termed a "quasimolecule". The interatomic potentials corresponding to relevant electronic states of this system are asymptotic at infinite nuclear separation to the atomic transition of interest. When the curve corresponding to the energy difference between the upper and lower states of a transition goes through an extremum, $\left(\frac{dv}{dr}\right)_{v'} = 0$. This gives rise to a satellite at the energy separation, v', in question. This is illustrated schematically in Fig.1.3.

Apart from the calculation for proton perturbers by Stewart et al (1973) and Le Quang Rang and Voslamber (1975) there is little quantitative work available on this effect. Moreover, the predictions of Stewart et al (1973) and Le Quang Rang (1975) are expected to be fairly

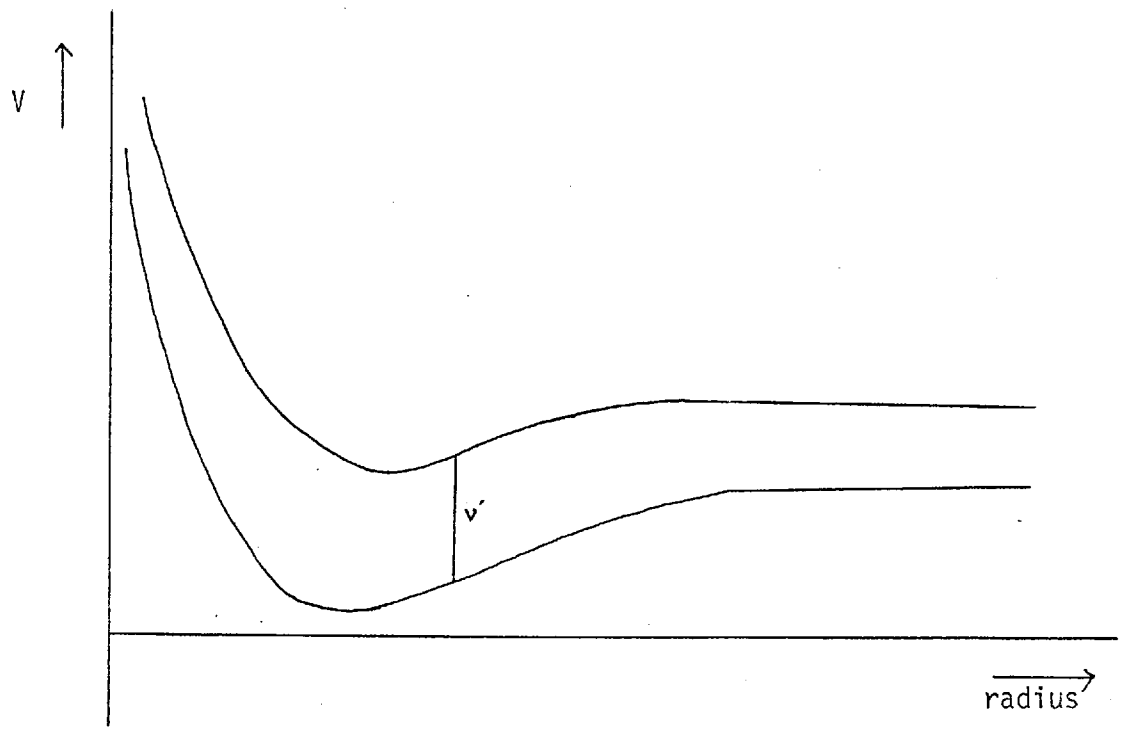

Fig 1.3 : Schematic illustration of extremum in difference between potential energy of upper and lower states of a transition.

specific to protons, although other ions may give qualitatively similar effects. However at high densities the probability of observing quasimolecular features will be greater since the perturber separations of interest are smaller, and deviations from the Stark shifts predicted by the usual theory correspondingly more significant. For example, Stewart et al (1975) predict extrema in the differences between the interatomic potential curves for proton perturbers at separations from $\sim 8\ a_o$ to $26\ a_o$. The mean interparticle separation for a plasma of electron density $n_e = 3 \times 10^{18}\ cm^{-3}$ is $\sim 80\ a_o$.

1.5.3 Plasma Satellite Features

Although the appearance of plasma satellites as predicted by Baranger and Mozer (1961) is not an effect concerned specifically with high density plasmas, there is some experimental evidence (Ya'akobi and Bekefi 1969) to suggest that such satellites may be excited by purely thermal fluctuations under conditions where the ratio of the electrical energy ($1/2 \cdot \varepsilon_o E_p^2$, where E_p is the collective field) to the particle kinetic energy ($3/2\ NkT$) is high. Since the ratio is equal to $0.015/N_D$ this requires that the number of particles in a Debye sphere is small, which condition is fulfilled for high density ($n_e \approx 10^{18}\ cm^{-3}$), relatively low temperature ($T_e \approx 20{,}000K$) plasmas. These conditions correspond to those reached in the source used in this investigation.

1.5.4 Quadrupole Interaction

The spectral line profiles of hydrogen in dense plasmas are all predicted to exhibit asymmetries due to the inhomogeneity of the electric microfields of the ions (see, for example, Sholin 1969). If the electric microfield was homogeneous, the relative intensities and shifts of the Stark components would be independent of the distribution

of perturbers (for a given net electric field) and, with a purely linear Stark effect, the profile would be symmetric.

The interaction between a perturbing ion and the optical electron can be written :-

$$V(r) = Ze^2 \left(\frac{1}{R} - \frac{1}{\sqrt{\{R^2 + r^2 - 2Rr\cos\theta\}}} \right)$$

where $\underset{\sim}{R}$ (0, 0, R) is the radius vector of the perturbing ion, $\underset{\sim}{r}$(x, y, z) is the radius vector of the atomic electron and θ is the angle between $\underset{\sim}{R}$ and $\underset{\sim}{r}$. By expanding the square root in terms of Legendre polynomials it can be shown that the interaction potential has the form

$$V = \lambda^2 V^{(2)} + \lambda^3 V^{(3)} + \lambda^4 V^{(4)} \ldots$$

where $\lambda = n^2 a_o R^{-1}$ and $\lambda^2 V^{(2)}$, $\lambda^3 V^{(3)}$, and $\lambda^4 V^{(4)}$ correspond to dipolar, quadrupolar and octupolar interactions respectively. Since the relative importance of quadrupole and higher order interactions depends on the parameter $\lambda = \frac{n^2 a_o}{R}$, corrections due to quadrupole interactions will be more important for smaller interparticle separations (R), i.e. for high densities.

Sholin (1969) shows that of the corrections giving rise to inhomogeneities in the electric microfield, quadrupole interactions play the dominant role, other corrections being of the next order in λ (for example quadratic Stark effect, octupolar interactions). In the case of Lyman α, Sholin (1969) shows that the quadrupole interaction shifts the red Stark component to longer wavelength and increases its relative intensity, while the blue component is shifted toward line centre and its relative intensity is decreased. Thus, for Lyman α, the quadrupole interaction produces an enhanced red wing asymmetry. Sholin (1969) predicts that, for Lyman α, the asymmetry will be proportional to $(\Delta\lambda)^{3/2}$.

Since the asymmetry depends on the inhomogeneity of the electric microfield, the effect will be most important at high field strengths (i.e. for close perturbers) when the gradient of the field across the emitter becomes important. Thus the asymmetry is expected to be increasingly important at higher densities.

1.5.5 Contribution of Perturber Radiation

Burgess (1968) showed that the inclusion of the coupling of the perturbing electron with the transverse radiation field, hitherto neglected in electron-impact broadening theories, gives rise to interference terms which produce asymmetries in the lines of ionized emitters. The percentage asymmetry at a given wavelength separation from line centre is shown (Burgess 1968) to be independent of electron density. Since the ordinary Stark width is proportional to the electron density for electron-impact broadened lines, the asymmetry will thus become more noticeable at high densities, i.e. when the wavelength at which a measurable percentage asymmetry occurs becomes comparable with the half-width of the line concerned (which, of course, increases with increasing n_e).

1.5.6 Debye Shielding

The electrostatic potential at a distance r from a charge q in a plasma is given by :-

$$V = \frac{q}{r} e^{-r/\lambda_D}$$

λ_D is the Debye radius, and is a measure of the distance to which the field of an individual ion or electron extends before it is effectively shielded by oppositely-charged particles.

The effect of Debye shielding on spectral line shapes will become important when the ratio of the interparticle separation R to

λ_D becomes large, as for the source used in the present investigation. Debye shielding will be most important for perturbers with impact parameters $\rho \gtrsim \lambda_D$, where the electrostatic field seen by the perturber will be considerably reduced due to the effects of Debye shielding. (Conversely, emitter-perturber correlations (i.e. electron-ion attraction) will be most important for small impact parameters $\rho < \lambda_D$, and will thus affect primarily the line wings).

For electron-impact broadened lines, typical impact parameters are usually much smaller than λ_D. For example, in this source for for electrons broadening Ar II Mult 6, typical impact parameters are of order 8.0×10^{-8} cm, compared with a Debye length of order 5.6×10^{-7}cm ($7.0\ \bar{\rho} \sim \lambda_D$). Thus typical perturbers will be unaffected by Debye shielding. Only close to line centre, corresponding to large impact parameters, will Debye shielding affect the line shape.

However for ion-broadened lines, typical impact parameters are larger by about an order of magnitude. For example, for H_α $\bar{\rho} \sim 8.5 \times 10^{-7}$cm for perturbing ions (i.e. $\bar{\rho} \sim 1.5\lambda_D$), so that Debye shielding might appreciably affect the line shape for this transition.

Unfortunately the lines of the Balmer series of hydrogen are very broad under the high density conditions in this pinch (the half width of H_α is ~ 30 Å at these densities. Thus in this source, the hydrogen lines usually lie underneath many strong Ar II transitions, making the hydrogen line profile studies impossible.

1.6 A Summary of the Work Presented in this Thesis

Chapter II describes the choice of diagnostic methods relevant to high density sources, and the application of several independent diagnostic techniques (two of which are fully spatially resolved) to determine the electron density of the dense z-pinch source. In each

case the special procedures are described which are necessary to overcome the problems of uncertainties in the plasma size and spatial inhomogeneities when observing sideways-on.

Chapter III discusses the historical background to the effect described as the plasma polarization shift, and Chapters IV and V describe measurements of such shifts for a number of ionization stages (for neutral and singly-, doubly- and triply-ionized emitters) at high electron densities. The temperature dependence of observed shifts is also investigated.

Chapter VI discusses some experimental evidence for the existence of measurable contributions to spectral line shapes due to perturber-radiation interactions which take the form of wing asymmetries for the profiles of Ar II and Ar III.

In Chapter VII measurements of the line wings of hydrogen Lyman α at high densities ($n_e \gtrsim 10^{18}$ cm^{-3}) are described. A number of satellite-like features in both the red and blue wings are observed. These features arise as a result of the structure of unbound quasi-molecules H Ar$^+$ and H Ar^{++}. Measurements of the asymmetry of the profile are also compared with theoretical predictions for quadrupole asymmetries.

CHAPTER II

A Dense (i.e. $n_e > 10^{18}$ cm^{-3}) Z-pinch Source and its Diagnostics

2.1 Apparatus

The source used in these experiments was a z-pinch, run in argon to produce, at the pinch stage, a dense ($n_e > 10^{18}$ cm^{-3}) but relatively low temperature plasma.

The 20 cm long discharge was driven by a low inductance (~ 15 nH) capacitor bank with a capacitance of 100 μF. This inductance should be compared with the inductance of the connecting cables (~ 75 nH) and of the pinch (~ 90 nH). The bank consisted of five capacitors of 20 μF, connected in parallel. The capacitor bank could be charged up to voltages of 10 KV, and was discharged through the z-pinch by the breakdown of an intervening spark gap. The density and temperature of the plasma could be varied by changing the filling pressure in the pinch. Filling pressures used were typically in the region 0.05 Torr to 1.5 Torr. The characteristics of the plasma could also be changed by varying the bank voltage. Bank voltages used were typically 3 KV to 7 KV. The source produces a column of plasma 20 cm long and about 1 cm in diameter. The z-pinch could be fitted with either a plain tube, or with a tube with side-arms for studying the V.U.V. emission of the pinch sideways on. Both tubes were constructed of pyrex and were 20 cm long and 10 cm in diameter. The plasma column could also be viewed end-on, through small holes in the centres of both the earthy and high voltage electrodes, which were made of brass.

The return current is carried outside the pinch through a gauze closely fitting the discharge vessel.

Plate 2.1 shows the z-pinch, with a tube with side arms.

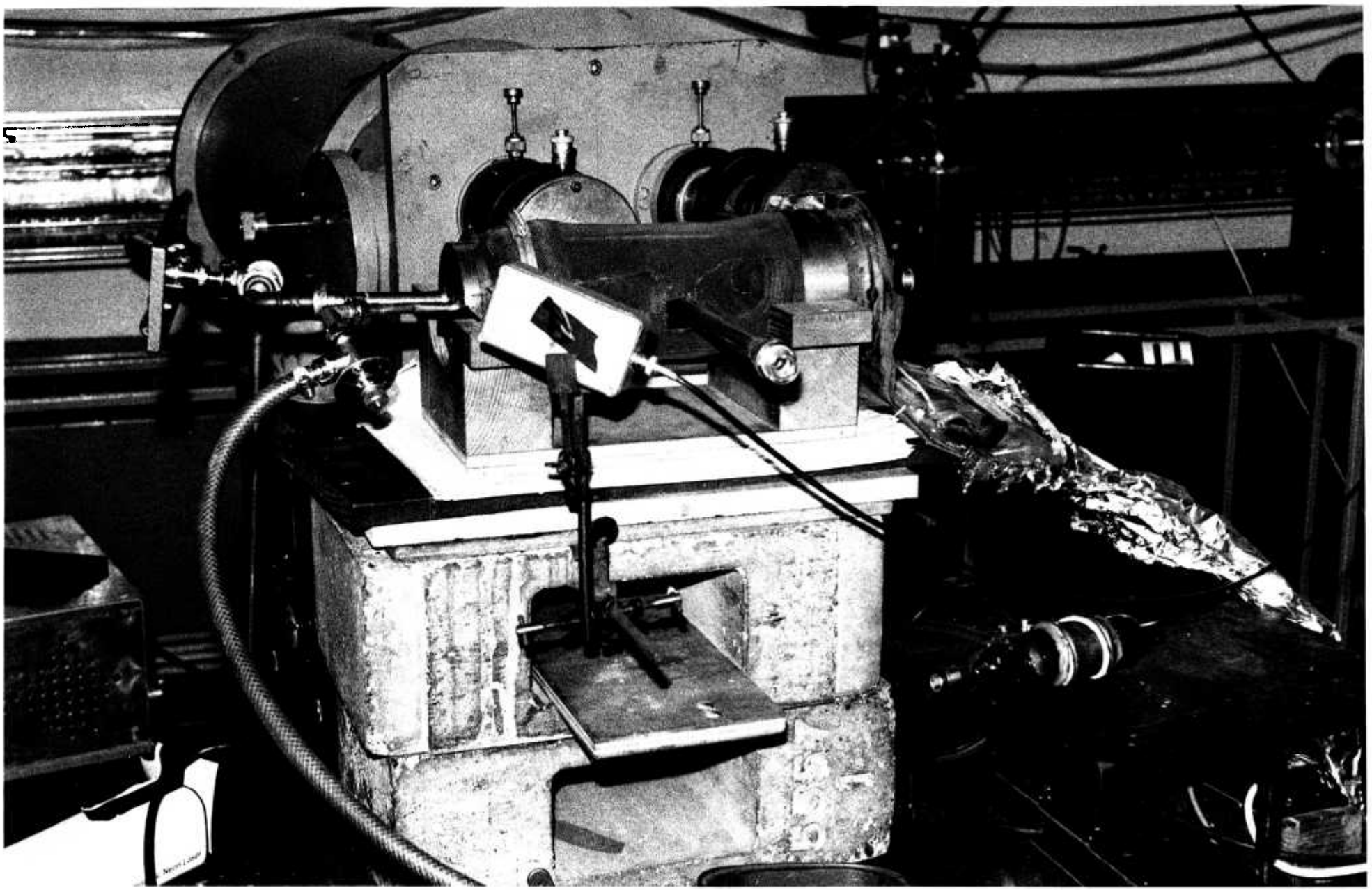

PLATE 2 . 1 : Z - Pinch Source

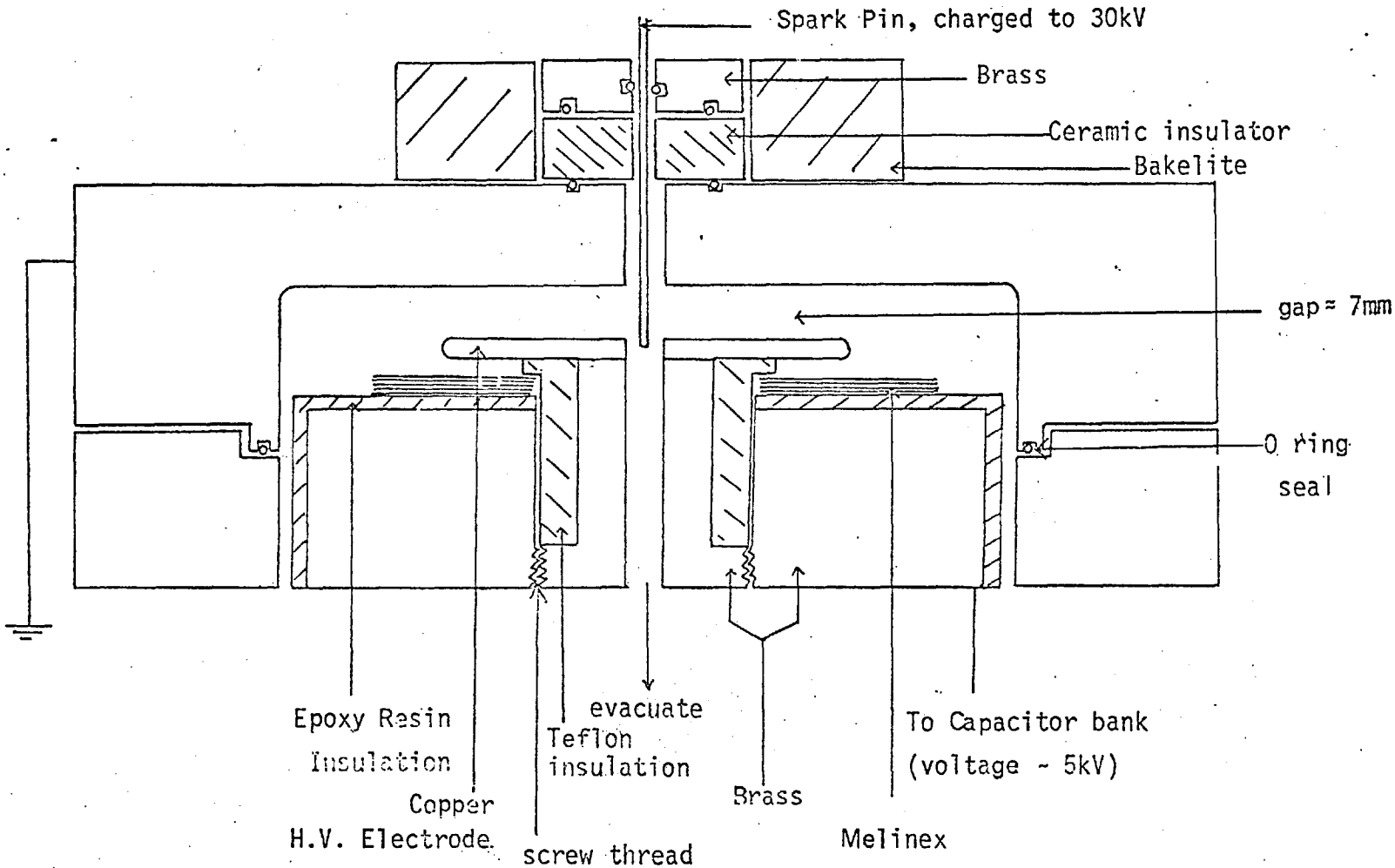

Fig 2.2 : Spark Gap Section.

The capacitor bank was discharged by breakdown of a low-pressure, low inductance spark gap, sketched in Fig.2.2. The working pressure in the gap was between 10^{-5} Torr and 10^{-6} Torr. This pressure was achieved by evacuation with a 3" oil-diffusion pump. At the lowest gap pressures, the capacitor bank and high voltage electrode of the gap could be charged up to 7 KV before the spark gap broke down spontaneously. The discharge was initiated by the breakdown of the air in the spark gap by applying a 30 KV pulse to a trigger pin, which was equidistant from the high voltage and earthy electrodes of the gap.

The pinch reaches peak compression after about 3 μsec. Plate 2.2(i) shows an oscillogram of the current trace for the plasma for a filling pressure of 0.2 Torr and a bank voltage of 5 KV. Plate 2.2(ii) shows the integrated spectrum of the pinch, from a photodiode placed near to the pinch. The time of peak compression (determined from the time at which the Ar II Mult 6 lines are broadest, as discussed in Section 2.3.1) is indicated on the current trace.

2.2 Gross Spectrum of the Pinch

Plate 2.3 shows a visible emission spectrum of the pinch, taken on Polaroid film with a Chelsea Instruments S100 spectrograph. The dispersion of the instrument is 40 Å/mm. The spectrum was taken sideways on to the pinch, with the spectrograph slit about 30 cm from the middle region of the pinch column.

The plasma consists chiefly of singly- and doubly-ionized argon, and the visible spectrum shows Ar II and Ar III lines. Visible hydrogen lines also appear in the spectrum, although at peak compression $H\alpha$ and H_β are both so broadened that they cannot be detected above the continuum level and the wings of broadened Ar II transitions which lie on top of the hydrogen profiles. As discussed

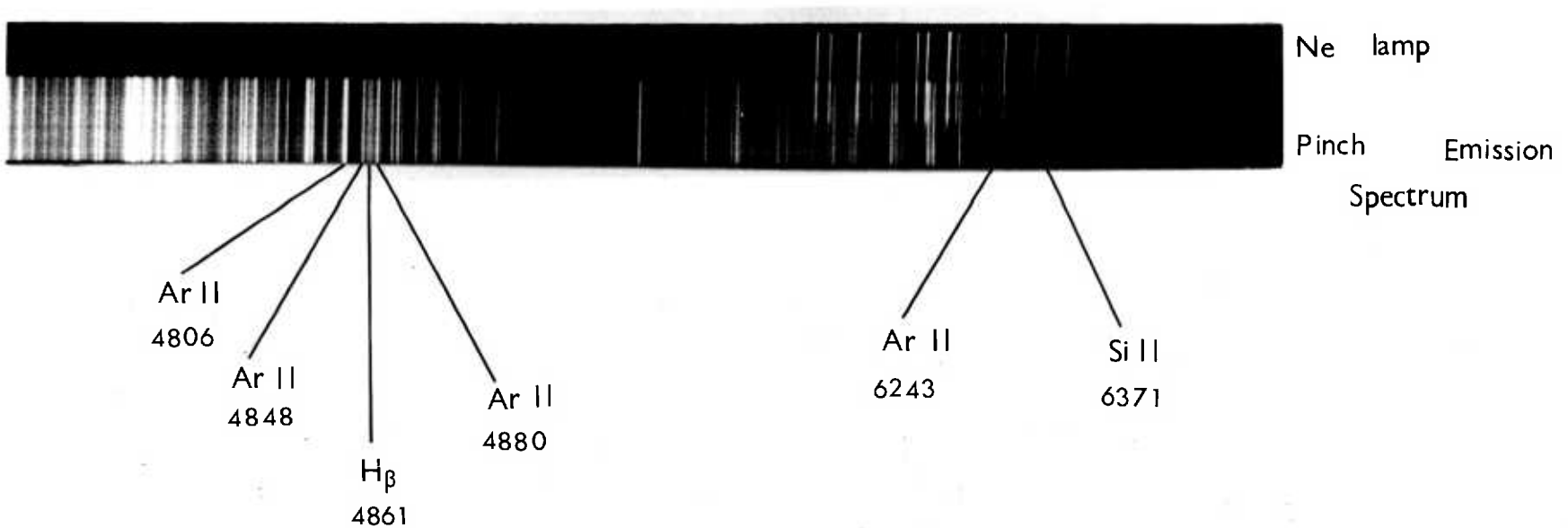
Ne lamp
Pinch Emission Spectrum
Ar II
4806
Ar II
4848
Hβ
4861
Ar II
4880
Ar II
6243
Si II
6371

PLATE 2.3

in Section 1.4.4, the middle (working) region of the plasma is free from electrode impurities (such as Cu II, Zn II).

Sodium and silicon impurities from the glass tube of the pinch also give rise to lines in the spectrum. However as discussed in Chapter IV, the sodium D-line line-widths indicate that at the time of peak compression these impurities emit from a less dense region outside the core of the pinch.

The chief gaseous impurity is nitrogen, which gives rise to U.V. impurity lines of N II, (N III), N IV as discussed in Chapter IV.

The pinch also shows carbon impurity lines (C III) in the ultraviolet spectrum, as discussed in Section 7.5.2.

2.3 Difficulties in Performing Diagnostic Experiments on High Density Sources

As discussed in Chapter I, there are many difficulties associated with performing diagnostic experiments on high density sources. The most serious problem is that of optical opacity along the line of sight. Before relevant diagnostic techniques can be chosen, it is necessary to make estimates of the opacity of the source, in order assess the importance of optical thickness considerations.

2.4 Optical Depth Considerations

2.4.1 Ar II Profiles

The optical depth may be determined by measuring the widths and intensities of two lines from the same multiplet. Assuming (after Griem 1964) that the lower state broadening of the lines can be neglected, all lines arising from the same upper state will have the same electron impact width. Even if the lower state broadening is significant, all lines within a multiplet will have approximately the same electron impact width if the multiplet splitting is small compared with the ℓ-splitting.

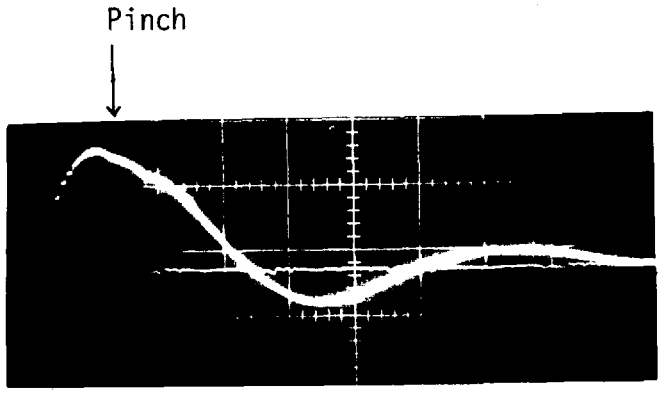

PLATE 2.2(i)

Current

.2 Torr

5 KV

5 μs/cm.

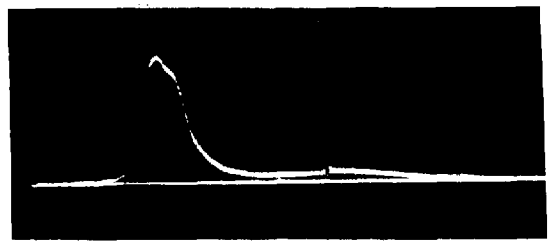

PLATE 2.2(ii)

Integrated Spectrum

5 KV. .1 Torr

2 μs/cm.

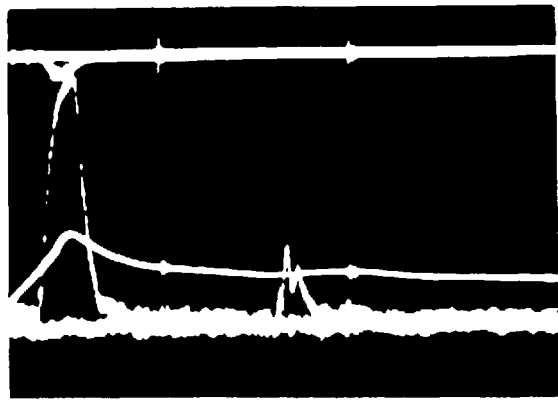

PLATE 2.4

He-Ne Laser Absorption.

Moreover, if the source is optically thin, the relative total intensities of the lines will be in the ratio of their respective $h\nu\ A_{21}\ g_2$ values. Provided the line widths are the same, the peak intensities will also be in the ratio of the $h\nu A_{21}\ g$ values.

Thus, knowing the relative intensities and widths of these two lines in the optically thin case, the optically thin intensities can be compared with the measured intensities and the optical depths at line centre can be determined.

The line profiles studied were those of Ar II Multiplet 6 at 4848 Å and 4806 Å ($3s^2\ 3p^4\ 4s\ ^4P$ - $3s^2\ 3p^4\ 4p\ ^4P^o$). Burgess (1965) measured the optically thin value to be 0.42 for the relative peak intensities of 4848 Å and 4806 Å, which is close to the LS coupling value.

The profiles were scanned from shot to shot, the reproducibility being ± 5%. The spectrograph used was a Hilger Watts medium quartz spectrograph, fitted with a scanning attachment and an RCA1P28 photomultiplier.

End-on observations suggested that the optical depth became appreciable at high bank voltages (e.g. 5 KV) and only at the lowest bank voltages (i.e. below 3 KV) did the intensity ratios and widths of these lines approach the values expected for an optically thin plasma. For example, with 5 KV bank voltage and 0.5 Torr filling pressure, the optical depth was estimated to be 1.1 at 4806 Å and 0.4 at 4848 Å, for end-on observation. Because of this high optical depth estimate, further experiments were carried out to determine the optical depth of the plasma end-on, as described below.

2.4.2 Absorption of Off-Resonance Laser Radiation

The optical depth of the plasma in the continuum, viewed end-on, was determined from measurements of the absorption of off-resonance laser radiation. First the optical depth at 6328 Å was measured

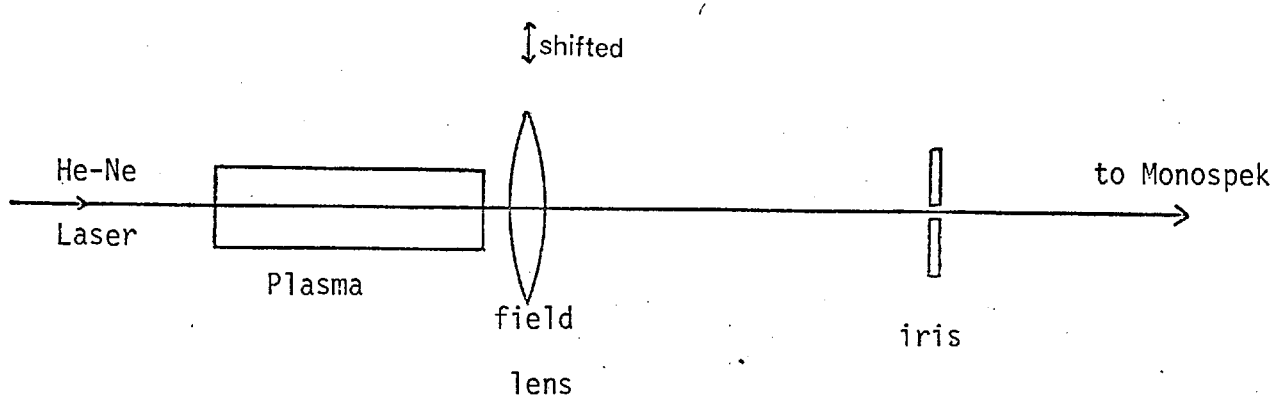

Fig2.1 : Apparatus for end-on absorption measurements.

using a Metrologic helium-neon laser. As may be seen on Plate 2.3, 6328 Å is well removed from the wings of Ar II 6243 Å and Si II 6371 Å which are the nearest transitions to this wavelength.

The apparatus is shown in Fig.2.1.

The light was dispersed by a Monospek 1000 monochromator, fitted with a 1200 lines/mm 5000 Å blazed grating. The signal was detected using an RCA 1P28 photomultiplier.

Plate 2.4 shows the oscilloscope traces on a 5 μsec/cm time base. The upper trace shows the photomultiplier output when the laser is turned off (i.e. pinch emission only). The lower trace is the photomultiplier output when the laser is turned on and the source is fired (showing the laser absorption and the pinch emission). At peak compression the percentage of the laser intensity transmitted is $< 3\%$.

The experiment was repeated with a lens inserted between the pinch and the monochromator, to ensure that possible shearing of the laser beam through less dense regions around the core of the pinch, would not result in misleadingly high measurements of the absorption. In this case, however, the measured transmission was still only $< 4\%$. Thus, even without a light-collecting lens, the proportion of the laser beam being sheared through less dense regions was less than 1%. The optical depth of the pinch end-on at 6328 Å was found to be $\tau \sim 3.5$.

The experiment was repeated using a C.W. dye laser tuned to 5820.5 Å as source. At this wavelength the measured transmission at peak compression was $< 5\%$, corresponding to an optical depth of $\tau \sim 3.0$.

Assuming that the optical depth is proportional to the cube of the wavelength (i.e. free-free absorption), the measured optical depth at 6328 Å suggests that at 5820 Å the percentage transmission

in the continuum should be $(5.5 \pm 1.4)\%$ which is consistent with the measured value of the percentage transmission.

Using Eqn.2.1 for the free-free absorption coefficient, these values of the optical depth can be used to estimate the electron density of the plasma. The electron density estimated from the end-on optical depth of the plasma at 6328 Å is 2.3×10^{18} $cm^{-3} \pm 15\%$. This value is in good agreement with the electron density determinations from three independent methods discussed in Sections 2.5.1, 2.8 and 2.9 below.

2.4.3 Conclusions from the Optical Depth Measurements

The experiments described above indicate that in any end-on observations, finite optical depth would severely limit the range of firing conditions over which measurements of line profiles could usefully be made. In any case, it was difficult to make density determinations and optical depth estimates from end-on observations because of the strong overlap of the various Ar II transitions. All subsequent diagnostic experiments and line-shape measurements were therefore made observing the plasma sideways-on rather than end-on, in which case the geometric depth of the plasma was only about 1 cm instead of 20 cm. This was in some ways inconvenient, since it introduces another unknown parameter into considerations - namely the geometric depth of the plasma involved, since the diameter of the plasma column is not known and varies with the firing conditions. However, information about the plasma size has been obtained from interferometric experiments described below, so this does not impose any severe limitations. More serious is the problem of radial inhomogeneity of the plasma along the line of sight. Information about the radial variation of the electron density is derived from an Abel inversion procedure, also described below (Sections 2.8 and 2.9).

2.5 Estimation of the electron density from measurements of the Half Widths of Ar II Lines

The electron density has been determined by a number of independent methods, summarised in Table 2.1. More accurate, fully spatially resolved methods will be discussed below (Sections 2.8 and 2.9). However, the density was first determined by the straightforward method of measuring the half widths of Ar II Multiplet 6 4848 Å and 4806 Å, viewed sideways-on to the discharge. Plate 2.7 shows the pinch emission at 4806 Å for a bank voltage 5 KV, and a filling pressure 1 Torr. The lines of Multiplet 6 were chosen because they have already been studied extensively, both experimentally and theoretically, and their broadening parameters are relatively well-known. Since 4848 Å is one of the weaker transitions of Multiplet 6, problems of optical opacity are less serious for this transition.

2.5.1 Broadening Parameter

Griem (1966) has calculated the electron impact broadening parameter Ω for the lines of Multiplet 6, where

$$\Omega = \frac{\text{width } W}{\text{electron density } n_e}$$

$$\Omega = 1.3 \times 10^{-18} \text{ Å/cm}^{-3} \text{ at } T_e = 30{,}000^{\circ}\text{K} \quad \text{(Griem)}.$$

Furthermore, Roberts (1968) checked by experiment the electron impact broadening parameters for the lines of Multiplet 6 in a high density ($\sim 10^{17}$ cm^{-3}) argon plasma. He found that at these densities

$$\Omega \approx 1.88 \times 10^{-18} \text{ Å/cm}^{-3} \text{ at } T_e \sim 30{,}000^{\circ}\text{K}.$$

2.5.2 This Experiment

In this experiment, the profiles of Ar II 4848 Å and 4806 Å were scanned from shot to shot, using a Monospek 1000 monochromator,

fitted with a 1200 lines/mm, 7000 Å blazed grating. The light signal was detected using an RCA 1P28 photomultiplier. The shot to shot reproducibility of the signal was 10% or better. Fig.2.3 shows typical profiles of Ar II 4848 Å for different times in the pinch at a bank voltage of 5 KV and a filling pressure of 0.5 Torr.

2.5.3 Deconvolution Procedure

The measured half-widths were corrected for instrumental broadening and Doppler broadening by a procedure discussed by Allen (1955).

The total width B of the Voigt profile of a spectral line at half maximum intensity is given by :-

$$B = (D^2 + 2.80\, G^2)^{\frac{1}{2}} + D$$

The broadening factors are resolved into a Gaussian term with half-($^1/e$) width g in the intensity expression $\exp(-x^2/g^2)$ and a Lorentzian term with half-half width d in the expression $1/(1 + x^2/d^2)$. D represents the sum of all the Lorentzian half-half widths :-

$$D = d_1 + d_2 + \ldots$$

G represents the sum of all the Gaussian half-($^1/e$) widths :-

$$G = (g_1^{\,2} + g_2^{\,2} + \ldots)^{1/2}$$

The electron impact broadening results in a Lorentzian of half-half width

$$d = n_e\, \Omega$$

The Doppler broadening results in a Gaussian distribution of half-($^1/e$) width

$$g_D = \frac{\lambda}{c}\left(\frac{2k\, T_e}{m_a}\right)^{1/2}$$

where m_a is the atomic mass.

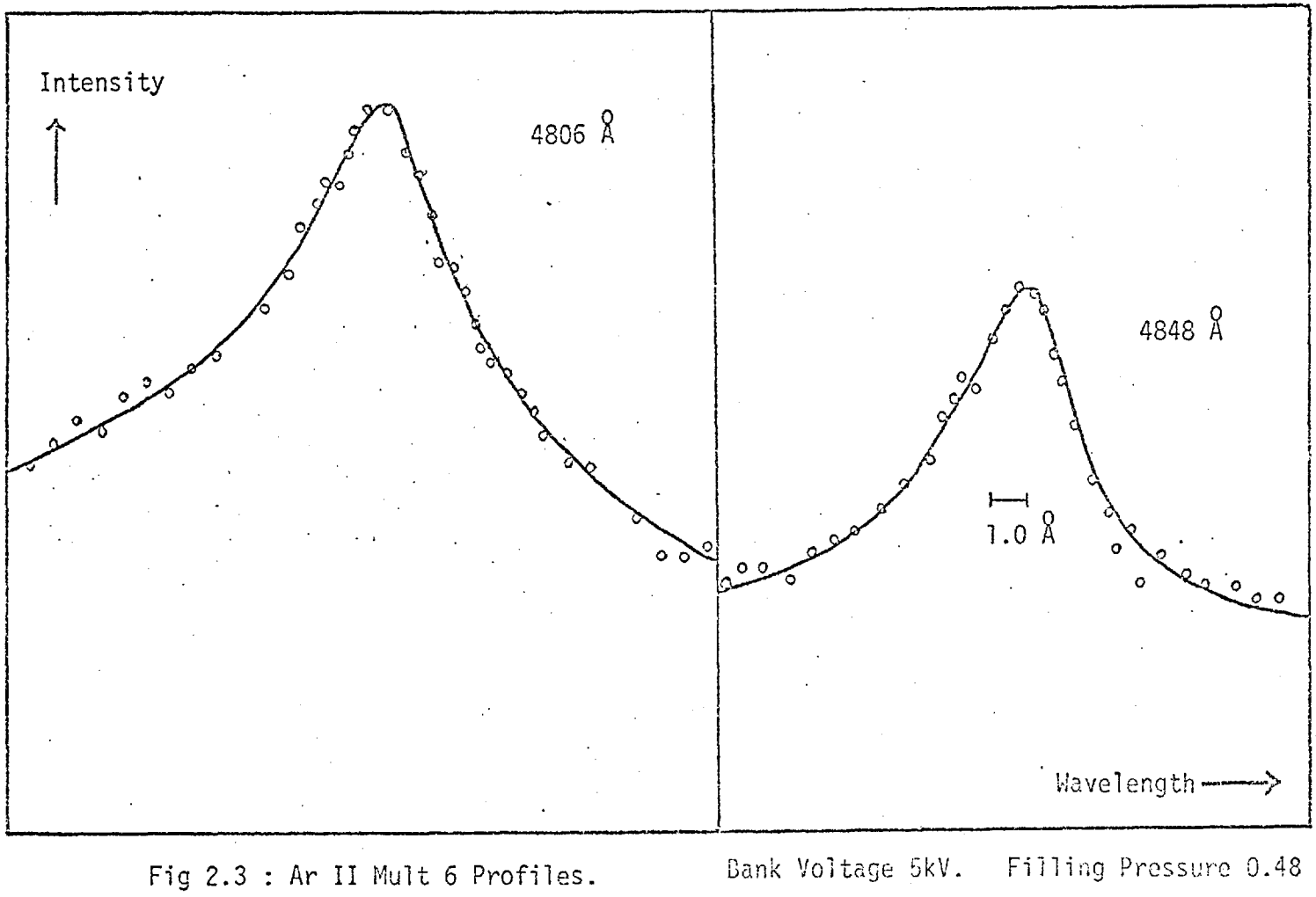

Fig 2.3 : Ar II Mult 6 Profiles. Bank Voltage 5kV. Filling Pressure 0.48 Torr

The instrument profile is a Voigt profile. For a perfect spectrograph the profile has a Lorentzian component

$$d = 0.14\ell$$

and a Gaussian component

$$g = 0.43\ell$$

where ℓ is the resolving distance from the first maximum to the first minimum.

2.5.4. Electron Density Estimates from Ar II Profiles

The electron impact widths of 4848 Å obtained from the measured half-widths by the method outlined above, were used to estimate the electron density using the Griem (1966) value for the electron impact broadening parameter. The variation of electron density with time at a bank voltage 5 KV, filling pressure 0.48 Torr is shown in Fig.2.4. The values of n_e for a bank voltage 5 KV and filling pressure 0.4 Torr are shown on the same graph for comparison.

The electron densities determined from the half widths of 4806 Å are also shown on the same graph - these are slightly higher since the widths of the more intense line will be broader because of absorption. The peak intensity ratios of 4848 Å and 4806 Å at the time of peak compression suggest that the optical depth at 4806 Å is $\tau = 0.18$ corresponding to a line centre optical depth for 4848 Å of 0.08.

The half widths for 4848 Å suggest that at peak compression the electron density is $\sim 2 \times 10^{18}$ cm^{-3}.

2.5.5 Sources of Error in Electron Density Estimates

The density values may be expected to be uncertain by $\pm$ 30%, as quoted for the uncertainty in the Griem (1966) theoretical broadening

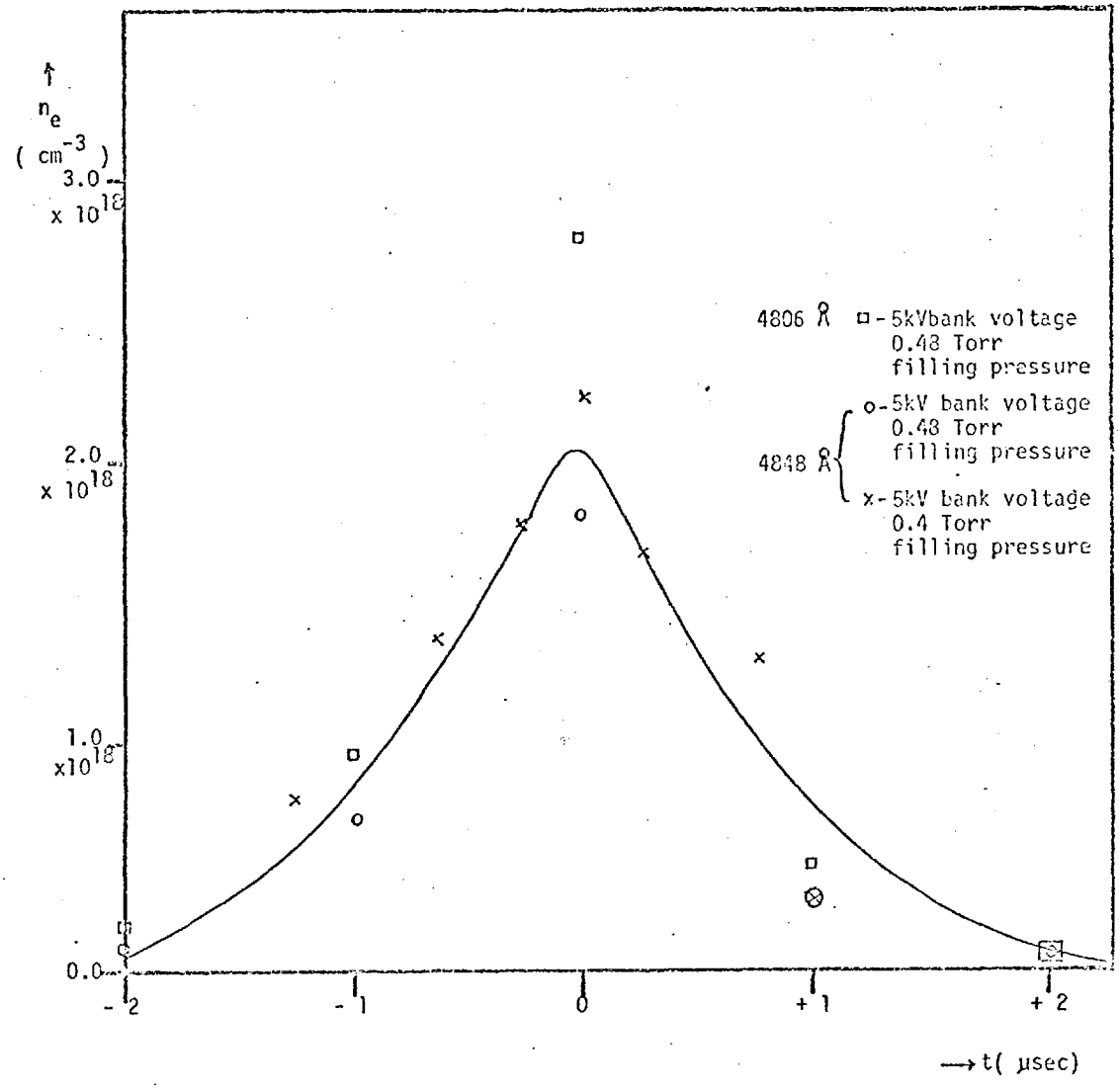

Fig 2.4 : Electron density, n_e, (from Ar II half widths) as a function of time, t.

parameter. Since the profiles of the Ar II lines were studied sideways-on, radial density variations might be expected to present a more serious source of error in these values. For this reason, the quoted electron densities are probably underestimates of the true electron density in the core of the plasma. As an absolute density determination for the core of the plasma, the use of the Ar II half-widths is rather limited because of uncertainties in the radial corrections. More accurate, spatially resolved measurements of n_e are discussed below in Sections 2.8 and 2.9. However, the approximate densities obtained from the half-width measurements are still of great importance to the studies of the Ar U.V. resonance lines discussed in Chapter IV, since these estimates set a lower limit on the density of the region from which the Ar II emission arises.

2.5.6 Asymmetries of Ar II Mult 6 Profiles

The profiles of Ar II Mult 6 4806 Å and 4848 Å both show enhanced blue-wing asymmetries, which are particularly marked at high densities. The interpretation of these asymmetries is discussed in Chapter VI.

2.6 Measurement of the Electron Temperature

2.6.1 Measurement of Temperature by resonant absorption

The temperature of the plasma was determined by a method first suggested by Burgess (1965) and treated in detail by Troughton and Wheeler (1969). The absorption of resonant laser radiation transmitted sideways through the plasma was studied. The absorption is proportional to the exponential of the optical depth, which is itself a function of temperature and electron density. As pointed out by Wheeler and Troughton (1969), the optical depth is independent of the electron density only if the temperature lies in the range 10,000K to 20,000K

for electron densities 4.10^{16} to 2.10^{20} cm^{-3}, and under these circumstances this method can be used to determine the plasma temperature to an accuracy of 1%. Outside this temperature range, the optical depth is a weak function of density, and with some knowledge of the electron density, the electron temperature can still be determined, although with some loss of accuracy.

2.6.2 Assumptions implicit in the Optical Depth Calculations of Wheeler and Troughton (1969)

Wheeler and Troughton (1969) assume that the optical depth of a plasma $\tau(\nu)$ at a frequency ν in one of its emission lines is :-

$$\tau(\nu) = \frac{h\nu}{4\pi} B(1,2) \int_a^b n(1) \left\{ 1 - \exp\left(\frac{-h\nu}{kT}\right) \right\} \Phi(\nu)\, dx$$

Where $\Phi(\nu)$ is the emission profile, (b-a) is the geometric thickness of the plasma in the x-direction, $n(1)$ is the population density of the lower state, and $B(1,2)$ is the Einstein intensity absorption coefficient. The exponential factor corresponds to contributions due to stimulated emission and is $\ll 1$ for temperatures of interest here.

The plasma is assumed to be collision-dominated, so that the emission and absorption profiles are the same, and the use of Boltzmann factor to evaluate the stimulated emission coefficients is justified.

Further, if collisional domination is valid right down to the ground state of the plasma emitting species, $n(1)$ can be related to the total number density of this species by Boltzmann statistics. Further, this total number density can be related to n_e by Saha equations and the equation of electrical neutrality. Hence $n(1)$ may be evaluated in terms of n_e.

The line profile $\Phi(\nu)$ is assumed to be broadened by electron impacts, so the usual dispersive shape may be used for $\Phi(\nu)$.

Hence Wheeler and Troughton (1969) calculate $\tau(\nu)$ for different n_e and T_e. There are a number of assumptions implicit in this treatment, which fall into two categories - those concerning the line profile, and those concerning plasma collisional domination.

2.6.2.1 Assumptions concerned with the Line Profile

Thermal Doppler broadening is assumed to be negligible compared with the electron-impact broadening. For the Ar II Mult 6 transitions this requirement is well satisfied in this plasma, since even at modest densities of order $n_e = 4 \times 10^{16}$ cm^{-3}, the neglect of Doppler broadening introduces errors of $< 10\%$ in temperatures of order 20,000K.

In addition, ion broadening has been completely neglected in the above treatment. This assumption is perfectly justified for the Ar II Mult 6 lines in this plasma, as will be discussed in Chapter VI.

In addition there are a number of assumptions in the impact-broadening theory used to calculate the dispersive line profile. These are fully discussed in Roberts (1967). For these Ar II lines there are two chief assumptions. Firstly that the free electrons suffer little change in motion on perturbing the emitter. This requires $T_e \geq 7{,}000$K. Secondly, it is assumed that the perturbing energy levels are non-degenerate, requiring $n_e << 2 \times 10^{20}$ cm^{-3}.

2.6.2.2 The Assumption that all the Energy Levels (including the ground state) are Collisionally Dominated

According to Griem the LTE approximation holds good if the radiative population rate of the ground state from the resonance level should be a factor of ten less than the corresponding collisional rate. However if strong self absorption takes place this requirement can be relaxed by a factor of ten (Griem 1964). For Ar II this requirement is then

$$n_e \geq 2.56 \times 10^{16} \ (T(eV))^{\frac{1}{2}} \ \text{cm}^{-3}$$

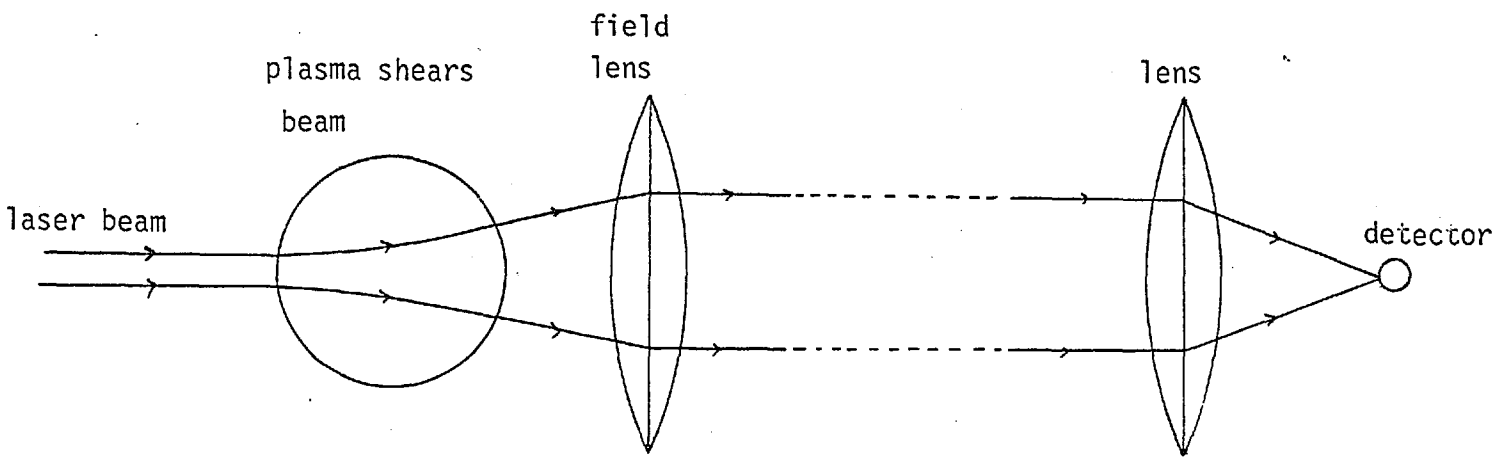

Fig 2.5 : Illustration of the use of a field lens to distinguish between shearing and absorption of the laser beam by the plasma. The sheared beam shown above is focussed at the detector, with no loss of intensity. Absorption of the beam results in a reduction in the intensity recorded at the detector.

This will be true for the present case, which deals essentially with the self-absorption of a non-resonance line. Hence in this case the requirement for collisional domination is already satisfied if the temperature is sufficiently low for Doppler broadening to be negligible.

Since $n_e \sim 10^{18}$ cm^{-3} and $T_e \sim$ 20,000K in this plasma, errors due to implicit assumptions in the theory should be negligible.

2.6.3 Temperature Diagnostics on this Pinch

Measurements of the optical depth indicated that the temperature of the plasma was in excess of 20,000K. Therefore the values of the optical depth calculated by Wheeler and Troughton (1969) for λ = 4880 Å were used to determine the temperature for different filling pressures, assuming the electron density is of order 2.10^{18} cm^{-3}. The errors involved in measuring the temperature in this region are rather greater than 1% since the method depends on the estimate of the density, which is itself only accurate to about $\pm$ 30%.

The geometric depth of the absorbing plasma was estimated from details of the variation of plasma size obtained from interferometric experiments discussed in Section 2.7. The laser used was an argon ion laser (Spectrophysics Model 164) tuned to Ar II 4880 Å. A field lens was placed between the pinch and the detection system, focussed at the pinch, to ensure that any possible shearing of the laser beam by radial density gradients in the plasma would not result in an erroneously high measurement of the laser absorption - Fig.2.5.

The variation of temperature with filling pressure for bank voltages 5KV and 3.6KV is shown in Fig.2.6. Fig.2.7 shows the variation of temperature with bank voltage for a filling pressure of 0.25 Torr. (Interferometric measurements showed that at this pressure the plasma size did not change much with bank voltage in the range 4.4KV to 6KV). The quoted values for the temperature might be

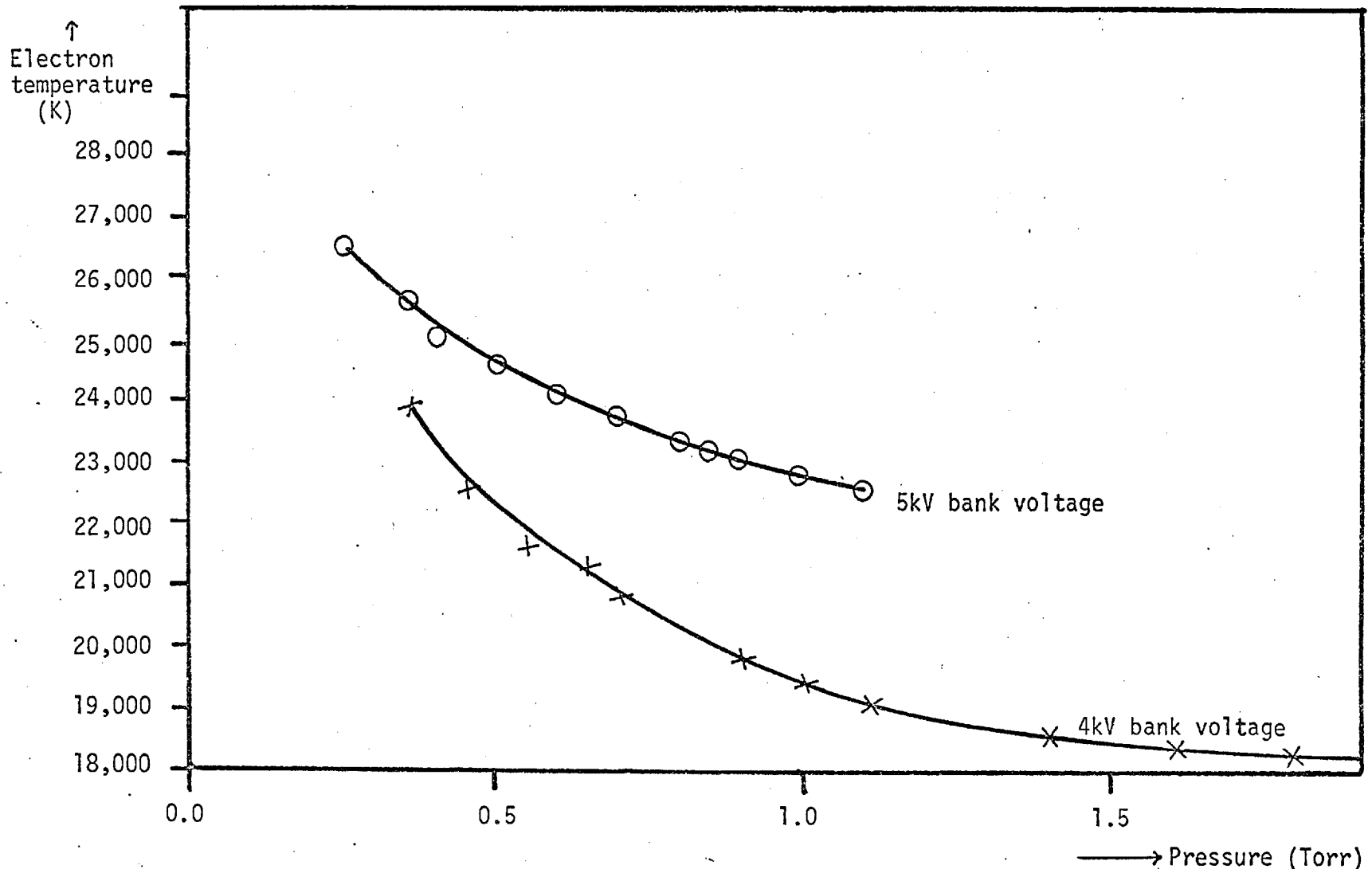

Fig 2.6 : Variation of electron temperature with filling pressure

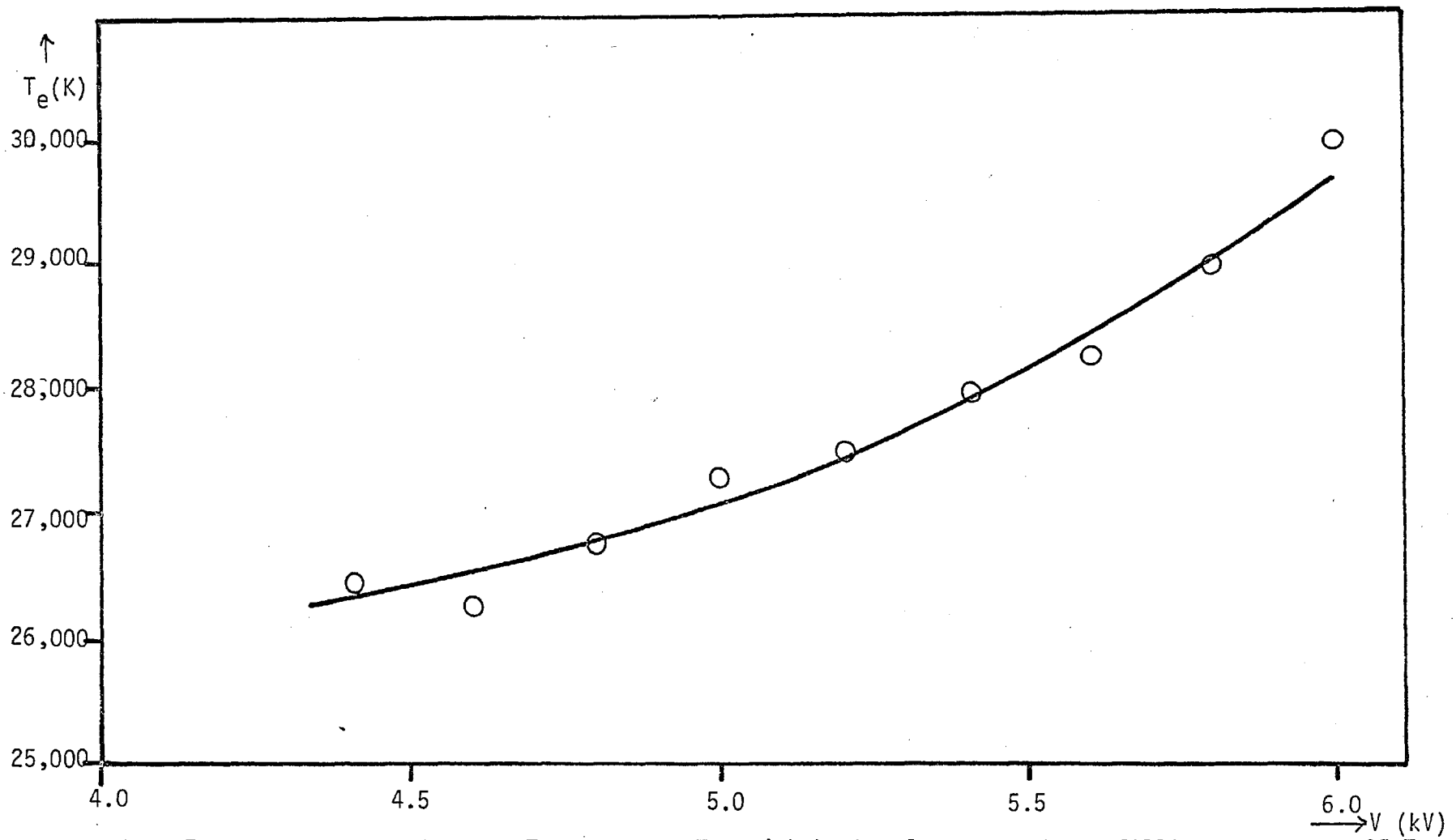

Fig 2.7 : Variation of Electron Temperature, T_e, with bank voltage, V, for a filling pressure 0.25 Torr

expected to be accurate to within $\pm$ 20% at worst, the errors arising from the uncertainties in the electron density and plasma size.

2.7 Preliminary Interferometric Studies

Studies of the electron density variation with pressure were made at bank voltages 4KV, 5KV and 6KV using a Mach Zehnder interferometer (see Fig.2.8) with a helium-neon laser source, observing sideways on to the pinch whilst simultaneously monitoring the continuum intensity.

The Mach Zehnder interferometer is shown in Fig.2.8.

Neglecting the refractive index effects due to changes in the neutral gas density in the path, the effective path change due to the plasma is N fringes where

$$N = \int \left\{ \frac{\mu - 1}{\lambda} \right\} dl$$

where μ is the refractive index of the electrons in the plasma.

$$\mu = \left(1 - \frac{\omega_p^2}{\omega^2}\right)^{1/2}$$

$$= \left(1 - \frac{4\pi n_e e^2}{m_e \omega^2}\right)^{1/2}$$

$$\approx \left[1 - \frac{2\pi n_e e^2}{m_e \omega^2}\right]$$

and $\omega = \frac{2\pi c}{\lambda}$

$$\therefore N = - \frac{e^2 \lambda}{2\pi m c^2} \int n_e \, dl$$

$$\approx \frac{1}{3.54 \times 10^{17}} \cdot \int n_e \, dl \quad \text{for} \quad \lambda = 6328 \text{ Å}$$

Plate 2.5 shows some typical oscillograms for Mach Zehnder fringes when firing at a bank voltage 5KV.

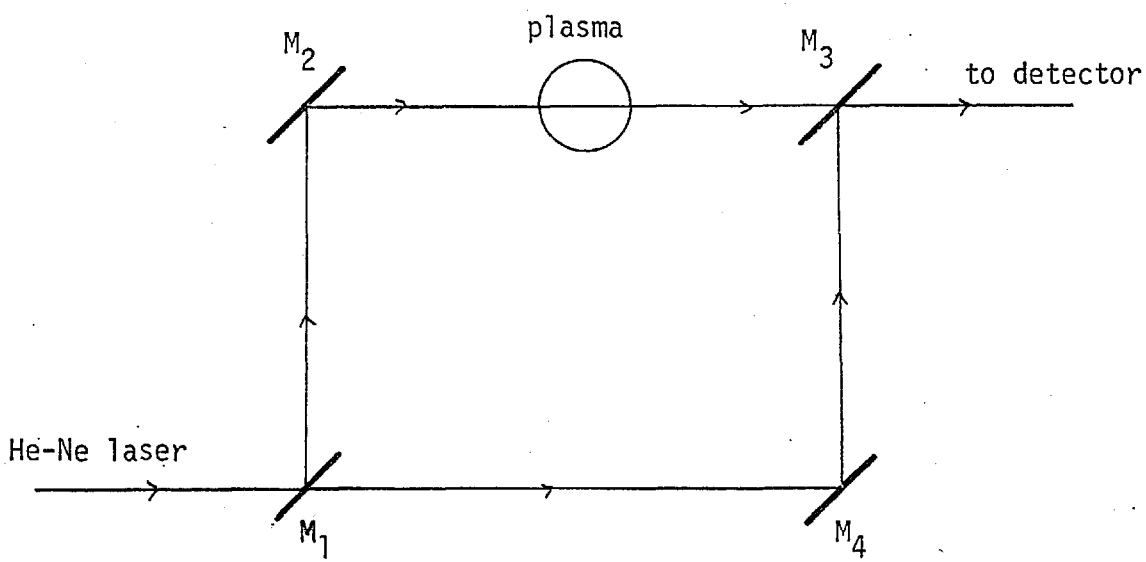

Fig 2.8 : Mach Zehnder interferometer. M_1 and M_3 are partially reflecting; M_2 and M_4 are totally reflecting.

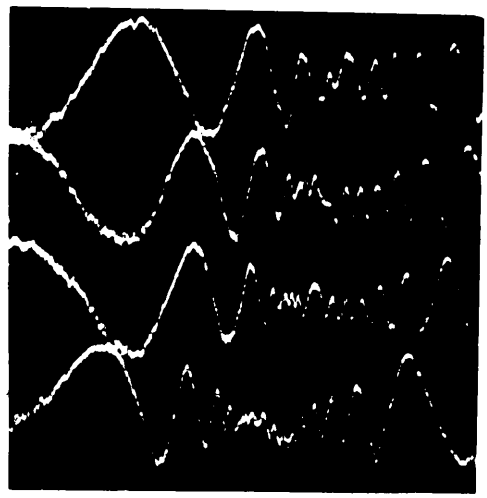

PLATE 2.5

Mach Zender Fringes.

5 KV Bank Voltage.

Filling Pressure (Top to bottom)

1.9, 1.7, 1.5, 1.3 Torr.

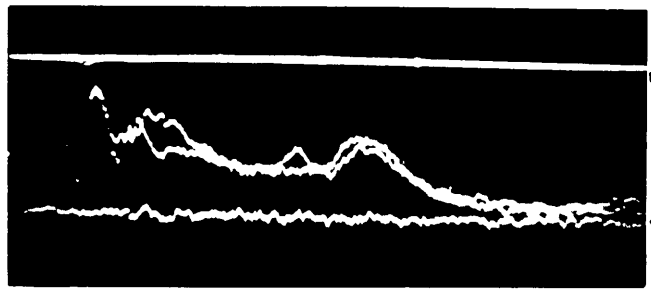

PLATE 2.6

Argon Ion Laser Absorption

(i) 5 KV .18 Torr (2 shots)

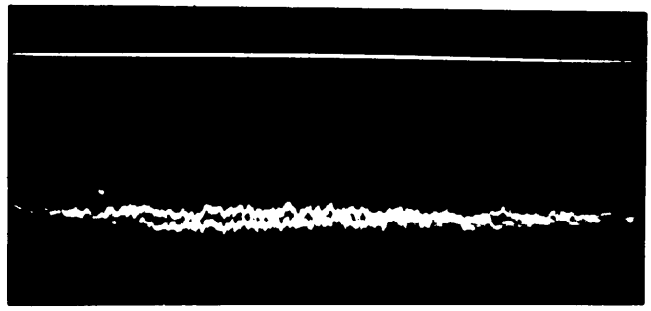

(ii) 5 KV .15 Torr

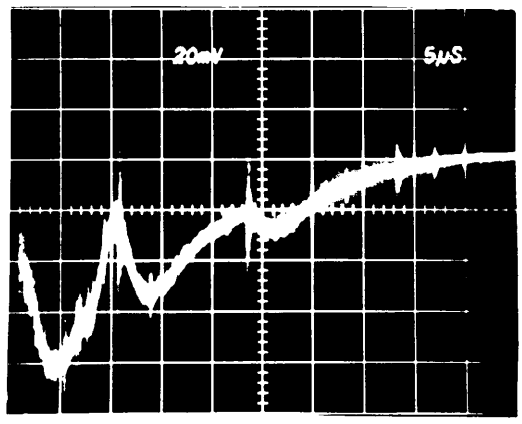

PLATE 2.7

Pinch Emission

at 4806 Å

The fringe count varies as $n_e l$, whilst the continuum intensity (assuming a Bremsstrahlung continuum) varies as $n_e^2 l$. Hence the measurement of fringe count and continuum intensity gave the form of the variation of both density n_e and size l of the plasma as a function of filling pressure.

Moreover the study of the absorption of resonant laser radiation discussed in the previous section fixed the absolute size of the plasma. When firing at 5KV, if the filling pressure was reduced to 0.16 Torr, the diameter of the plasma was the same as the diameter of the beam, since at filling pressures of 0.16 Torr and below, the absorption of the beam is considerably smaller than expected, most of the beam travelling round the plasma, not through it. This is illustrated in Plate 2.6 which shows two absorption traces, one for $P = 0.18$ Torr with the beam being absorbed, the other for $P = 0.15$ Torr with the beam partially tracking around the outside of the plasma, the absorption being drastically reduced in this latter case. Thus it was possible to fix the size of the plasma for one set of conditions, and, from this, with the interferometry results to determine the exact size and density of the plasma for other conditions.

Figs.2.9 and 2.10 show the variation of plasma size and density with filling pressure at bank voltages of 4KV, 5KV and 6KV.

These estimates of the electron density are likely to be underestimates. The chief source of error arises from the difficulty in counting a large number of fast fringes near to the time of peak compression (up to 10 fringes per μsec), the fringe contrast near peak compression being greatly reduced because of the absorption of the laser beam by the plasma. The estimates given in Figs.2.9 and 2.10 assume the source produces a homogeneous cylinder of plasma at peak compression. Correction for radial density gradients in the plasma by an Abel inversion procedure (as discussed in the next section)

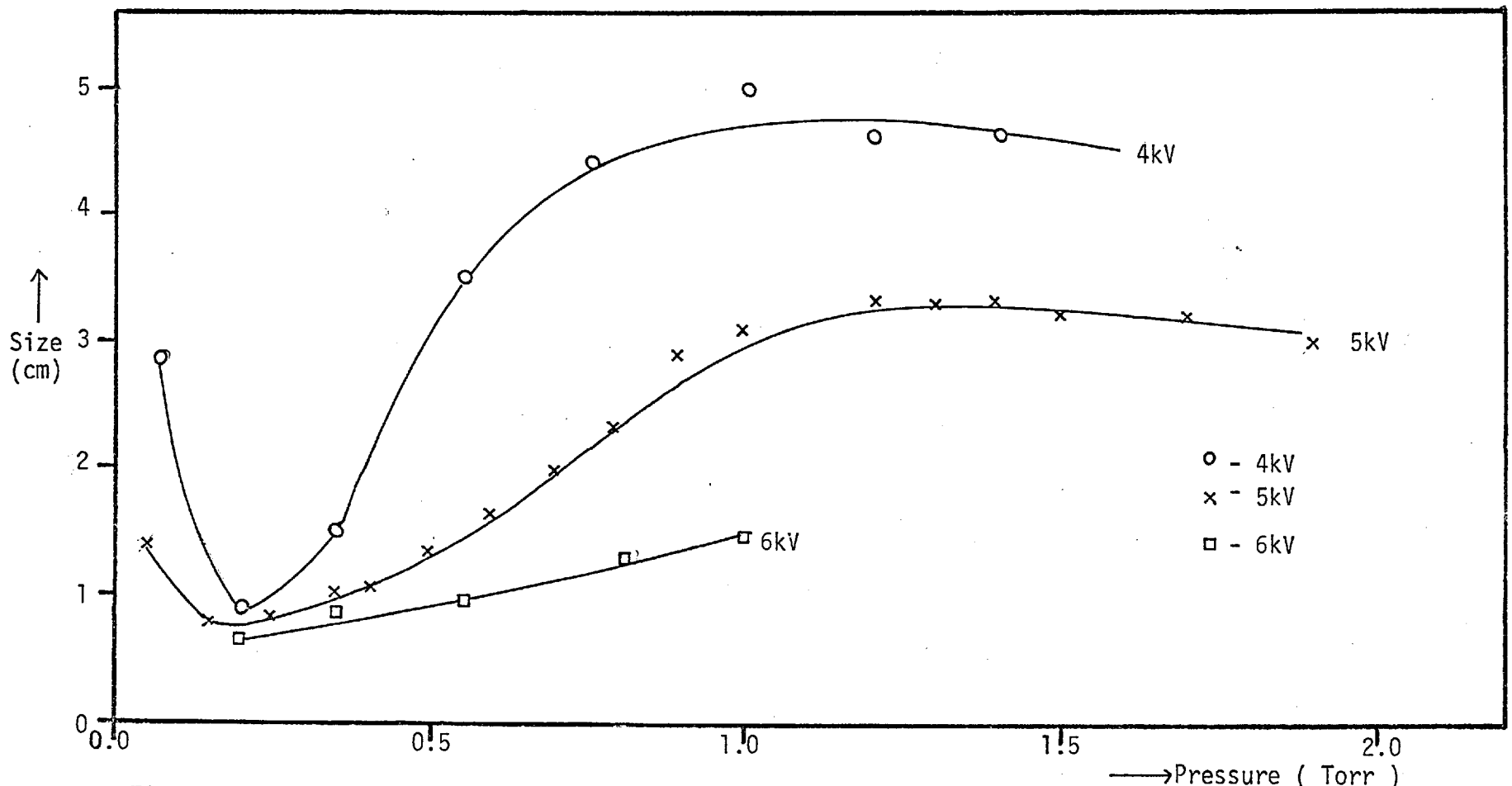

Fig 2.9 : Variation of plasma size (determined from interferometric measurements) with filling pressure.

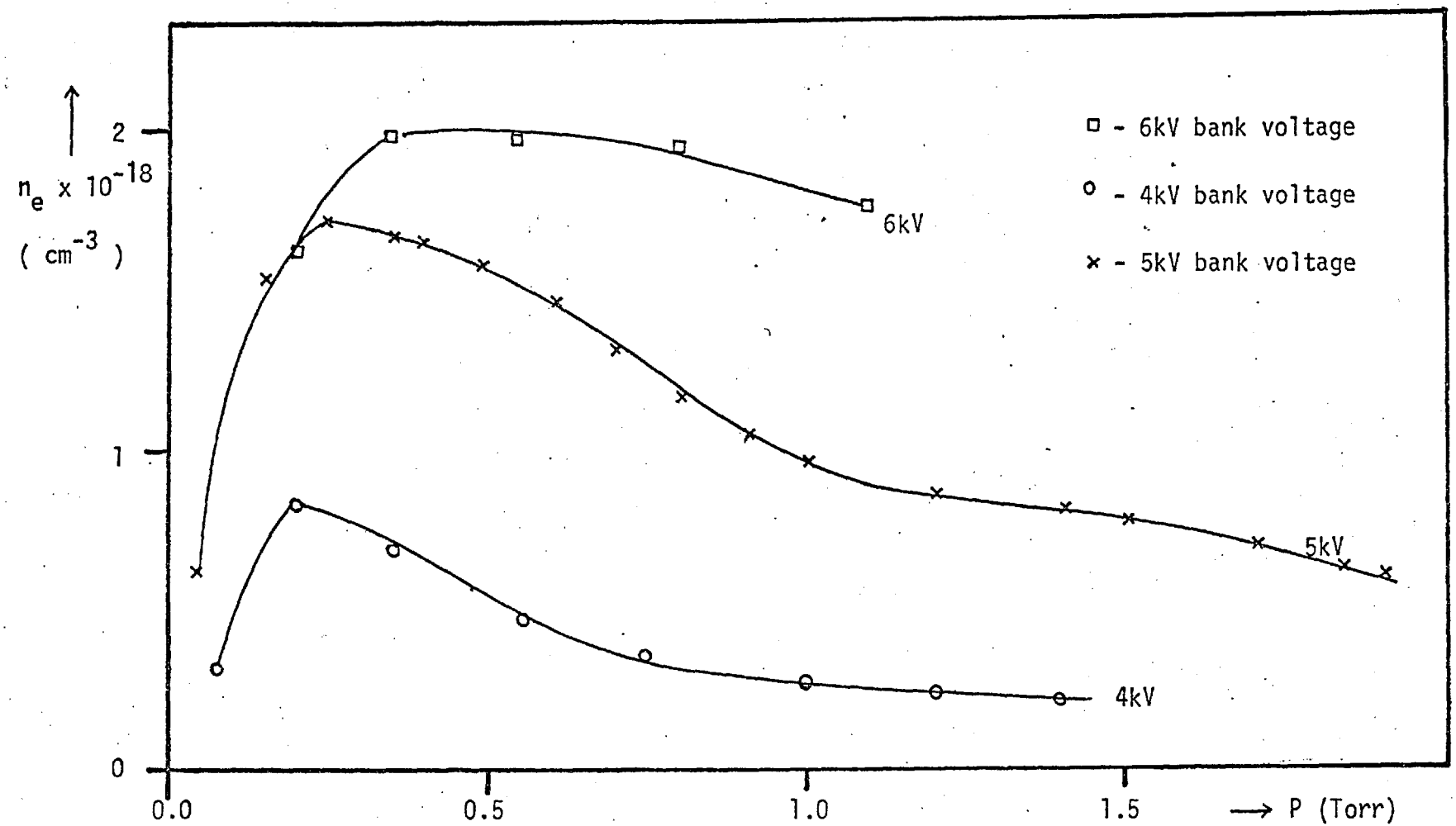

Fig 2.10 : Variation of electron density (from interferometric experiments) with filling pressure, P.

yields core densities up to two times higher than the values predicted by this method. Two such Abel inverted determinations of n_e, one from absorption measurements and the other from interferometry, will now be discussed.

2.8 Radial Variation of Electron Density from Continuum Absorption Studies

2.8.1 Method

The radial variation of the electron density was determined by measuring the radial variation of the continuum absorption at 6328 Å using a helium-neon laser background source. As suggested by the experiments described in Section 2.2, the continuum absorption of the plasma at 6328 Å might be expected to be appreciable even when observing sideways-on to the plasma. For example, using Eqn.2.1 below for the free-free absorption coefficient in this plasma, the optical depth of the plasma sideways-on is estimated to be of order $\tau \approx 0.13$, assuming the plasma diameter is of order 1 cm and $n_e \sim 2 \times 10^{18}$ cm^{-3}, as found from the half-width measurements discussed in Section 2.3.1. Therefore density determinations can be made by studying the radial variation of continuum absorption rather than the continuum emission intensity, thus avoiding the problem of determining relative values of the emission intensity for different off-axis positions. The apparatus is sketched in Fig.2.11.

2.8.2 Abel Inversion Procedure

The laser absorption was measured at different off-axis heights h. At a height h

$$I = I_0 \exp - \int_{-x_1}^{+x_1} a(r)\,dx$$

where a is the absorption coefficient

$$\ln\left(I_{o/I}\right) = \int_{-x_1}^{x_1} a(r)\,dx$$

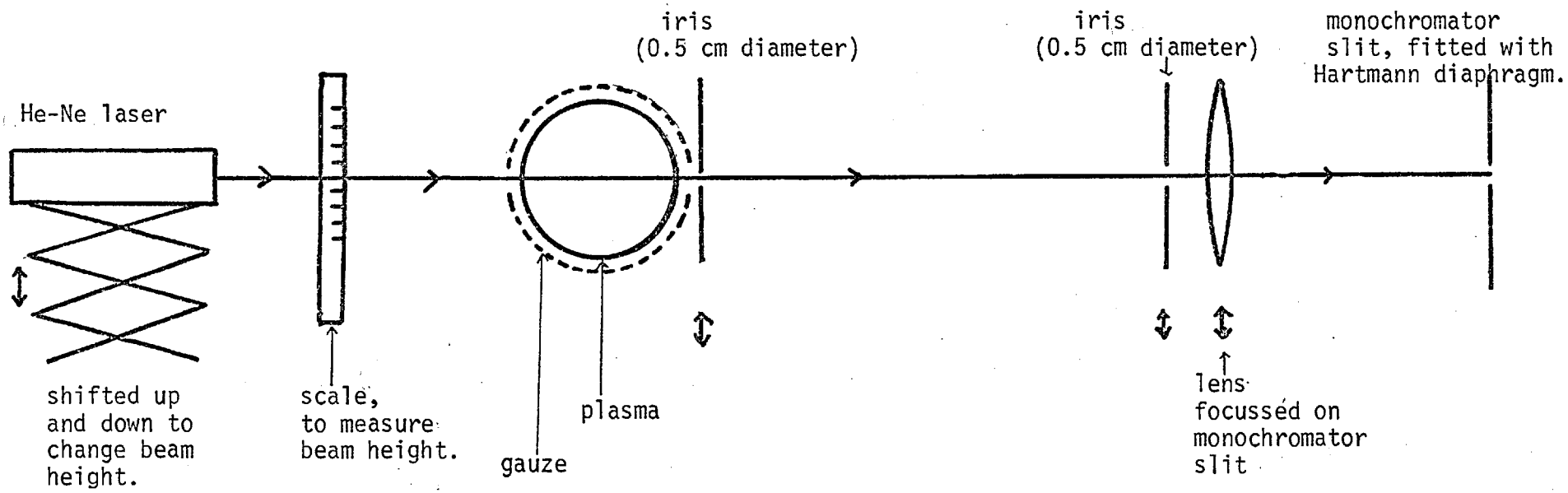

Fig 2.11 : Apparatus for measuring the radial variation of continuum absorption.

This expression can now be Abel inverted

$$F(y) = 2\int_0^{x_1} f(r)\, dx$$

$$F(h) = F(y) = 2\int_h^{r_o} \frac{r\, f(r)}{\sqrt{(r^2-h^2)}}\, dr$$

This expression Abel inverts to

$$f(r) = -\frac{1}{\pi}\int_r^{r_o} \frac{F'(y)}{\sqrt{(y^2-r^2)}}\, dy$$

So

$$\alpha(r) = -\frac{1}{\pi}\int_r^{r_o} \frac{\frac{d}{dy}(\ln I_o/I)}{\sqrt{(y^2-r^2)}}\, dy$$

The measured values of $\ln(I_o/I)$ were plotted as a function of y, and the smoothed data was Abel inverted by two methods.

The first method involved a straight numerical integration. The plasma was divided into 20 'onion skins', in each of which $\alpha(r)$ is constant.

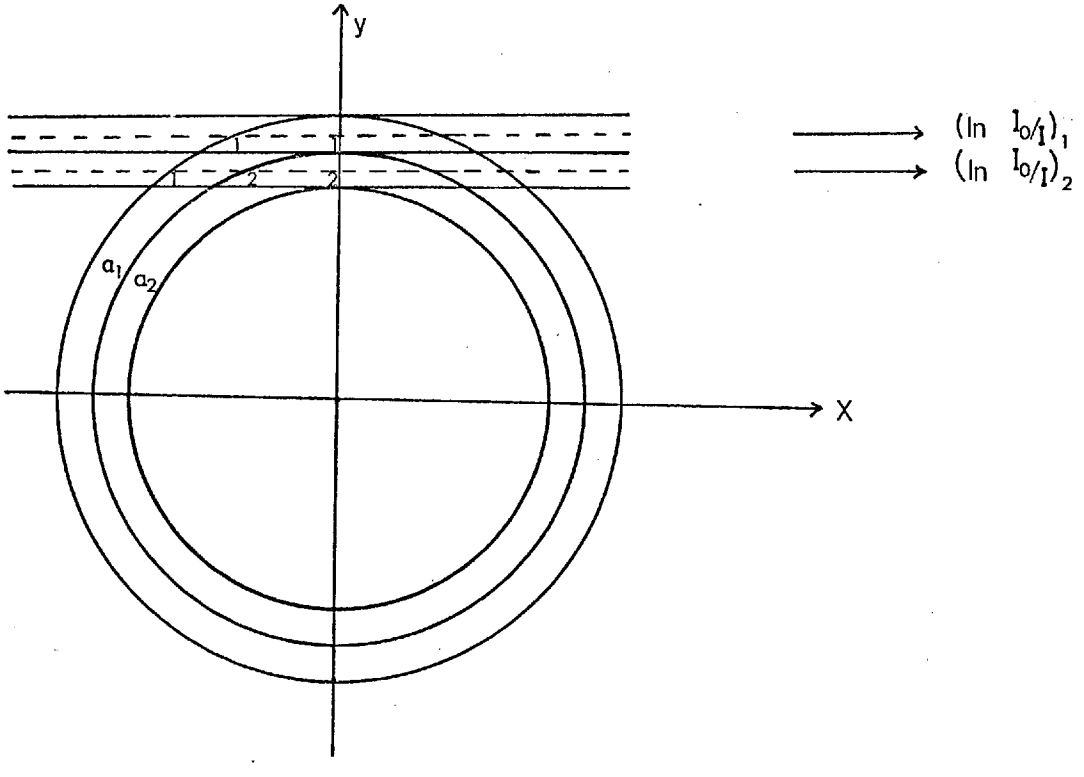

$$\ln\left(\frac{I_o}{I}\right)_1 = a_1 \times \text{chord length}_{11} \quad \sim \text{ gives } a_1$$

$$\ln\left(\frac{I_o}{I}\right)_2 = a_1 \times \text{chord length}_{12} + a_2 \times \text{chord length}_{22}$$

$$\sim \text{ gives } a_2$$

Thus the values of a_1, a_2, a_3 etc. are built up in a self-consistent way.

The second method involves fitting a polynomial to $\ln(I_o/I)$. Using a computer program written by Fielding (private communication), the measured values of $\ln(I_o/I)_j$ are multiplied by a matrix of coefficients to give a_j. The fitting coefficients are calculated by Bockasten (1961) by substituting a 3rd degree polynomial for the experimental curve.

The free-free absorption coefficient is related to the electron density by :-

$$a = \frac{4}{3}\left(\frac{2\pi}{3kT_e}\right)^{1/2} \frac{n_e n_z Z^2 e^6}{h c m^{3/2} \nu^3}$$

where Z is the charge on the ions in the plasma (Spitzer 1956). Assuming the plasma consists approximately equal concentrations of Ar II and Ar III at densities $n_e \sim 10^{18}$ cm^{-3} (Burgess 1965)

$$a = \frac{4}{3}\left(\frac{2\pi}{3kT_e}\right)^{1/2} \cdot \frac{2}{3} \frac{n_e^2 Z^2 e^6}{h c m^{3/2} \nu^3} \qquad (2.1)$$

Hence the values of a_j can be used to determine $(n_e)_j$.

2.8.3 Electron Density Measurements from Continuum Absorption

Fig.2.12 shows $(n_e)_j$ versus radius for a bank voltage of 5KV and a filling pressure of 0.5 Torr, one set of density values being

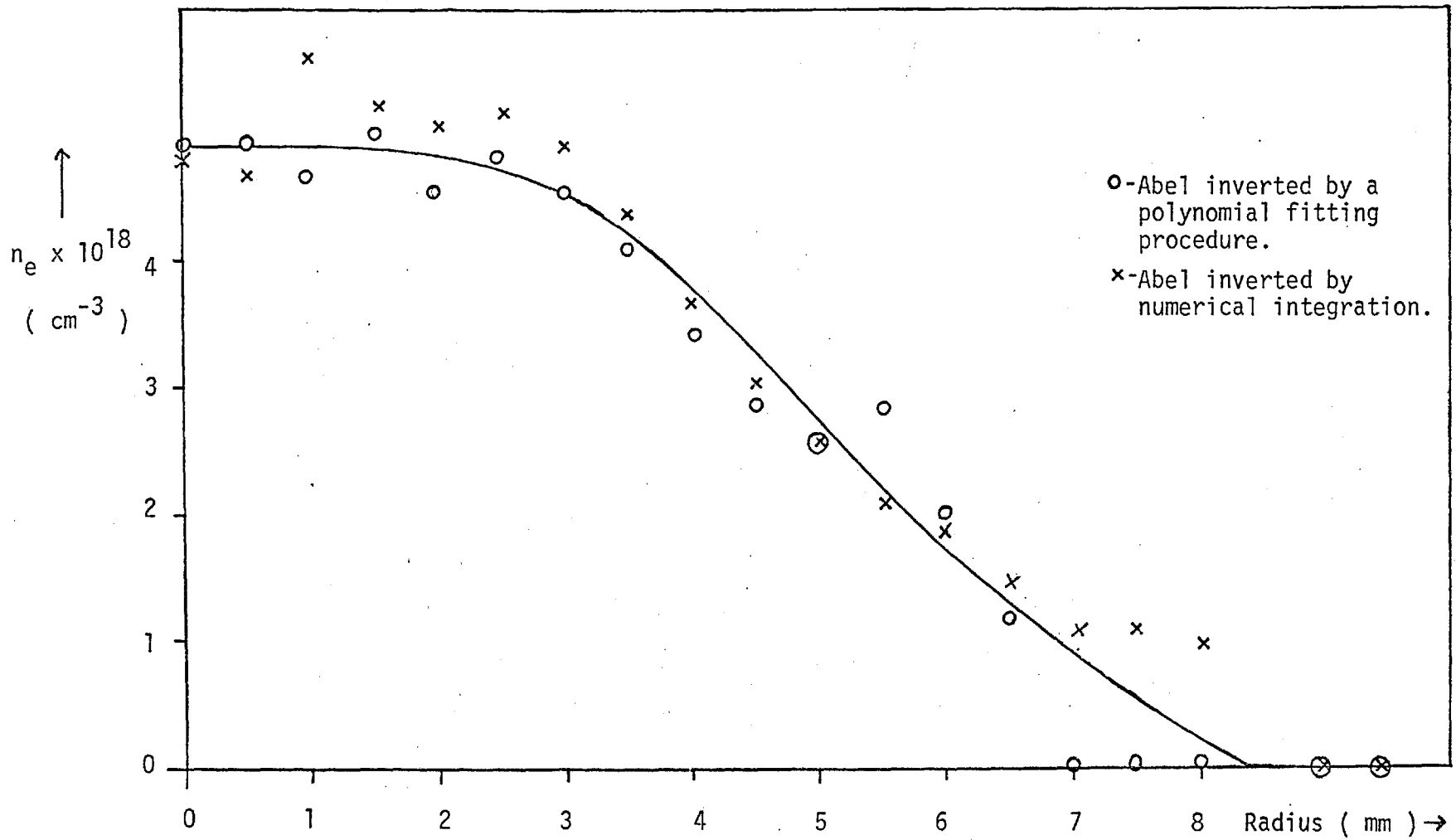

Fig 2.12 : Radial variation of electron density, n_e, calculated from continuum absorption

obtained by numerical integration and the other set by a computer polynomial-fitting procedure.

The chief source of error in these measurements is the poor shot-to-shot reproducibility of the absorption traces, which is particularly marked near the core of the plasma (typically $\pm$ 35%). This is probably due to shearing of the laser beam through less dense plasma regions (which would result in an overestimate of n_e). This assumption would be consistent with the findings of the end-on absorption experiment described in Section 2.4.2. Measurements of the absorption along the length of the plasma column (where shearing was negligible) gave a density estimate in excellent agreement with the other diagnostic experiments, as may be seen in Table 2.1. However, for the sideways-on absorption experiment, the uncertainty in the measurement of α gives rise to errors $\sim \pm$ 17.5% in n_e. In addition, the assumption that Ar II and Ar III ions are present in approximately equal concentrations (Eqn.2.1) might give rise to errors $\sim \pm$ 15% in the estimation of n_e.

Thus the density estimates obtained by this method are only accurate to $\sim \pm$ 33%.

More accurate fully spatially resolved density measurements are discussed below.

2.9 Radial Variation of Electron Density from Interferometric Measurements

2.9.1 Method

Fig.2.8 shows the Mach Zehnder interferometer used in these experiments. The laser beam was narrowed by pinholes so that the beam diameter was of order 1 mm. This should be compared with the diameter of the plasma column, which was typically 10 - 20 mm.

The number of fringe shifts up to peak compression was measured

as a function of off-axis height h. The smoothed data was then Abel-inverted by the polynomial-fitting program described in the previous Section 2.8. This program is given in Appendix 1.

2.9.2 Sensitivity of Abel-inversion Routine

The sensitivity of the Abel-inversion routine was tested by computing the radial distribution of fringe shifts which would be yielded by several hypothetical density distributions. Two Gaussian density distributions of equal area and with peak densities differing by a factor of two produce radial fringe shift distributions which differ by at least 2 fringe shifts (i.e. $\sim$ 50%) for all radial positions greater than 2mm from the core. Since the measured fringe counts are accurate to $\pm$ 1/2 fringe at these radii, such a difference would be easily measurable. Fig.2.13 shows the two hypothetical fringe shift distributions with their corresponding Abel inversions. Measurements taken at larger radii are particularly accurate, since the fringes are of large modulation; nearer the axis, problems of counting many fast fringes of small modulation become serious. However, this test indicates that the core density given by an Abel inversion procedure is heavily weighted in favour of the wings of the fringe distribution. Thus the accuracy of the estimate depends chiefly on the accuracy of the fringe-counting in the wings of the distribution. Since the fringe counts in the wings are accurate to $\pm$ 1/2 fringe, the effect of introducing a systematic error of 1/2 fringe into the fringe count measurements in the wing was investigated. In no case did this introduce an error of more than 25% into the core density, and it usually resulted in errors of only $\pm$ 20%.

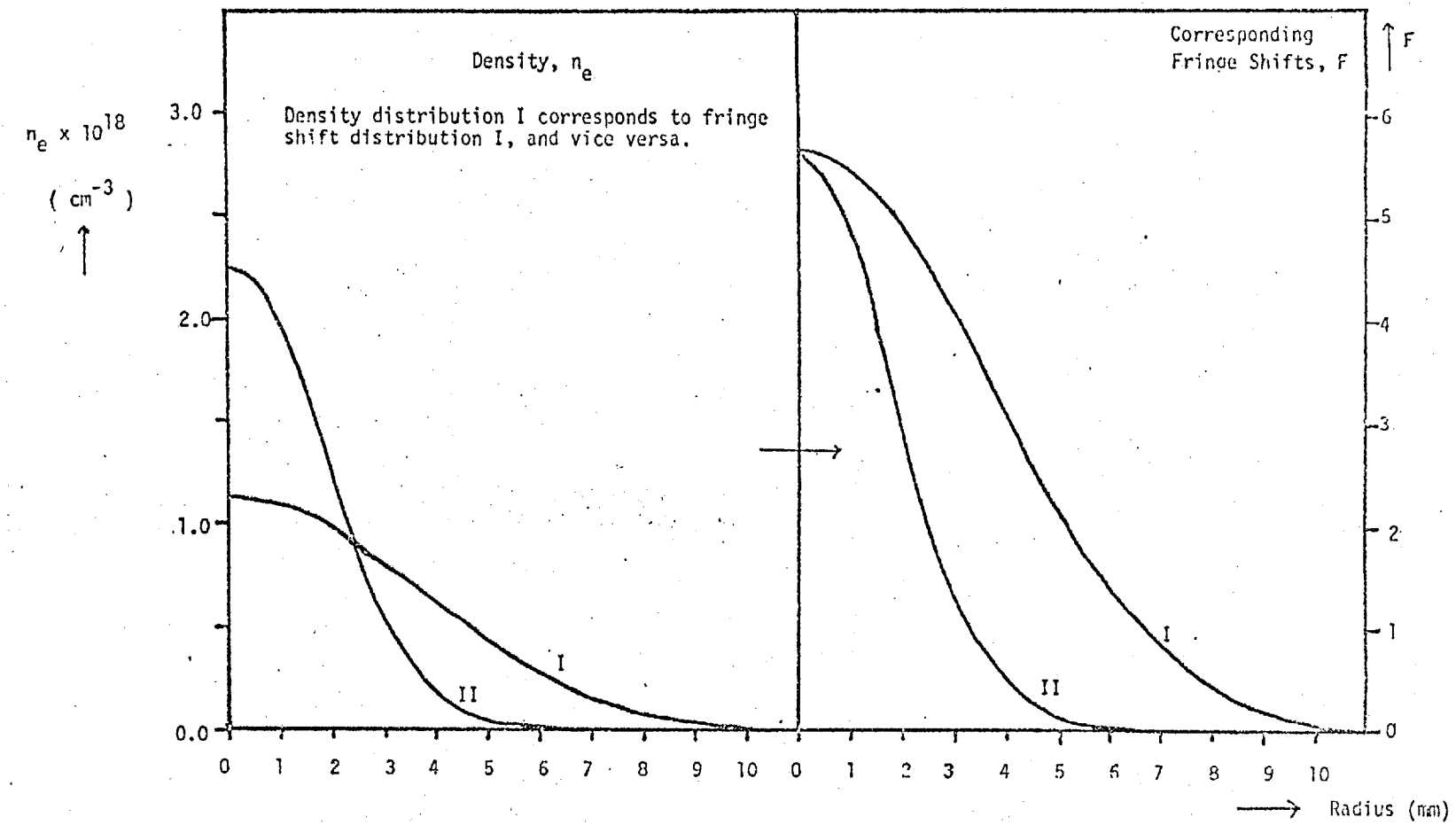

Fig 2.13 : A test of the sensitivity of the Abel inversion routine by computing the fringe shift distributions corresponding to two Gaussian density distributions of equal area but different peak intensity.

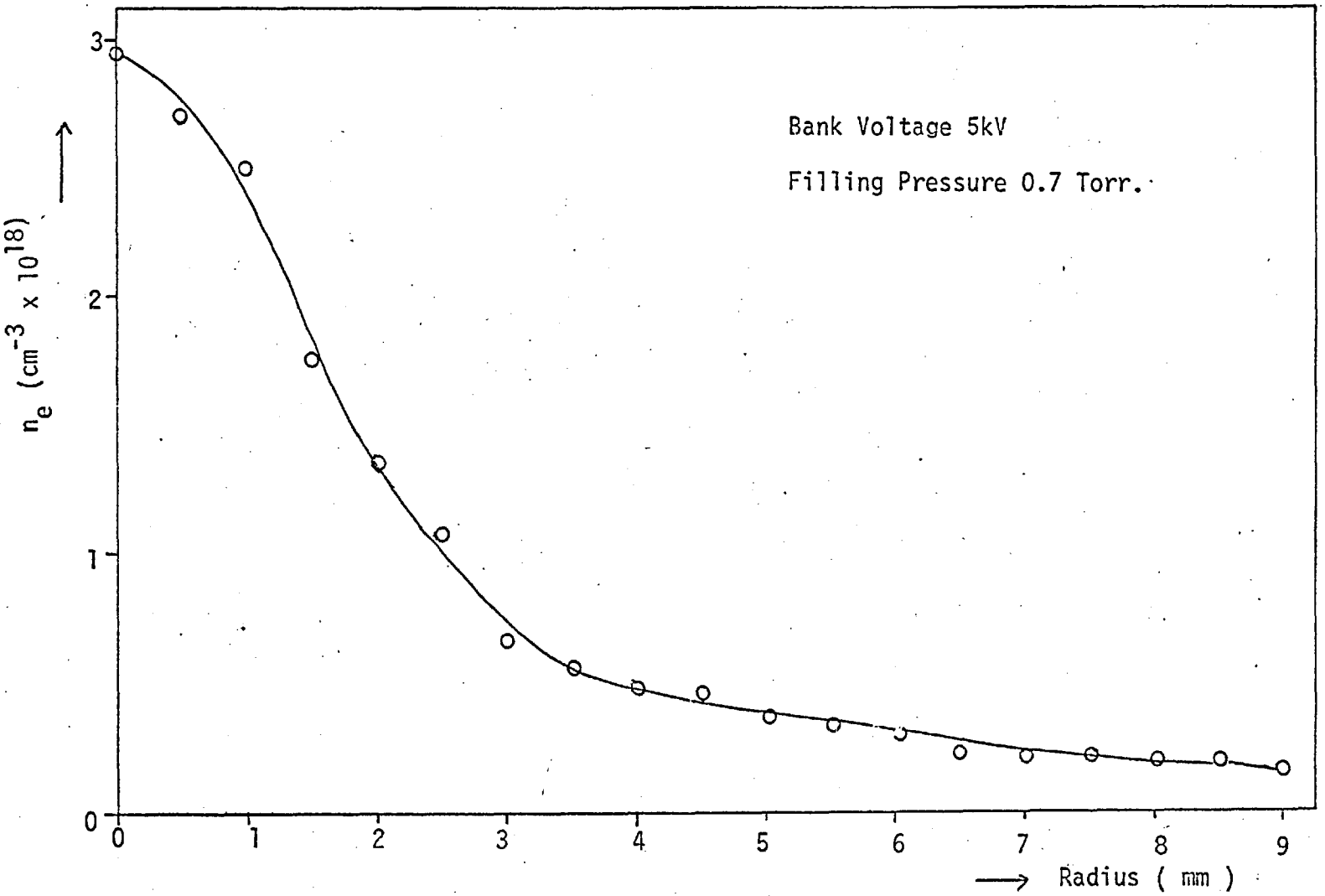

Fig 2.14 : Typical Radial Electron Density (n_e) Distribution.

2.9.3 Results

The radial density variation across the plasma column depends on the filling pressure in the pinch and the bank voltage. Fig.2.14 shows the radial variation of electron density for a typical filling pressure of 0.7 Torr and a bank voltage of 5KV. The radial variations of density for other filling pressures and bank voltages used are given in Appendix 2.

Fig.2.16 shows the variation of plasma size (defined arbitrarily as the radius at which $n_e = 10^{18}$ cm^{-3}) with filling pressure at bank voltages 5KV and 6KV. Fig.2.15 shows the variation of core electron density with filling pressure at bank voltages of 5KV and 6KV.

The results suggest that the electron density does not alter significantly with filling pressure except for very low filling pressures. As discussed above, because of the errors involved in fringe-counting, these values are expected to be accurate to $\pm$ 25%.

2.9.4 Density Estimates from Compression Ratio

A rough density estimate can also be obtained simply from the pinch diameter, and hence the compression ratio at a given filling pressure. The pinch diameter was estimated from the interferometric measurements of the radial variation of electron density described above (Section 2.9.3). It is interesting to compare this value with the core electron density measured directly from the interferometric technique. As can be seen in Fig.2.17, the comparison is very reasonable, suggesting trapping efficiencies of between 60% and 80%, a reasonable value from other investigations (e.g. Nation, I. 1960).

2.10 Conclusions

Diagnostic experiments were particularly difficult on this source because of the high electron density. Problems of optical opacity severely limited the range of useful measurements that could

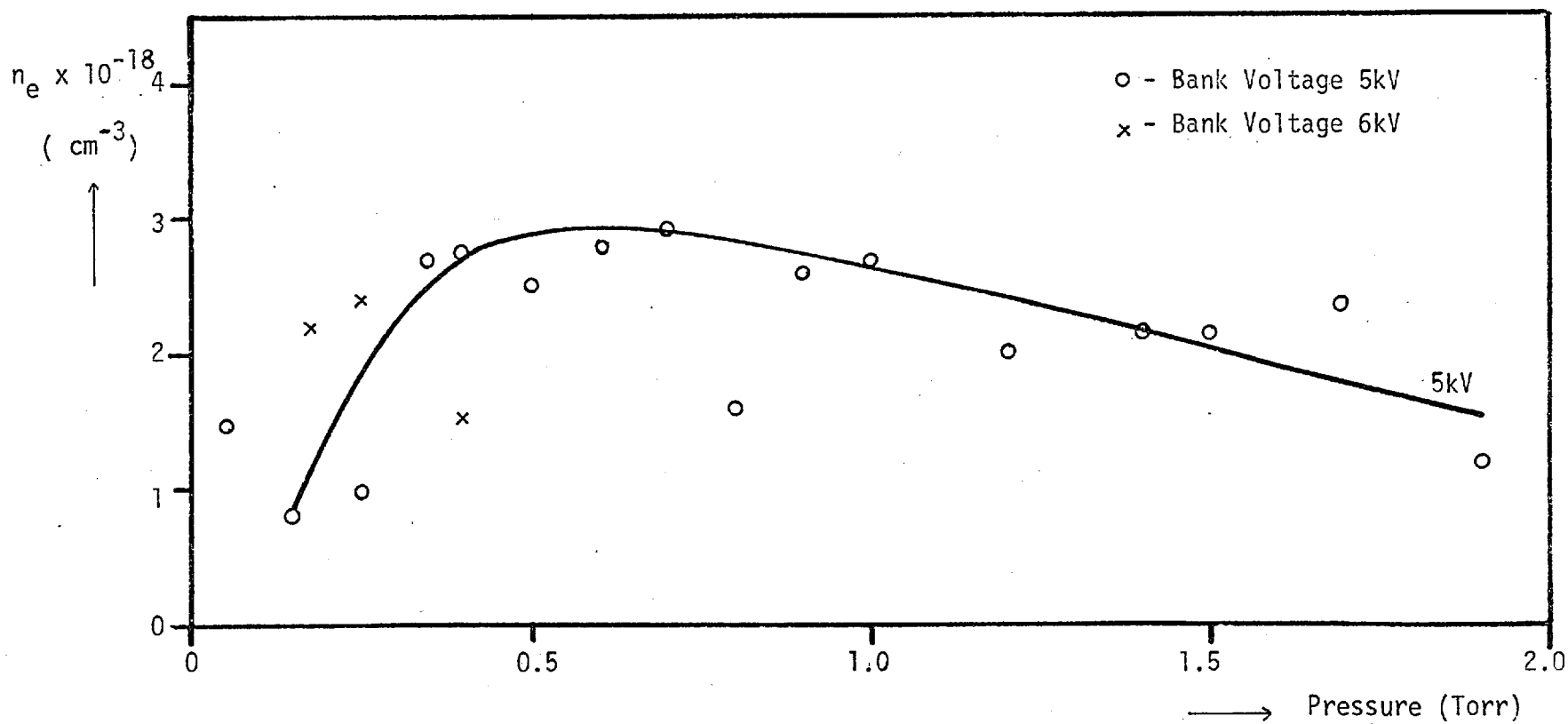

Fig 2.15 : Variation of electron density, n_e, with filling pressure.

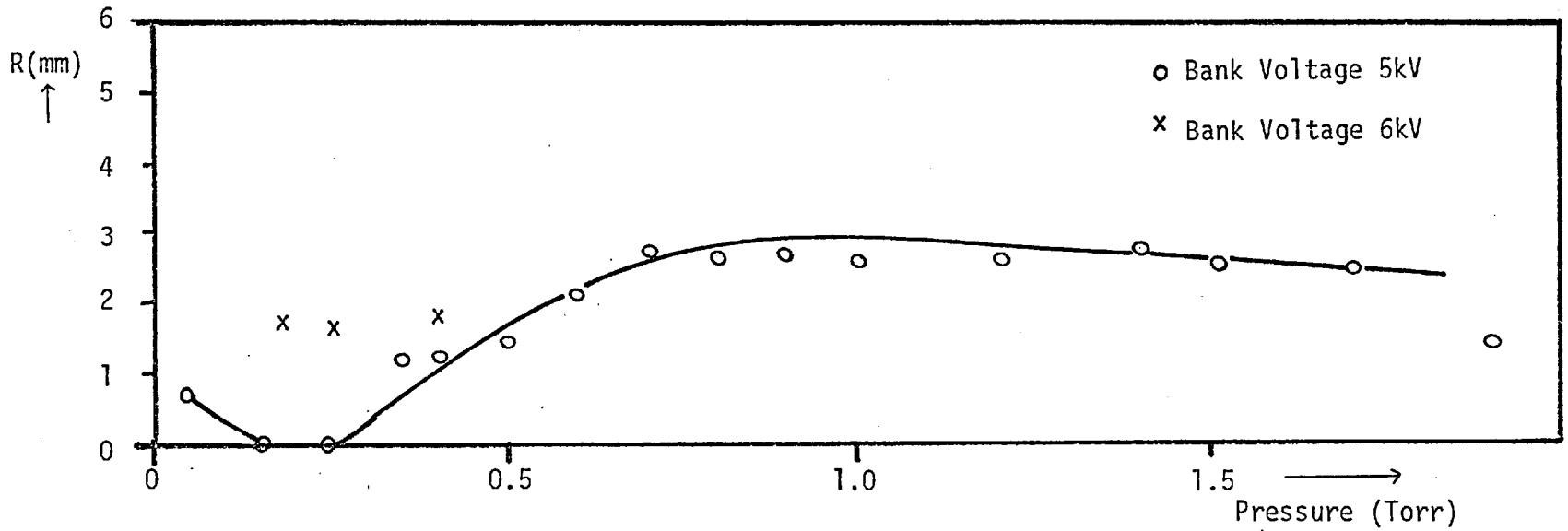

Fig 2.16 : Plasma radius, R, as a function of filling pressure.
R is arbitrarily chosen as the radius for which the electron density has fallen to $10^{18} cm^{-3}$.

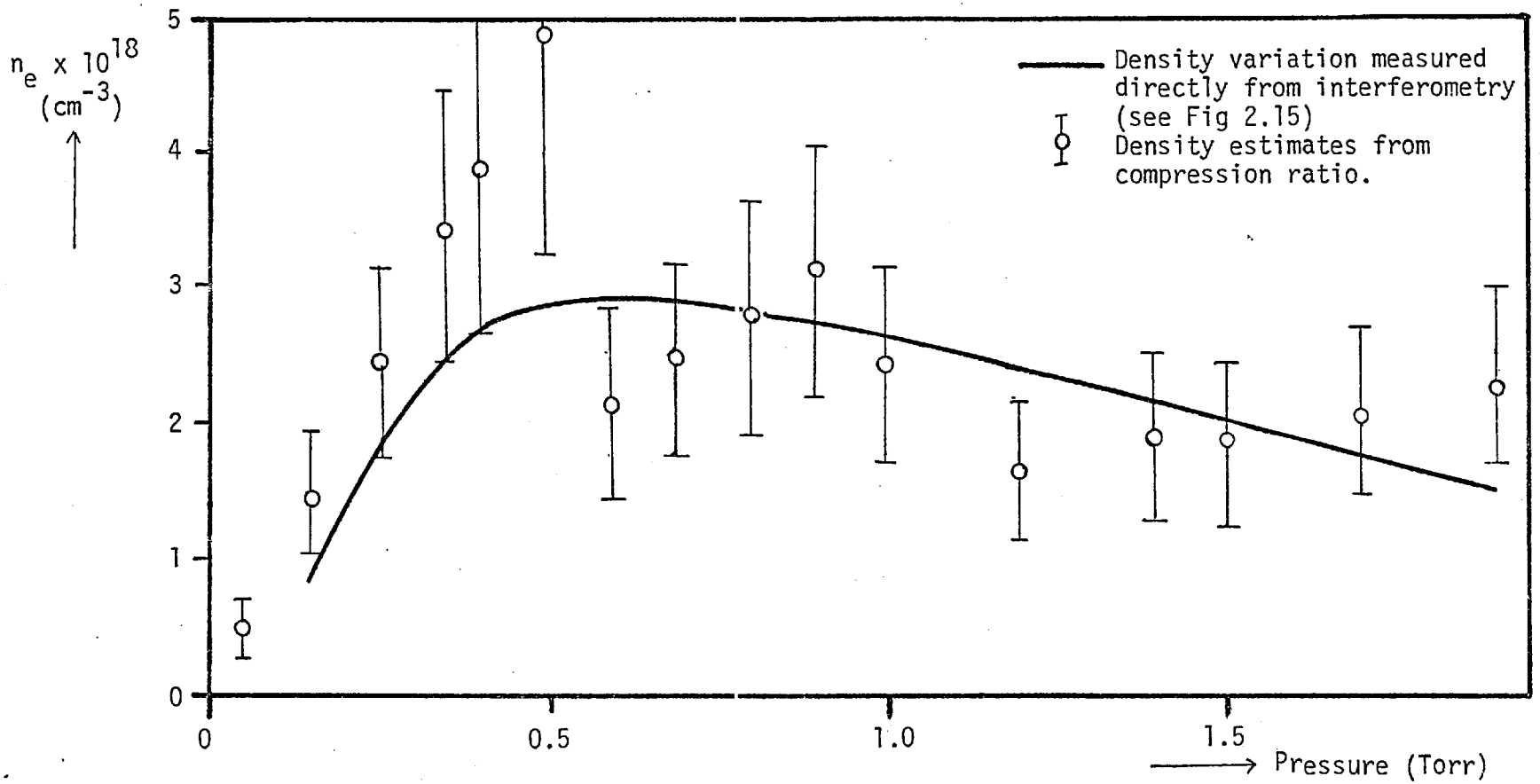

Fig 2.17 : Electron density, n_e, estimated from compression ratio, shown as a function of filling pressure.

be made end-on to the source. In addition, radial inhomogeneities impose further restriction on sideways-on observations.

The electron density has been determined by a number of independent methods, two of which are fully spatially resolved. The results of the density diagnostic experiments are summarised in Table 2.1. These results show a high degree of mutual consistency.

The spatially resolved interferometric density determinations are most accurate, and these results are in agreement with independently determined estimates from fully spatially resolved continuum absorption studies. In addition, the Ar II half-width studies and the preliminary interferometric studies discussed in Section 2.7, although less accurate, both yield density estimates which are in good agreement with the spatially resolved estimates. The remaining density estimates (from end-on continuum absorption and from the compression ratio) are essentially cross checks. Both yield density estimates which are consistent with the density diagnostic experiments discussed above.

Problems of radial inhomogeneity were less serious in the electron temperature determination. The electron temperature (determined by resonant absorption) was found to be $\sim$ 25,000K ($\pm$ 20%), the error arising from uncertainties in the electron density and plasma size. The temperature was dependent on the firing conditions, with temperatures from 22,000K to 27,000K being easily obtainable.

TABLE 2.1

A Summary of Experiments Used to Determine the Electron Density

Method	Discussed in Section	Electron Density for 5KV bank voltage, 0.5 Torr filling pressure	Maximum Density	Comments
Spatially Resolved Interferometry	2.9.3	2.8×10^{18} cm^{-3} ($\pm$20%)	3.0×10^{18} cm^{-3} ($\pm$25%)	Fully spatially resolved.
Ar II Mult 6 Half-Width Measurements, Sideways-on.	2.5	2.0×10^{18} cm^{-3} ($\pm$30%)	2.5×10^{18} cm^{-3}	Underestimate, due to radial inhomogeneities. Lower limit on density in the region of Ar II emitters.
Interferometry and Continuum Emission	2.7	1.6×10^{18} cm^{-3} ($\pm$30%)	1.7×10^{18} cm^{-3}	Underestimate due to radial inhomogeneities.
End-on Measurement of continuum absorption	2.4.2	2.3×10^{18} cm^{-3} ($\pm$30%)	—	Estimate.
Compression Ratio	2.9.4	$\sim 3.0 \times 10^{18}$ cm^{-3}	—	Overestimate, since it assumes 100% trapping. Error probably $< 40\%$.
Spatially Resolved continuum absorption	2.8	4.8×10^{18} cm^{-3} ($\pm$33%)	—	Overestimate, due to laser beam shearing. Fully spatially resolved.

CHAPTER III

The Plasma Polarization Shift

3.1 Introduction

In the model put forward by Griem and co-workers, Berg et al (1962), Greig et al (1970), the interaction of an ionized emitter with the plasma environment has been predicted to produce spectral line shifts, called plasma polarization shifts in the literature, additional to the usual shifts produced by mechanisms normally included in pressure broadening calculations. This interaction will produce, time-averaged, an excess of negative charge in the vicinity of the emitter. Some of this net charge is assumed to lie within the bound electron orbits of the emitter, and will thus distort the energy level structure of the emitter. This charge will shield the nuclear charge from the optical electron, and give rise to spectral line shifts.

This effect is not included in ordinary Stark broadening theories, since these theories make no inclusion of the shielding of the core charge from the optical electron by perturbing electrons.

3.2 The Importance of the Plasma Polarization Effect

As well as being of fundamental interest, the plasma polarization shift will be important in many practical situations. It might be expected to be the dominant effect for highly-ionized emitters and in dense plasmas, and as such it may represent the ultimate restriction on wavelength accuracies in laser-produced plasmas. For example, using the estimate of Greig et al (1970) (see Section 3.4.5 below) the predicted polarization shifts are between 1 Å and 3 Å for the O VI and K IX lines observed in a laser-generated plasma of electron density 7×10^{20} cm^{-3} and temperature 40 eV (Burgess, Fawcett and Peacock 1967). (Burgess et al (1967) found that these predicted shifts were too large by at least an order of magnitude in this case. The reasons for this discrepancy are discussed in Section 3.4.6 below).

Moreover, the polarization shift is likely to be of fundamental importance to the diagnostics of laser-compressed plasmas, and could even affect opacities in stellar interiors.

3.3 Limitations of Previous Work on the Plasma Polarization Shift

3.3.1 Experimental

Some of the previous measurements of plasma polarization shifts are summarised in Table 3.0 below. The experiments are discussed in greater detail in Section 3.4 below. Most of the experiments have been concerned with the resonance lines of He II, and in particular with He II 304 Å.

For many non-resonance lines, the energy level shifts due to the plasma polarization effect are comparable for the upper and lower levels of the transition. When the shifts of the upper and lower levels partially cancel one another, the resulting wavelength shift is frequently negligibly small.

For many of the U.V. lines studied, uncertainties in wavelength standards are likely to prejudice the validity of shift measurements.

In addition, problems of optical opacity are often important for resonance lines, and care should be taken in the interpretation of "flat-topped" or self-reversed profiles. For such profiles shift measurements are based on line wing measurements and symmetry arguments. However care should be exercised in applying such arguments, since many different effects can give rise to asymmetries in line wings (see Chapter VI), which might be erroneously interpreted as shifts in the case of "flat-topped" lines.

3.3.2 Theory

The existing theoretical estimates are discussed in detail in Section 3.4 below. The plasma polarization effect is a complex effect which is very difficult to treat rigorously, since it is essentially an

TABLE 3.0

Experimental Studies of Plasma Polarization Shifts

Experiment	Lines	Shift	Agreement with theory	Comments
Day & Griem 1965	Visible N II lines	$0 \pm .15$Å	Griem 1966	
Berg 1966	Visible He II 4686 Å	0	Griem 1966	Revision of Berg 1962 measurement
Burgess & Cooper 1965	Visible Ar II lines	0	Griem 1966	Shift to width measurements
Burgess, Fawcett & Peacock 1967	O VI K IV C VI	0.2 Å	Burgess & Peacock 1971	Greig 1970 estimate too big by a factor of 10.
Chowdhury 1969	Ar II 4806 Å shift to width d/w measure-ment	$d/w \sim .1 \pm 10\%$	Griem 1966 in magnitude. Berg 1962 in temperature dependence	
Greig, Griem, Jones & Oda. 1970	Resonance Line of He II 304 Å	~ 0.05Å $\pm 20\%$	Semiclassical theory out-lined in same paper (Greig 1970)	"Flat-Topped"
Gabriel & Volonte. 1973	First 4 He II u.v. Resonance lines	~ 0.10Å $\pm 10\%$	None. Burgess & Peacock 1971 & Griem 1974 are of right order.	Self-reversed lines.
Goto and Burgess. 1974	First Eight He II u.v. Resonance lines	0.03Å	Burgess and Peacock 1971.	
Griem and Neiger. 1976.	He II u.v. Resonance lines 304 Å 256Å) 243Å)	$\sim .07 \pm .05$Å $\sim .03$Å	Greig 1970 Griem 1973	Optically thick lines. Measurements disagree with Goto and Burgess 1974, and Gabriel and Volonte 1973 by a factor of 2.

n-body problem. Thus both the semiclassical and quantum mechanical treatments of the effect are of a very approximate nature.

More specific criticisms of the existing theories are discussed below in Sections 3.4.9, 3.5 and 3.4.6.

In view of these shortcomings it would be wrong to attach too much weight to the existing theoretical estimates of the effect, although in the absence of any more rigorous theories they must form the starting point for any discussion.

3.4 Historical Background

3.4.1 The Berg (1962) Experiment

The plasma polarization shift was first suggested in 1962 by Berg et al as the reason for an unexplained shift measured for one of the He II lines studied by the authors. He II 4686 was apparently shifted by ~ 1 Å to the blue under conditions where its full-half width was near 4 Å ($n_e \sim 10^{17}$ cm^{-3}). Berg et al (1962) treated the effect as follows. The time-averaged charge density at a distance r from the emitting ion in the Zth ionization stage was estimated from the thermal equilibrium relation.

$$\rho(r) = eN\left\{\exp\left[-\frac{(Z-1)\,e^2}{kT\quad r}\right] - \exp\left[+\frac{(Z-1)\,e^2}{kT\quad r}\right]\right\}$$

Assuming all perturbing ions to be singly charged, and expanding the exponentials

$$\rho(r) \approx -2(Z-1)\frac{Ne^2}{rkT}\left[1 + \frac{(Z-1)^2}{6}\left(\frac{e^2}{rkT}\right)^2 + \ldots\ldots\right]$$

The correction item $\frac{(Z-1)^2}{6}\left\{\frac{e^2}{rkT}\right\}^2$ in the expression of the exponential was assumed to be negligible. Thus the shielding charge within a distance r from the nucleus was taken as :-

$$e\,\Delta Z = \int_0^r 4\pi r^2 \rho \, dr$$

$$\approx -4\pi (Z-1) N \frac{e^2 r}{kT} \qquad (1)$$

This entirely classical result was used to estimate the shift of hydrogenic energy levels from

$$\Delta E_n = \Delta\left(-Z^2 \frac{E_H}{m^2}\right) \approx -2Z \cdot \Delta Z \frac{E_H}{n^2} \qquad (2)$$

where $E_H = \frac{e^2}{2a_o}$ is the ionization energy of hydrogen. With (1) and (2) and the Bohr radius $r = \frac{n^2 a_o}{2}$ the level shifts predicted by this quasi-classical estimate finally were

$$\Delta E_n = 16\pi \cdot E_H \left(\frac{E_H}{kT}\right) a_o^3 N n^3 \frac{(Z-1)}{Z} \qquad (3)$$

This predicted a blue shift which was in fair agreement with the measured shifts of 4686 Å found by these authors.

3.4.2 Further experiments for singly-ionised emitters

The years immediately following the publication saw several experiments attempting to detect similar shifts for other singly ionised emitters. Day and Griem (1965) studied the widths and shifts of some lines of singly ionised nitrogen in a T-tube plasma; and Burgess and Cooper (1965) investigated Ar II lines in a z-pinch discharge in argon. In neither of these experiments was there found any evidence for the polarization shifts predicted by the estimate of Berg (1962).

Subsequently Berg (1966) reported a revised measurement for the shift of He II 4686 Å. With improved spectral resolution and reduced

plasma impurities, this measurement failed to reproduce the earlier results for 4686 Å. Instead two Si III lines were found in the blue wing of He II 4686 at 4683.018 Å and 4683.774 Å, which would not have been resolved in the previous experiment and could have simulated the blue shift measured for He II 4686 Å.

3.4.3 The Griem (1966) Quantum Mechanical Estimate

In 1966 Griem proposed a new theoretical treatment of the effect which predicted shifts up to an order of magnitude smaller than the Berg (1962) estimate, consistent with the null results found experimentally by Day and Griem (1965), Burgess and Cooper (1965) and Berg (1966). In this new treatment the perturbing electron is considered to be bound in highly excited states, so that the states of interest are those of the doubly excited ion or atom preceding the emitting ion in the ionization sequence. Using the Saha equation to find the relative probability of having a doubly excited state, the perturbing charge density is derived. This treatment predicts energy level shifts of the form :-

$$E_n = + \frac{8}{3} \sqrt{2\pi} \; E_H \; \left(\frac{E_H}{kT}\right)^{3/2} \; a_o^{\,3} \; N_e \; Z\left(\frac{Z-1}{Z}\right)^{3/2} n \qquad (4)$$

This yields shifts which are considerably smaller than those predicted by Berg's semiclassical estimate (3).

3.4.4 The Chowdhury (1969) Experiment

In 1969 Chowdhury reported an experiment on the shift to width ratio of Ar II 4806 Å which was in good agreement with the Griem (1966) estimate (4). The measured temperature dependence of the shift to width ratio could be fitted to the T_e^{-1} variation which would be in agreement with the temperature dependence predicted by the Berg (1962) estimate (Eqn.3) for the plasma polarization shift.

3.4.5 The Greig (1970) Experiment and Semiclassical Estimate

In 1970 Greig et al reported a new experiment on He II 304 Å, which showed a blue shift in agreement with a new semiclassical theory of the effect presented by the authors in the same paper. He II 304 Å was studied in a T-tube plasma of $n_e \sim 3 \times 10^{17}$ cm^{-3}, $T \sim 4$ eV, and was found to be blue-shifted by ~ 0.05 Å. Like the early Berg estimate (Eqn.3), the semiclassical treatment proposed by Greig et al for resonance lines was based on the use of a Boltzmann factor to determine the perturber charge distribution

$$N(r) = N \exp\left(\frac{e^2}{rkT}\right) \tag{6}$$

where N is the electron density averaged over the whole plasma volume.

However, quantum mechanical effects were allowed for in the perturber distribution. When $r \approx a_o$ the quantum mechanical perturber charge distribution would be considerably smoothed out and Greig et al suggested that Eqn.(6) should be replaced by

$$N(r) \approx N \exp\left(\frac{E}{kT}\right)$$

where E is close to the ionization potential of neutral helium. Hence the time-averaged perturber charge density within the nth Bohr orbit of the ion is estimated to be

$$\Delta Z = -N \exp\left(\frac{E}{kT}\right) \cdot \frac{4\pi}{3}\left(\frac{n^2 a_o}{Z}\right)^3$$

Using $E_n = \frac{Z^2}{n^2} E_H$ for the energy levels of the radiator the energy level shifts predicted are thus

$$\Delta E_n = \frac{8\pi}{3} n^4 \frac{N_e}{Z^2} E_H a_o^3 \exp\left(\frac{X_{Z-1}}{kT}\right) \tag{7}$$

where X_{Z-1} is the ionization potential of the preceding ion in the

ionization sequence.

3.4.6 Criticism of the Greig (1970) Estimate by Burgess and Peacock (1971).

In the high density laser-produced plasma studied by Burgess et al (1967), O VI lines and the C VI Lyman series remained unshifted to within $\pm$ 0.05 Å, whereas the formula of Greig et al (Eqn.7) predicted large shifts of a few angstroms. Burgess and Peacock (1971) criticised the use of the Boltzmann factor in the Greig (1970) estimate. They pointed out that in the vicinity of an emitting ion there cannot be thermal equilibrium in the distribution of perturber velocities, since the perturber velocities will be directly related to their potential energies. They suggested that only at distances of order, or greater than, r_o, the interparticle distance, would collisions randomise the perturber velocities, and justify the use of the exponent in the Boltzmann factor of the Greig et al (1970) treatment. Burgess and Peacock therefore proposed that the Greig (1970) estimate be modified by replacing X_{Z-1} with $\frac{(Z-1)e^2}{r_o}$ giving shifts :-

$$\Delta E_n = \frac{8\pi}{3} n^4 \frac{N_e}{Z^2} E_H a_o^3 \exp\left\{\frac{(Z-1)e^2}{r_o kT}\right\} \qquad (8)$$

The resulting shifts are then typically a few orders of magnitude smaller than those estimated by Greig (1970), depending on the ionization stage concerned.

3.4.7 The Experiment of Gabriel and Volonté (1973)

Photographic studies of the first four resonance lines of He II at 10^{18} cm^{-3} were reported by Gabriel and Volonté (1973a). All the lines studied were unfortunately strongly self-reversed. However, by considering the wings of the lines, shifts were obtained for Ly_α, Ly_β, Ly_γ, Ly_δ, which suggested that in particular Ly_γ and Ly_δ were shifted by a measurable amount, which was not in quantitative

agreement with either the Greig (1970) or the Burgess and Peacock (1971) estimates. They found satisfactory agreement with the $n^2(n^2 + 1)$ scaling of the wavelength shift predicted for resonance lines by both estimates. The discrepancy between their results and the shifts predicted by Burgess and Peacock suggested that while the correction was justified on physical grounds, yet it underestimated the shifts measured because of the choice of r_o as the cutoff factor.

3.4.8 The Griem (1973) Semiclassical Estimate

Griem (see Gabriel and Volonté, 1973b) suggested that the semiclassical formula be revised, using a mean value $r \approx \frac{1}{2} \frac{n^2}{Z} a_o$ for the radius at which the Boltzmann factor is cut off. This predicts shifts of the form

$$\Delta E_n = \frac{8\pi}{3} n^4 \frac{N_e}{Z^2} E_H a_o^3 \exp\left\{\frac{4Z(Z-1) E_H}{n^2 kT_e}\right\} \qquad (9)$$

This modification introduces a further n-dependence into the shifts.

3.4.9 The Griem (1974) Quantum Mechanical Estimate

At this time Griem (1974) also proposed a fully quantum mechanical treatment of the effect. Using continuum wavefunctions of the one electron system for the case of strong Coulomb interactions, this estimate gives energy shifts of the form :-

$$\Delta E_n = \frac{(4\pi)^2}{3} \frac{(Z-1)}{Z^2} n^4 E_H \left\{\frac{4E_H}{kT}\right\}^{1/2} \cdot a_o^3 N_e \qquad (10)$$

Gabriel and Volonté (1973b) presented a full comparison of their results (first reported in Gabriel and Volonté 1973a) with the new theoretical estimates available. Their results showed little evidence to support the further n-dependence introduced by the Griem (1973) semiclassical estimate (Eqn.9). This estimate seriously overestimated shifts for low n and underestimated the shifts for Ly_δ . The

agreement with the measured shift for Ly_γ would therefore appear to be purely fortuitous. Their agreement with the quantum mechanical estimate of Griem (1974) (Eqn.10) was fair. Although the estimate tended to consistently overestimate the shifts by a factor of about 1.4, such a discrepancy is hardly surprising in view of the approximate nature of the theory.

3.4.10 Inclusion of a "Back Reaction", as suggested by Gabriel and Volonté (1973)

Gabriel and Volonté (1973b) also pointed out a close similarity between the polarization shift effect and the theory of dielectronic satellites (Gabriel and Jordan, 1969), since both effects involve the shift of a line under the influence of an additional perturber. They suggested that the theories of the polarization shift should include a "back reaction" of the kind considered in dielectronic satellite theory. All the current theories of the polarization shift derive a shift that is entirely due to the screening of the nucleus-bound electron interaction by the perturber, assuming the perturber state is independent of the state of the radiating electron. This assumption is not entirely valid, since when the bound electron undergoes a transition, this might be expected to produce a change of the perturber state which leads to a further component of the shift. For dielectronic satellites, while screening produces a blue shift, the inclusion of a back reaction of this kind produces red shifts, at least for the lower satellites. This suggests that allowing for the back reaction in polarization shift theory will produce a red-shifting effect, as well as the blue-shifting effect produced by screening.

In particular the authors pointed out that if the additional perturbing electron is considered as bound in a high orbital, as in the early quantum mechanical treatment by Griem (1966) (Eqn.4), the shift effect corresponds to the emission of high dielectronic satellites

and is, in general, negligible. Under most conditions only free perturbers are expected to produce measurable polarization shifts.

3.4.11 The Goto and Burgess (1974) Experiment

Goto and Burgess (1974) studied eight members of the helium resonance series from n = 2 to n = 9 photographically at an electron density 10^{17} cm^{-3}. Their experiment confirmed that the Greig (1970) estimate (Eqn.7) grossly overestimated the magnitude of the shifts expected. The quantum mechanical treatment of Griem (1974) (Eqn.10) predicted shifts too small to be detected for the lines up to $n \approx 4$, consistent with the findings of this experiment but for higher members the theory overestimated shifts by about an order of magnitude. Their results were in agreement with the semiclassical estimates of Burgess and Peacock (1971) (Eqn.8) and Griem (1973) (Eqn.9) and did not permit any choice to be drawn between the two estimates, although they pointed out that because of the additional n-dependence, Griem (1973) (Eqn.9) predicted an unrealistically large shift for Ly_α, which would have been easily detected if present.

3.4.12 The Volonté (1975) Treatment

In 1975, Volonté presented an improved version of Griem's (1974) quantum mechanical treatment, which led to a smaller estimate of the shielding charge. The shifts predicted were reduced by one order of magnitude, leading to good agreement with the semiclassical approach of Greig (1970) as corrected by Burgess and Peacock (1971). The agreement with experimental data for the He II lines is good at lower densities ($\sim 10^{17}$ cm^{-3}) while at higher densities ($\sim 10^{18}$ cm^{-3}) large discrepancies were still found.

Although this treatment goes some way towards bridging the gap between the quantum mechanical and semiclassical approaches to the problem, the agreement between current theories is still far from satisfactory.

3.5 Some Comments on the Time-Averaging Assumptions on which Polarization Shift Estimates are based.

As pointed out by Burgess (1964), existing theories of the polarization shift are based on questionable time-averaging assumptions. All the theoretical estimates mentioned above begin by estimating the correction to the nuclear charge due to shielding, Δq, seen by the optical electron. This is typically some small fraction ($\sim 10^{-4}$) of an electronic charge. It is then argued that this charge lies within the bound orbits of the emitter for all time, distorting the energy level structure.

It could be argued that this assumption is incorrect, and that a correct (classical) interpretation is that either no electron penetrates the core, or at least one does. This then constitutes a 'strong collision', and it will completely disrupt the emitter. It would in this case be completely wrong to interpret this collision in terms of emitter energy level shifts, as above.

3.6 Summary

It is important to remember that all the theoretical approaches to the problem are very crude, since this is essentially a very difficult calculation to carry through in detail. Moreover, agreement between experimental results and theory, and indeed between the experiments themselves is still very poor.

All the measured shifts have been relatively small, and justification for the theories has been based on the agreement of small predicted and measured shifts, where the experimental errors and other sources of uncertainty might be expected to be serious. Little work has been done experimentally on ions of higher Z. No attempts have yet been been made to study the Z-dependence of the effect for a given ion. Although many of the theories predict large shifts for ions of higher Z,

the production of dielectronic satellites might be expected to become more important than the polarization shift for highly ionized emitters, when the probability of finding the extra electron in a bound orbit is greater. Apart from the work of Chowdhury (1969) little has been done to investigate the strong temperature dependence of the polarization shift as predicted by current theoretical estimates.

3.7 This Experiment

The varying temperature dependence of several of the shift estimates is illustrated in Figure 4.4 for the Ar II U.V. resonance lines. The wavelength shift to density ratio is plotted as a function of electron temperature, for the range of electron temperatures available in this source.

The following chapters describe measurements of the polarization shift for the resonance lines of a number of different ion stages. Ions of Z = 1, 2, 3 and 4 have been investigated. Because of the $n_e \exp\left(\frac{\text{Constant}}{T}\right)$ dependence of the polarization shift, the shifts predicted for emitters under the special ultradense, low temperature conditions of this source are strikingly large.

The shifts predicted for the emitters studied are given in detail in Tables 3.1 to 3.6. These values are determined for an electron density 2×10^{18} cm^{-3}, which, as discussed in Chapter II, is the lower limit of the density at peak compression, and hence the shifts presented are also lower limits of the predicted shifts. The shifts are calculated by using estimated effective principal quantum numbers for the levels concerned and finding the energy shift for the upper and lower levels. In many cases the predicted shifts even exceed the unshifted wavelengths of the lines concerned.

The ordinary Stark shifts, calculated by using effective Gaunt factors and semiempirical estimates as discussed in Appendix 3, are

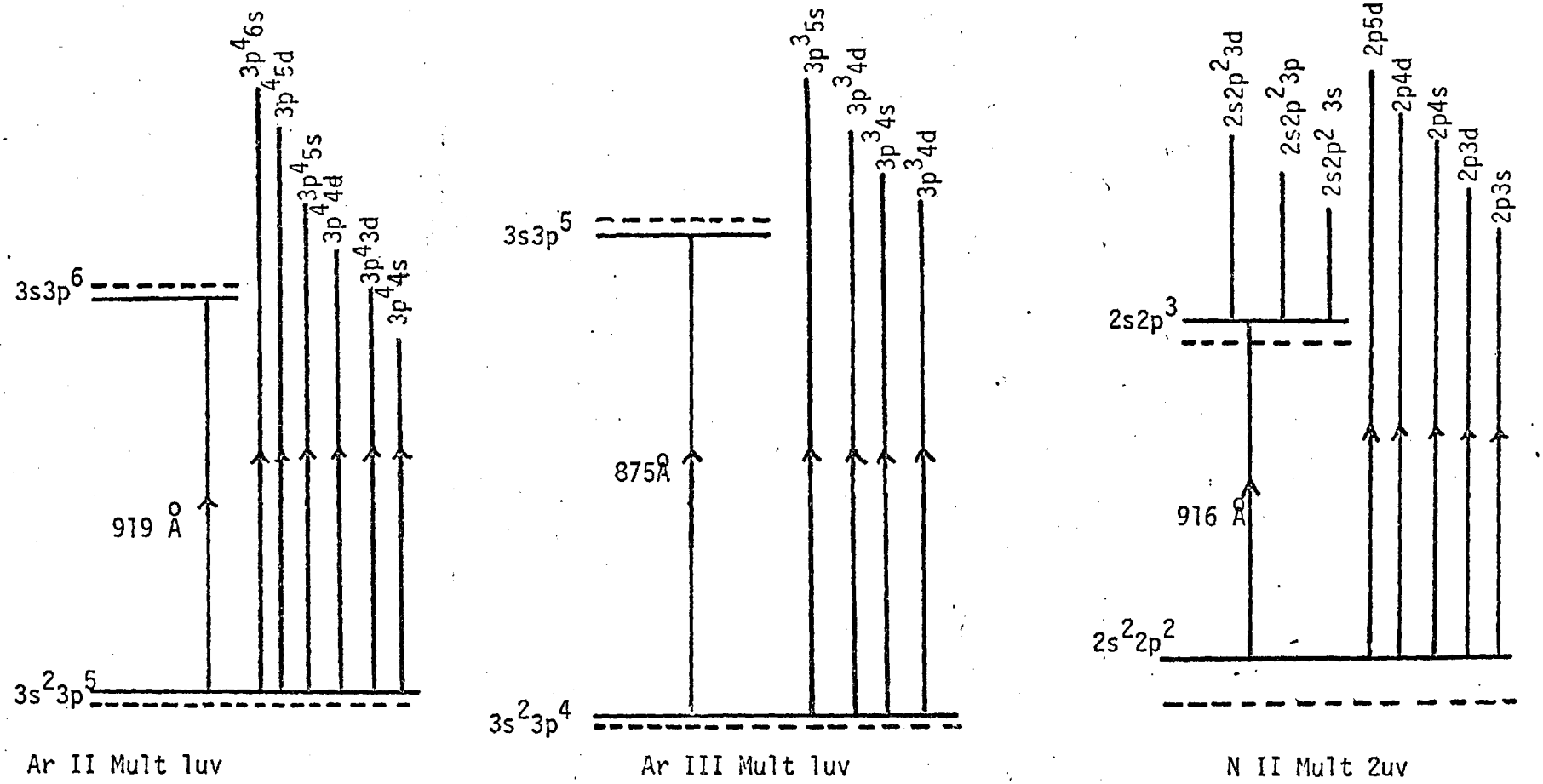

Fig 3.1 : Schematic of Stark shifts for ArII Multluv, ArIII Mult 1uv, NII Mult 2uv.

----- Field

——— No field

given in the same tables for purposes of comparison. The shifts are all less than 0.013 Å, and are not expected to be in error by more than $\pm$ 50%, as discussed in Appendix 3. Thus the ordinary Stark shifts are generally much smaller than the predicted polarization shifts, and too small to be detected in this experiment. Moreover, for Ar II Mult 1.U.V., Ar III Mult 1.U.V. and N II Mult 2.U.V. the ordinary Stark shifts are blue shifts since the impact broadening is dominated by interactions between the upper and lower states of the transition (see Fig.3.1). Thus in these cases there is no possibility of cancellation between ordinary Stark shifts and polarization shifts to give zero measured shifts.

The assumption that Ar II is in thermal equilibrium in z-pinch sources such as the source used in this experiment has long been established (see, for example, Burgess (1964)). Thus the use of the Greig estimate is justified for Ar II.

The strong temperature dependence of the estimates has also been investigated and compared with the dependence predicted, shown in Fig.3.1.

The experimental procedure, the results, and their implications are discussed in the following chapters.

TABLE 3.1

Predicted Shifts for the Ar II Mult 1.U.V. resonance lines at 919.78Å and 932.05Å, for an electron density 2×10^{18} cm^{-3} and a temperature 25,000K.

Polarization Shift Estimate	Predicted Polarization Shift	Ordinary Stark Shift
Griem 1966 (quantum mechanical)	- 0.012 Å	- 0.013 Å (Semiempirical Estimate - See Appendix 3)
Greig 1970 (semiclassical)	- 9.52 Å	
Burgess and Peacock 1971 (semiclassical)	$- 7.2 \times 10^{-3}$ Å	
Griem 1973 (semiclassical)	+ 284,174,794.0 Å	
Griem 1974 (quantum mechanical)	- 0.115 Å	
Volonté 1975 (quantum mechanical)	$- 1.08 \times 10^{-3}$ Å ×2	

A negative sign indicates a blue shift.

TABLE 3.2

Predicted Shifts for the Ar II Mult 4.U.V. resonance lines at 730.929 Å and 725.550Å for an electron density 2 x 10^{18} cm^{-3} and temperature 25,000K.

Polarization Shift Estimate	Predicted Polarization Shift	Ordinary Stark Shift
Griem 1966	- 0.0113 Å	+ 0.09 Å (Griem 1974)
Greig 1970	- 12.56 Å	
Burgess and Peacock 1971	- 9.6 x 10^{-3} Å	
Griem 1973	+ 159,751,331.0 Å	
Griem 1974 (quantum mechanical)	- 0.297 Å	
Volonté 1975	- 1.4 x 10^{-3} Å ×2	

A negative sign indicates a blue shift.

TABLE 3.3.

Predicted Shifts for Ar III Mult 1.U.V. Resonance Lines, $3p^4\ {}^3P\text{-}3p^5\ {}^3P$, ($\bar{\lambda}$ = 879.06 Å), for an electron density 2×10^{18} cm^{-3} and temperature 25,000K.

Polarization Shift Estimate	Predicted Polarization Shift	Ordinary Stark Shift
Griem 1966	- 0.018 Å	- 0.006 Å (semiempirical estimate ~ see Appendix 3)
Greig 1970	- 1043.67 Å	
Burgess and Peacock 1971	$- 3.67 \times 10^{-3}$ Å	
Griem 1973	$+ 1.716 \times 10^{19}$ Å	
Griem 1974	- 0.299 Å	
Volonté 1975	$- 1.0 \times 10^{-3}$ Å $\times 2$	

A negative sign indicates a blue shift.

TABLE 3.4

Predicted Shifts for the N II Mult 2.U.V. Resonance Lines at $\bar{\lambda} \sim 916.34$ Å, ($2s^2\ 2p^2 - 2s\ 2p^3$) for an electron density 2×10^{18} cm^{-3} and a temperature 25,000K

Polarization Shift Estimate	Predicted Polarization Shift	Ordinary Stark Shift
Griem 1966	-9.90×10^{-3} Å	- 0.0014 Å (semiempirical estimate see Appendix 3)
Greig 1970	- 3.94 Å	
Burgess and Peacock 1971	-5.3×10^{-3} Å	
Griem 1973	+1,594,401,008.0 Å	
Griem 1974	- 0.165 Å	
Volonté 1975	-7.8×10^{-4} Å x 2	

A negative sign indicates a blue shift.

TABLE 3.5

Shifts for N IV Mult 3.U.V. Lines at $\bar{\lambda} \sim 923.15$ Å, for an electron density 2×10^{18} cm^{-3}, and a temperature 25,000K.

Polarization Shift Estimate	Predicted Polarization Shift
Griem 1966	- 0.016 Å
Griem 1974 (quantum mechanical)	- 0.172 Å
Burgess and Peacock 1971	$- 1.2 \times 10^{-3}$ Å
Griem 1973	$+ 8.1 \times 10^{38}$ Å

A negative sign indicates a blue shift.

TABLE 3.6

Predicted Shifts for Sodium D Lines ($\bar{\lambda}$ = 5891.8 Å) for an electron density 2×10^{16} cm^{-3} and a temperature 25,000K.

Polarization Shift Estimate	Predicted Polarization Shift	Ordinary Stark Shift
Griem 1966	Zero shift	+ 0.012 Å (Griem 1974)
Burgess and Peacock 1971	- 0.0123 Å	
Griem 1973	- 0.0123 Å	
Griem 1974	Zero shift	

A negative sign indicates a blue shift.

CHAPTER IV

Ar II and Ar III U.V. Resonance Line Studies

4.1 Apparatus

The Ar II and Ar III U.V. resonance lines emitted by the z-pinch source described in Chapter II were studied. The z-pinch tube was connected by a side arm 20 cm long and 1 cm in diameter to a 1 metre normal incidence scanning vacuum monochromator, in order to observe the plasma column sideways on. The system was necessarily windowless and the monochromator was evacuated by an 8" diffusion pump to a working pressure in the region 10^{-5} to 10^{-6} Torr. The gas flow between the high pressure ($\sim$0.5 Torr) pinch side-arm and the low pressure (10^{-5} Torr) monochromator was regulated by the nylon block assembly, sketched in section in Figure 4.1. The block was machined so that when in place it cleared the slits by ~10 μ. Since the slit widths were typically 50 μ this meant that the gas leakage around the slits was completely negligible compared with the leakage through the slit (which is itself small and, in any case, inevitable). It was found that this clearance was just sufficient for the nylon block not to interfere with the opening and closing of the slits. The method of sealing was thus preferable to a conventional O-ring seal onto the slit jaws themselves, since the O-ring tends to pull the slit jaws open when the system is evacuated.

The monochromator was fitted with an R.C.A. 1P21 photomultiplier coated with a scintillator, operating at gains of typically 10^6. The scintillating coating on the photomultiplier was sodium salicylate. The chief disadvantage of using a visible-sensitive photomultiplier coated with a U.V. sensitive scintillator is that the detector is sensitive to scattered light of all wavelengths, including scattered visible light. The alternative is the use of a solar-blind photomultiplier.

Fig 4.1 : Nylon block assembly for windowless interfacing of high pressure source to low pressure spectrograph.

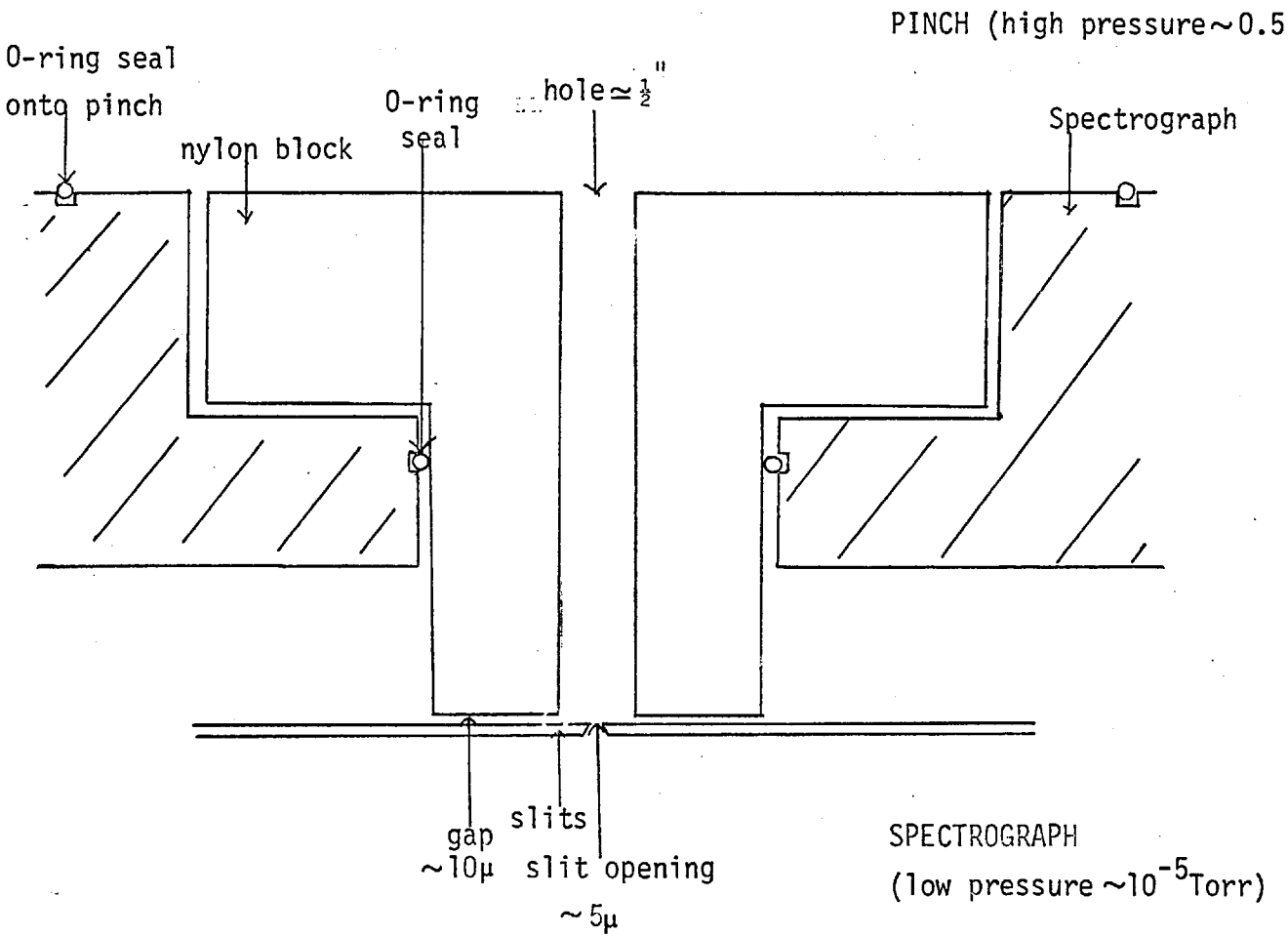

While the solar-blind photomultiplier offers the enormous advantage of peak sensitivity at about 900 Å, which corresponds to the spectral region of interest in these experiments, the main drawback is that the photomultiplier itself must be evacuated to a working pressure of 10^{-5} Torr. The stray light level in the monochromator was reduced to such a level that the scattered visible light was entirely negligible compared with the U.V. signal from the pinch in the region of 900 Å. Use of a solar-blind photomultiplier was therefore found to be unnecessary.

The grating used in these experiments was a Bausch and Lomb platinum-coated replica ruled at 3600 lines/mm, with one end of the grating separately ruled with 200.32 lines/mm for alignment and focussing purposes. The reciprocal dispersion of the grating was 2.8 Å/mm. The quoted blaze was 364 Å although in practice the blaze was found to be nearer 500 Å (R. Driver, 1973. Ph.D. Thesis).

The profiles of the resonance lines from the discharge were scanned from shot to shot, the signal reproducibility being $\sim \pm 5\%$.

4.2 Wavelength Standards

The wavelength standards used for these experiments were the same Ar II U.V. resonance lines at 919.7815 Å and 932.0528 Å emitted by a cooled cathode discharge, (described in Appendix 4). The lines are sharp and unshifted under these conditions, and so can be used to establish a wavelength standard, and to give the instrument width. The entrance and exit slits were both set at 50 μ. By advancing the gearing on the wavelength scale manually the instrument could be scanned in steps of $\sim 1/20$ Å. Using a stepping motor to advance the wavelength scale it was found that the wavelength scale could be re-set to within 1/60 Å, providing the setting was always approached from the low wavelength side to avoid backlash in the gearing system. Errors in resetability represented the ultimate restriction which the equipment set on shift measurements. The instrument profile at Ar II 919 Å

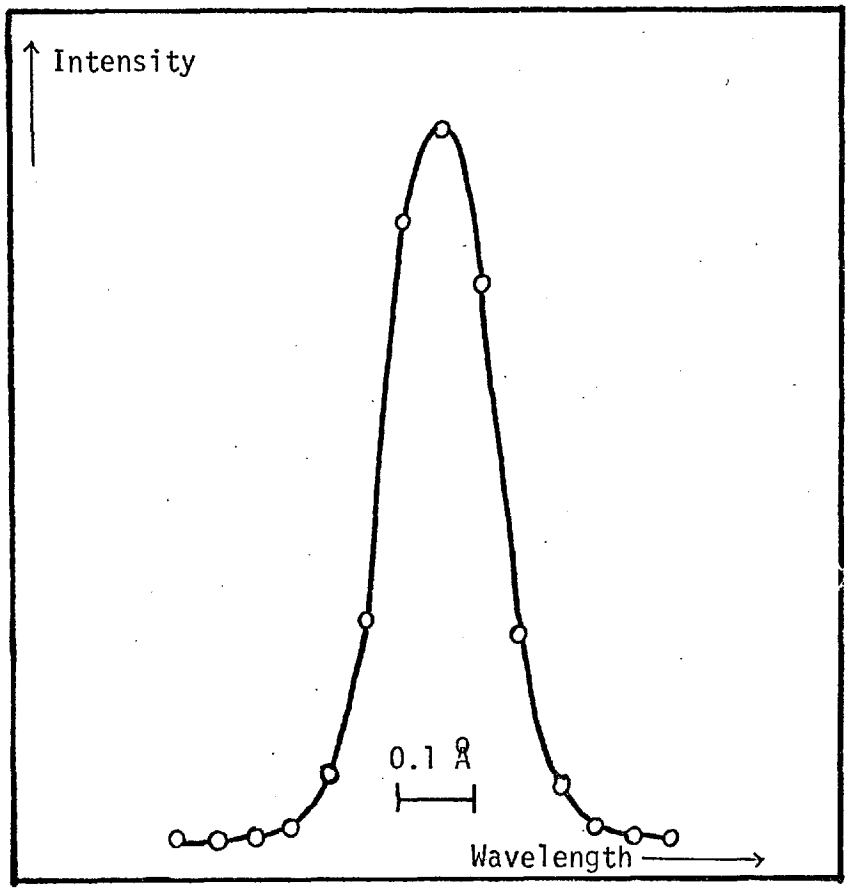

Fig 4.2 : Instrument Profile - Ar II Mult 1uv 919 Å
emitted by a cooled-cathode discharge.

under these conditions is shown in Figure 4.2. The full half-width is ~ 0.147 Å with the slits set at 50 μ.

4.3 Results: Ar II Mult l.U.V. Profiles

Figure 4.3 shows typical profiles for Ar II 919 Å and 932 Å. The half-half widths of these lines are typically about 1/3 Å. The lines were scanned in steps of about ~ 1/20 Å. The profiles were usually scanned out to ~ 2 Å in the wings, although one set of profiles was scanned ± 5 Å into the wings of 919 Å.

The profiles of Ar II 919 Å and 932 Å were found to be unshifted to better than 1/20 Å with respect to their wavelengths as emitted by the cooled cathode discharge. The measured shifts for the lines are summarized in Table 4.1. Comparison with the theoretical estimates at this density (Table 3.1) shows that the predicted magnitude of the shift is overestimated by between one and ten orders of magnitude.

Moreover the measured wavelength positions are apparently unchanged by altering the pinch firing conditions. Figure 4.4 compares the measurements with the temperature dependence predicted by some of the estimates. The wavelength shift to density ratio is plotted as a function of electron temperature. The results show no evidence for the strong temperature-dependent trend predicted by either the quantum mechanical approach of Griem (1974) or by the semiclassical estimates of Greig (1970) or Griem (1973). The only semiclassical estimate consistent with the measured null results is that of Burgess and Peacock (1971). This formula was in any case only suggested as an order-of-magnitude estimate for the shift, and as such makes no greater claims to rigour.

The revised version of the Griem (1974) quantum mechanical estimate, suggested by Volonté (1975), predicts small shifts of order 10^{-3} Å, which are consistent with the null results of this experiment.

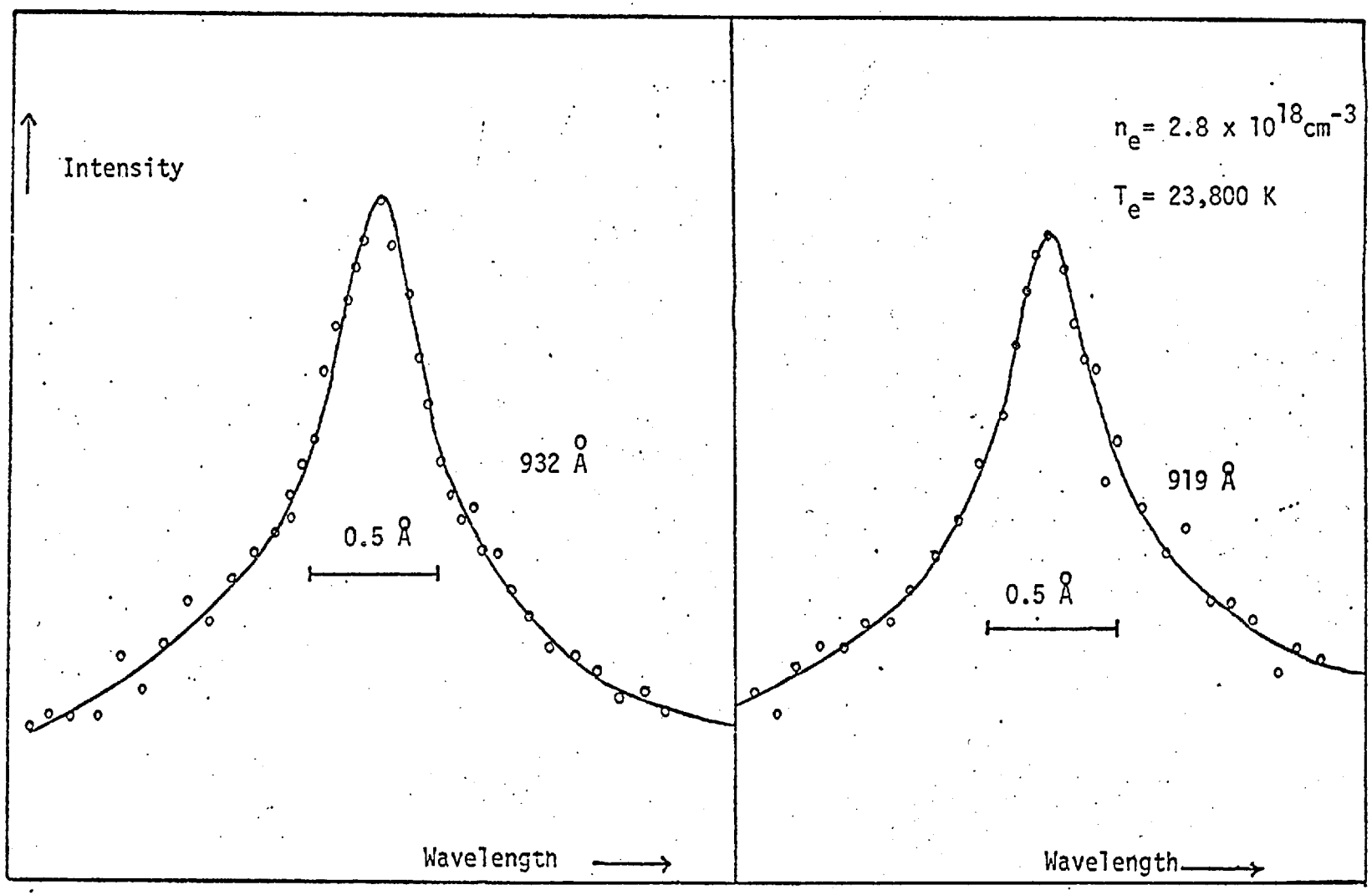

Fig 4.3 : Ar II Mult luv Profiles.

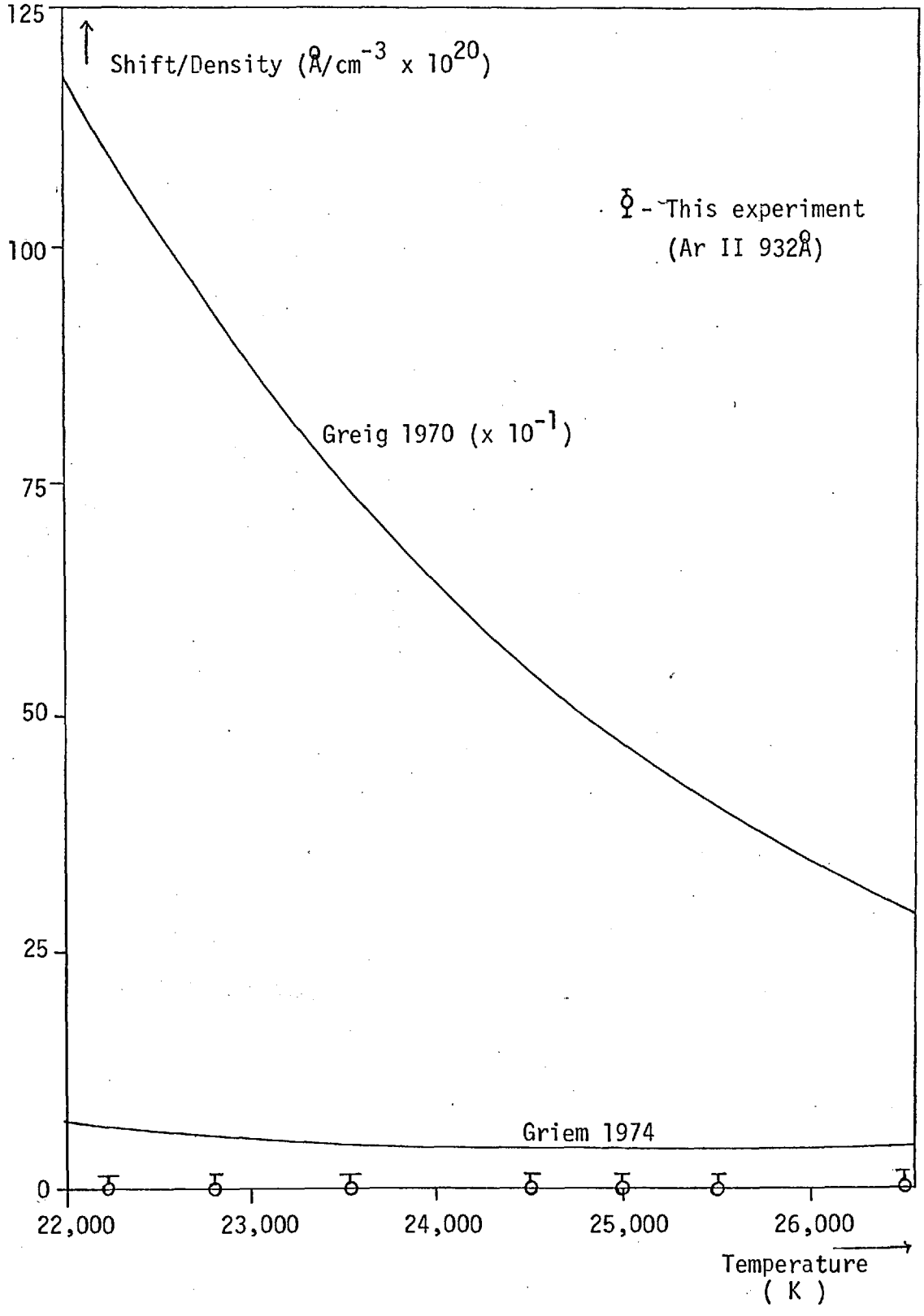

Fig 4.4 : Comparison of experimental measurements of the shift of of Ar II 932Å with some temperature-dependent theoretical predictions. The estimates of Burgess and Peacock (1971) and Volonte (1975) yield shifts too small to be shown on this scale.

The original estimate by Griem (1974) predicts shifts of order 0.12 Å, which are overestimates by at least a factor of two.

4.4 Results: Ar III U.V. Resonance Profiles

4.4.1 Shift Measurements

The Ar III Mult 1.U.V. resonance lines were scanned in steps of 1/6 Å from 869 Å to 889 Å. Typical Ar III Mult 1.U.V. profiles are shown in Figure 4.5. Since it was not possible to excite the Ar III Mult 1.U.V. lines in the cooled cathode, instead the Ar II Mult 1.U.V. lines from the cooled cathode were used as wavelength standards, these lines being the nearest reliable standards emitted by the source. Since these standards lie some 50 Å from the Ar III lines, the errors in shift measurements will be somewhat larger in this case. All the Ar III U.V. resonance lines (except 878.73 Å) show slight red shifts of order 0.2 Å. Ar III 878.73 Å consistently shows evidence of a blue shift of $\sim$0.2 Å (due perhaps to overlap with the red wing of 875.53 Å, or to some undetected impurity line in the blue wing of 878.73 Å itself). Table 4.2 summarises the measured shifts of these lines for different pinch conditions. A comparison of the findings with the shifts predicted theoretically (Table 3.3) shows that the existing theories grossly overestimate the shift (sometimes by as much as 20 orders of magnitude). Although there is indeed some evidence for an unexplained shift of these lines, it is a small red shift, and as such it cannot be adequately explained in terms of any of the existing polarization shift theories.

Although the wavelength standards are not so accurate for these lines since they are based on Ar II Mult 1.U.V., which lies about 50 Å to the red of the Ar III Multiplet, it is unlikely that the errors arising from inaccuracies in the wavelength standards will be greater than $\pm$ 1/6 Å, which is the accuracy to which the wavelength shifts of the Ar III lines have been measured. To account for the apparent red

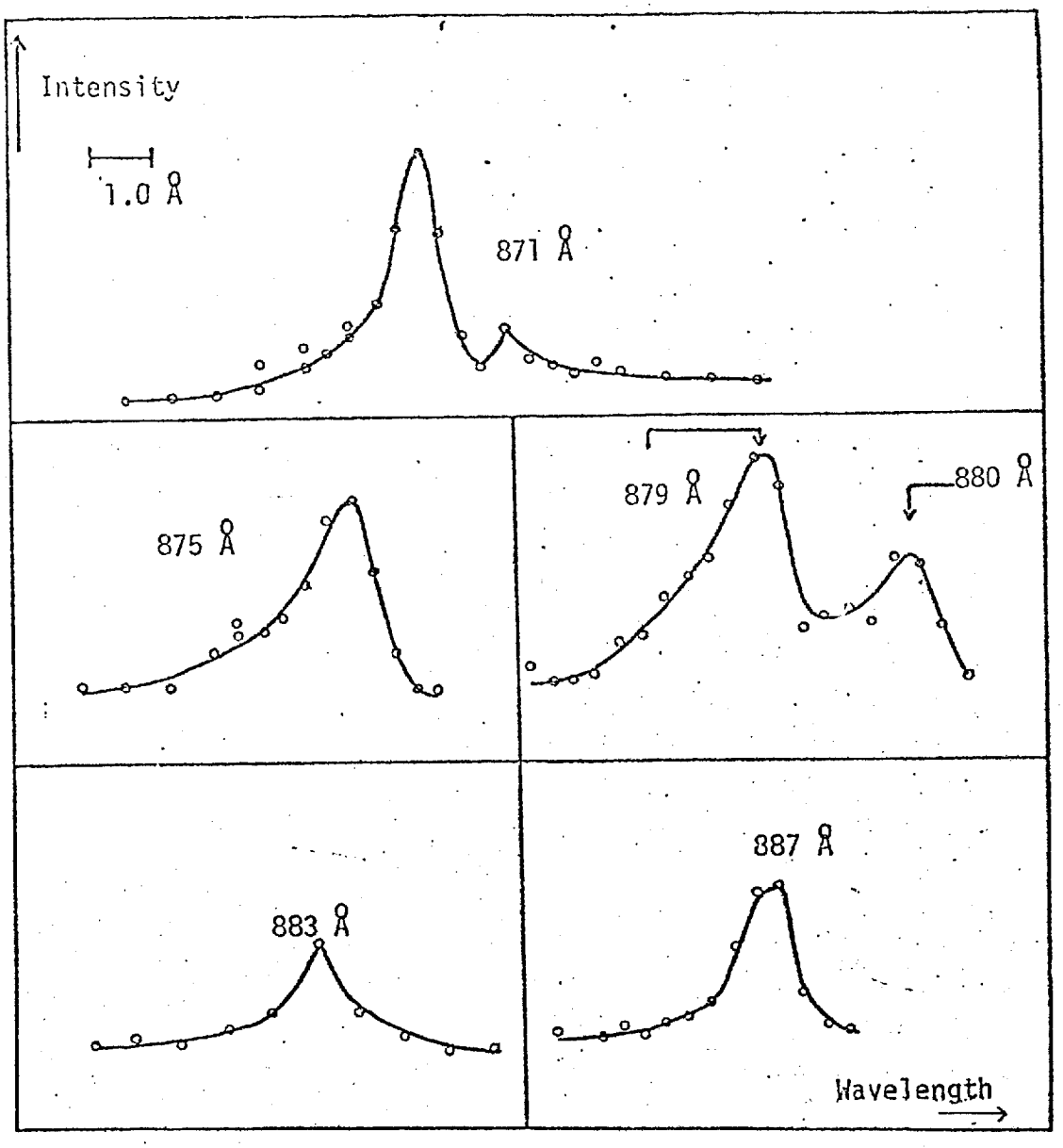

Fig 4.5 : ArIII Mult 1uv Profiles, for $n_e = 1.3 \times 10^{18}$ cm^{-3}, $T_e = 27{,}000$ K

shifts of about 0.17 Å for the Ar III lines the measurements of the Ar II standards would have to be in error by about 0.04 Å, which would be quite consistent with the measured accuracy of ± 1/20 Å for the wavelength standards at 919 Å, 932 Å. However the largest measured red shift of 0.28 Å at 887 Å would correspond to an error of -.07 Å in the measured position of 919 Å - which is unlikely, in view of the quoted errors. Thus there is some evidence for an unexplained red shift for the lines of this multiplet, although it is unlikely to be greater than 0.28 Å and it is probably more likely to be of order 0.17 Å (± 0.17 Å).

4.4.2 Asymmetries of the Ar III Lines

One of the most interesting features of the Ar III Mult 1.U.V. profiles is the marked asymmetry shown by all the lines in this multiplet. This asymmetry takes the form of an enhanced blue wing as is clearly seen in Figure 4.5. By comparison, the instrument profiles and the Ar II profiles studied with the same instrument and grating are highly symmetric. The possible sources of this asymmetry will be discussed in Chapter VI.

The asymmetry makes it particularly difficult to make polarization shift measurements for the Ar III lines, because of the problem of deciding where the line centre lies. The asymmetry rules out the possibility of using the line wings as well as the peak intensity to determine the position of line centre.

4.5 Ar II Mult 4 U.V. Resonance Line Profiles

Further polarization shift investigations were carried out on some of the Ar II U.V. resonance lines in Multiplet 4 U.V. at about 700 Å.

The wavelength standards used for these lines were the same lines emitted by a microwave cavity, fitted round one of the side arms

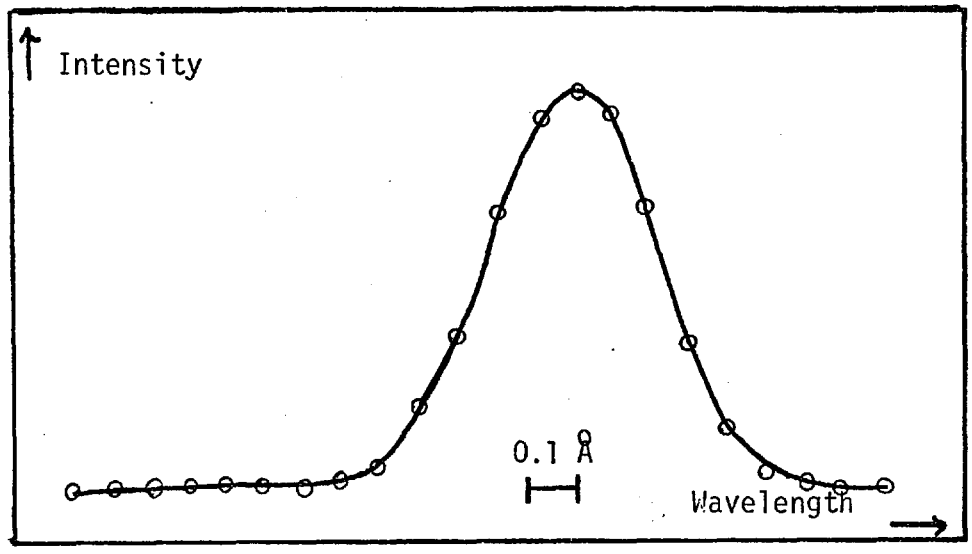

Fig 4.6 : Instrument Profile - Ar II 737.5Å from microwave source.

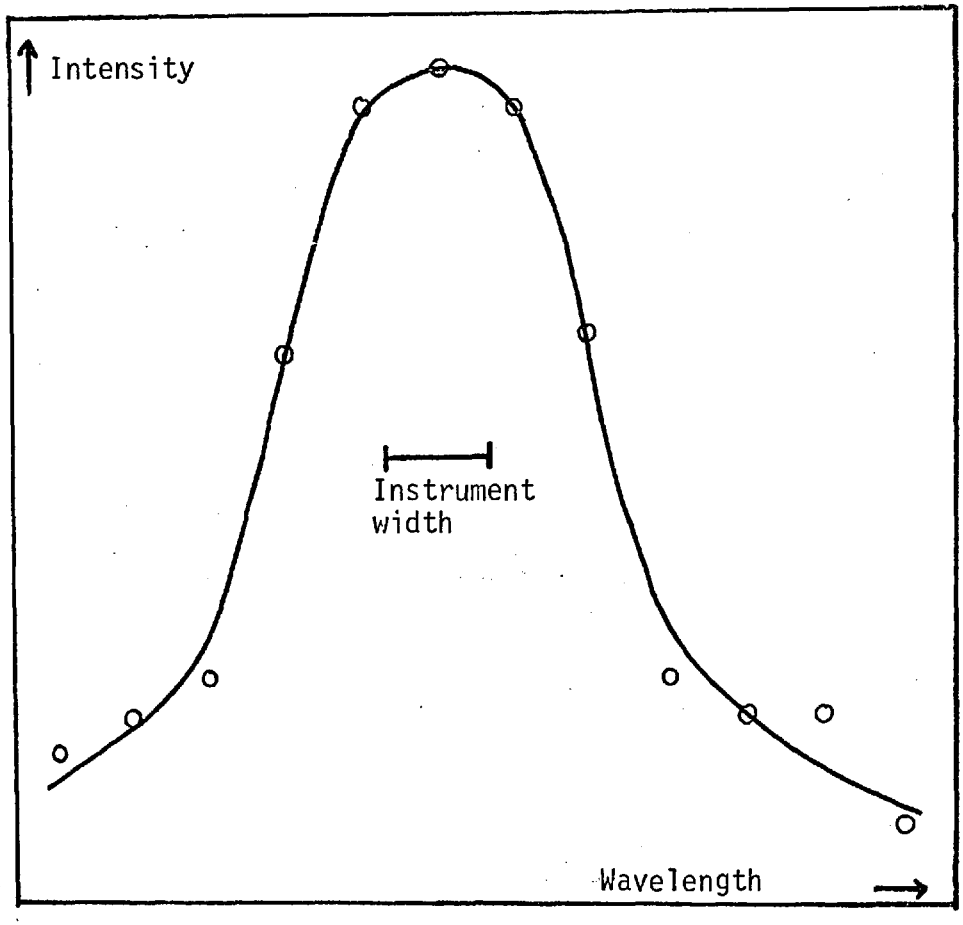

Fig 4.7 : Ar II 731 Å profile for bank voltage 5kV and filling pressure 0.09 Torr.

of the pinch. The reasons for using a different wavelength standard in this region are purely historical. The microwave cavity was run at powers of typically 10 watts and currents of 50 mAmps. The cavity was tuned so that the glow was confined to the region inside the cavity. The lines emitted were sharp and unshifted, and one of the fainter Ar II transitions (737.457 Å) was used to measure the instrument profile in this region (Figure 4.6). Three Ar II lines emitted by the microwave source were used to establish a wavelength scale and to determine the unshifted line positions.

Figure 4.7 shows a typical profile for Ar II Mult 4.U.V. 730.929 Å. The widths and shifts measured for different pinch conditions are summarized in Table 4.3, and may be compared with the shifts predicted for these lines in Table 3.2.

The blue shifts measured for 725.550 Å are likely to result from the overlap with 723.361 Å. For this reason, it was not possible to make any useful measurements of the width of this line. However the scans show 730.929 Å to be well removed from the nearest transitions.

The Stark shifts calculated for this multiplet are small. Using the broadening parameter calculated for one of the lines of this multiplet (730.929 Å) by Griem (1974), the Stark shift and width for this line may be found. At a density 2×10^{18} cm^{-3}, T $\sim$ 20,000°K, the Stark width of this line is 0.08 Å and the shift is 0.08 Å to the red. Thus the measured red shift for this line $\sim$ 0.12 Å is in good agreement with the ordinary Stark shift predicted for this line. This strongly suggests that any polarization shift to the blue for this line is very small. Even if the electron density is as high as 3×10^{18} cm^{-3}, the residual polarization shift would only be $\sim$ 0.02 Å. Table 3.2 shows that most of the existing theories overestimate this shift. Greig (1970) predicts $\Delta\lambda \sim -13$ Å, for Griem (1974) $\Delta\lambda \sim -.3$ Å, and for Griem (1973) $\Delta\lambda \gg \lambda_o$. Even the Griem (1966) estimate of

.0113 Å at $n_e = 2 \times 10^{18}$ cm^{-3} is likely to be an overestimate. Negligibly small shifts are predicted by Burgess and Peacock, 1971 ($\sim 10^{-2}$ Å) and Volonté, 1975 (10^{-3} Å), both of which would be consistent with the findings of this experiment.

The width of the line is found to be ~ 0.4 Å compared with the predicted Stark width of 0.08 Å at these densities. The measured half-half width is larger than the predicted Stark width by a factor of 4, because the transition is optically thick in this plasma.

4.6 Conclusions

Many of the existing predictions for the polarization shift are found to seriously overestimate the shifts of the Ar II and Ar III U.V. resonance lines at these densities (for example, Greig 1970, Griem 1973 (semiclassical) and Griem 1974 (quantum mechanical)). Only the estimate of Volonté 1975 (quantum mechanical) and Burgess and Peacock 1971 (semiclassical) predict negligibly small shifts consistent with the findings of this experiment.

TABLE 4.1

Summary of Shifts Measured for Ar II Mult 1.U.V.

Bank Voltage 5 KV.

Filling Pressure (Torr)	919 Å	932 Å
0.150	0.0 ± 0.05 Å	0.0 ± 0.05 Å
0.2	+0.02 ± .17 Å	-0.07 ± .17 Å
0.22	0.0 ± .05 Å	0.0 ± .05 Å
0.35	+ .05 ± .08 Å	-0.03 ± .08 Å
0.4	+0.01 ± .08 Å	-0.03 ± .08 Å
0.5	0.0 ± 0.05 Å	0.0 ± 0.05 Å
0.7	-0.05 ± .05 Å	+0.10 ± .05 Å
0.95	+0.14 ± 0.08 Å	+0.05 ± 0.08 Å

TABLE 4.2

Summary of Shifts of Ar III, Mult 1.U.V

Bank Voltage 5 KV

Filling Pressure (Torr)	871.10 Å	875.53 Å	878.73 Å	879.62 Å	883.18 Å	887.40 Å
0.2	+0.16 Å	+0.22 Å	-0.06 Å	0 Å	+0.19 Å	+0.28 Å
0.350	+0.09 Å	+0.25 Å	-0.19 Å	+0.16 Å	+0.16 Å	+0.19 Å
0.4	+0.06 Å	+0.13 Å	-0.06 Å	0 Å	+0.13 Å	+0.13 Å
0.5	+0.16 Å	+0.28 Å	0 Å	-0.19 Å	+0.19 Å	+0.25 Å
0.6	+0.16 Å	+0.28 Å	-0.22 Å	0 Å	0 Å	+0.19 Å
0.7	+0.16 Å	+0.19 Å	0 Å	+0.16 Å	+0.19 Å	+0.19 Å
0.95	+0.09 Å	+0.28 Å	-0.06 Å	+0.09 Å	+0.19 Å	+0.22 Å

TABLE 4.3

Summary of Shifts Measured for Ar II, Mult 4.U.V.

Filling Pressure (Torr)	Bank Voltage	Ar II 737.5 Å	Ar II 725.55 Å	Ar II 730.93 Å
0.1	5 KV	0.0 Å	-	-
0.05	5 KV	-	-0.8 Å	+0.12 Å
0.15	5 KV	-	-	+0.12 Å
0.09	5 KV	-	-0.8 Å	+0.12 Å
0.3	5 KV	-0.25 Å	-	+0.25 Å
0.6	5 KV	+0.25 Å	-0.2 Å	+0.25 Å
0.9	5 KV	-	-	+0.25 Å
0.05	6 KV	-	-	+0.20 Å
0.08	6 KV	-	-0.5 Å	+0.12 Å

CHAPTER V

Polarization Shifts of N II, N IV and Na I Lines

5.1 N II and N IV Lines

The N II Mult 2.U.V. resonance lines and the N IV Mult 3 U.V. lines arising from low concentration impurity nitrogen ions in the pinch were studied. The shifts predicted for these lines are given in Tables 3.4 and 3.5. The estimates available for N IV are limited, since the lines are not resonance lines, and hence it has been claimed (Griem 1974) that the Greig (1970) semiclassical estimate is not applicable.

The apparatus used for these experiments was the same as that described in Section 4.1, except that the instrument was fitted with a different grating. The grating used was a 1200 lines/mm, Bausch and Lomb Al/MgF_2 coated grating, blazed for 1200 Å. The entrance and exit slits were set at 5 μ, giving an instrument full-half width of 0.37 Å, as measured by exciting the Ar I U.V. resonance lines in a d.c. discharge in one of the side arms of the pinch.

Figure 5.1 shows a typical scan of the lines from the pinch, together with the unshifted line positions. Many of the nitrogen lines lie too close to be resolved and their positions are probably perturbed by the wings of the Ar II Mult 1.U.V. lines, so only approximate measurements of the shifts may be obtained.

The Ar II Mult 1.U.V. lines emitted by the plasma were used as wavelength standards, since the experiments of the previous chapter established that these lines were unshifted to ± 0.05 Å.

Table 5.1 summarises the shifts measured for the N IV and N II lines. These may be compared with the shifts predicted for these lines in Tables 3.4 and 3.5. The experiment sets an upper limit of $-1/2$ Å on the shift of the N IV lines and $+0.3$ Å on the shift of the N II lines.

The shifts predicted by theory are shown in Tables 3.4 and 3.5.

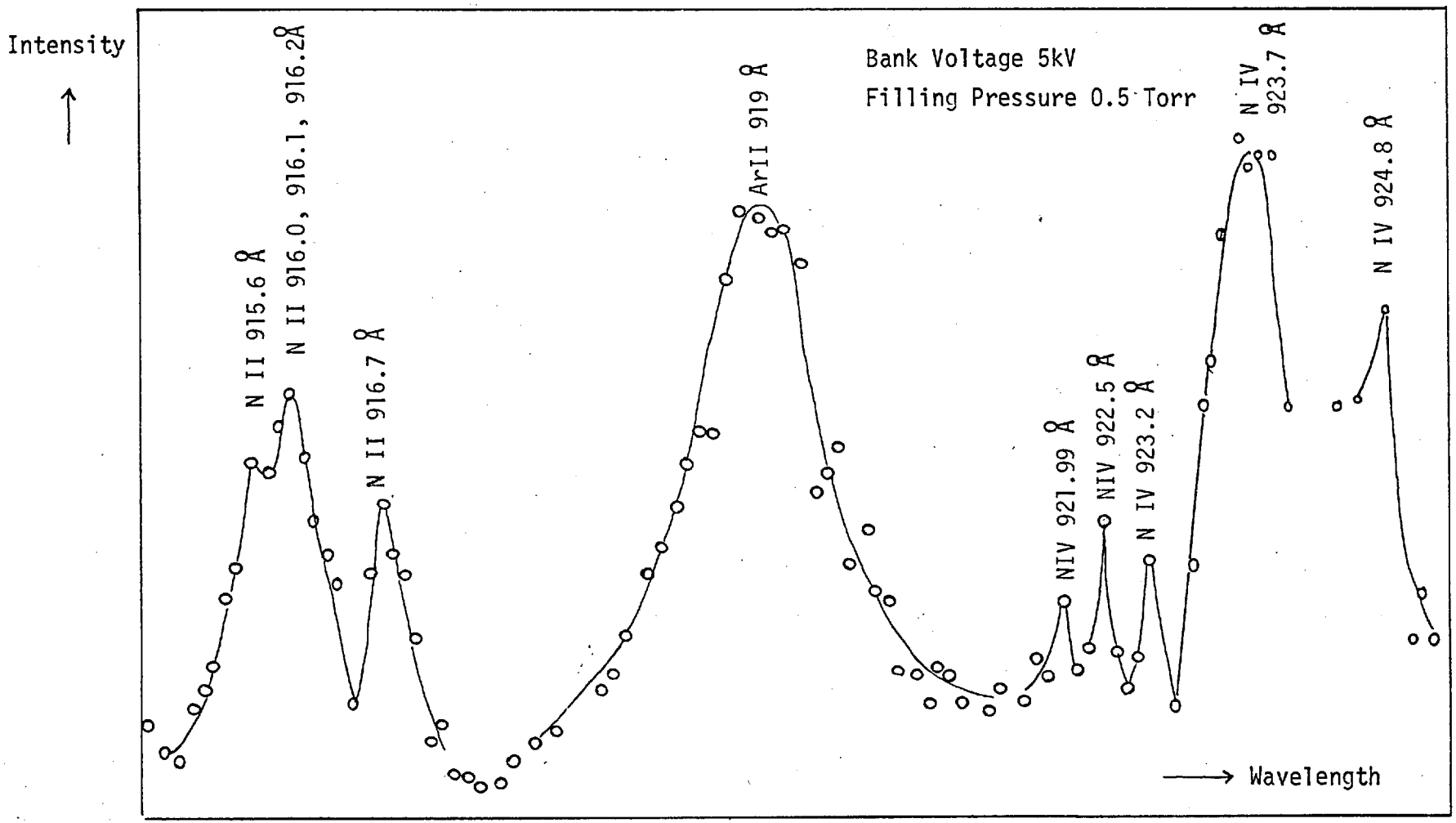

Fig 5.1 : Scan of N II and N IV Profiles studied

The blue shifts of the N IV lines are consistent with the estimates of Griem (1966), Burgess and Peacock (1971) and Griem (1974), although the Griem (1973) semiclassical estimate is too large by 39 orders of magnitude. The red shifts found for N II are not satisfactorily explained by any of the theories. In particular no measurable blue shift of ~0.16 Å as predicted by Griem (1974), nor of ~ 4.0 Å as predicted by Greig (1970), could be detected. The Griem (1973) semiclassical estimate overestimates the magnitude of the shift by ten orders of magnitude.

5.2 Studies for Neutral Emitters

Many of the theoretical estimates yield non-zero shifts for neutral emitters. In particular the semiclassical estimates do not give zero shifts for $Z = 1$, although in the vicinity of a netural emitter the local excess of charge as a result of the polarization of the plasma might be expected to be very small, if not actually zero. Although the plasma is too hot for Ar I emission an attempt was made to study the shifts for the resonance lines of some other neutral emitters in low concentration in the plasma.

5.3 Neon I Lines

The similarity between the ionization potentials of Ne I and Ar II (Ne I at 21.564 eV and Ar II at 27.629 eV) suggested that it might be possible to excite neutral neon in the plasma (which consisted chiefly of singly-ionised argon). However, it was found that reabsorption of the Ne I resonance emission by cold neon outside the core of the pinch and in the spectrograph precluded the measurement of the shifts of these lines.

5.4 Na I Lines

Shift measurements were made on the sodium D-lines, arising from impurity sodium from the pinch walls.

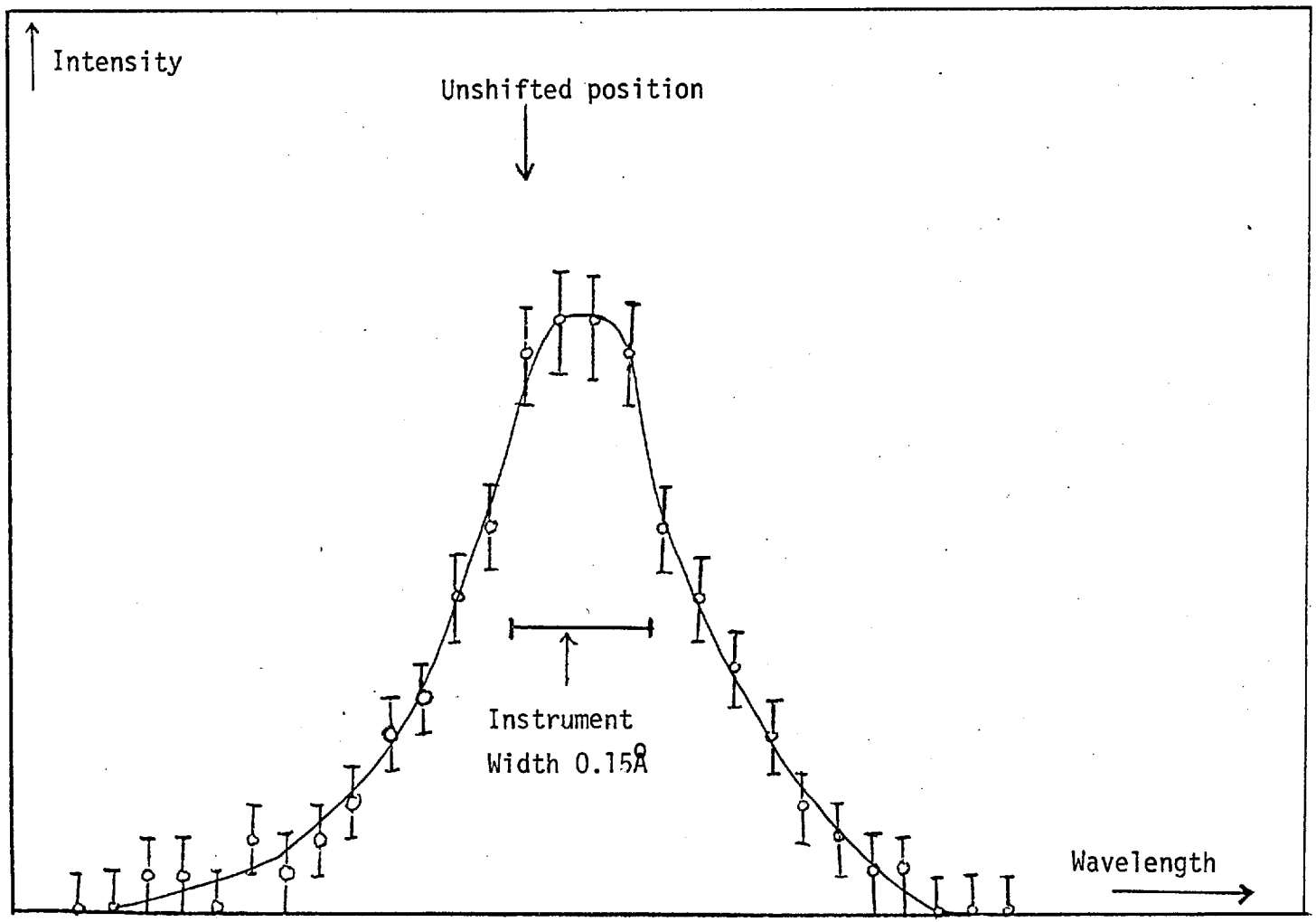

Fig 5.2 : Na I 5890Å Profile for bank voltage 6kV and filling pressure 0.4 Torr.

The profiles were scanned from shot to shot, using a Monospek 1000 monochromator and an RCA 1 P28 photomultiplier. A sodium lamp, run at low voltages so that the lines were optically thin and unshifted, was used as a wavelength standard for the sodium D-lines.

Figure 5.2 shows a scan of Na I 5890 Å. From the widths of these lines, it became clear that the sodium emission was not coming from the densest part of the plasma, but from a region where the electron density was only $\sim 2.10^{16}$ cm^{-3}. The expected shifts under these conditions are shown in Table 3.6. The predicted shifts vary between 0 and 0.013 Å to the blue, and at this density Griem (1974) predicts a Stark shift of 0.012 Å to the red.

The shift of 5890 Å was found to be 0.017 Å to the red $\pm$ 0.017 Å, the limiting factor being the resolution of the monochromator. This suggests that any blue shift of the line is smaller than the 0.012 Å shift predicted by both of the semiclassical estimates, (Griem 1973, Burgess and Peacock 1971), and is probably zero. It is not possible to draw any firmer conclusions since the small shifts involved are of the same order as the resolution of the monochromator.

TABLE 5.1

Summary of Shifts Measured for N II and N IV Lines

Bank Voltage 5 KV		
Filling Pressure	=	0.5 Torr
N II	915.61	+ 0.3 Å
N II	916.02	0.0 Å
N II	916.70	+ 0.15 Å
N II	916.21	+ 0.15 Å
N IV	922.00	+ 0.05 Å
N IV	922.52	- 0.15 Å
N IV	923.06	- 0.3 Å
N IV	923.22	- 0.5 Å
N IV	923.68	- 0.2 Å
N IV	924.28	- 0.3 Å

CHAPTER VI

Observations of Asymmetries in the Emission Profiles of Ar II and Ar III Lines

6.1 Introduction

As already mentioned in Chapter IV, the measured emission profiles for the Ar III Mult 1.U.V. resonance lines all show marked asymmetries, with an enhanced blue wing (see Fig.6.1). Detailed analysis of the profiles of Ar II Mult 1.U.V. (Fig.6.2) described in the same chapter indicates that these lines also show signs of a similar, though much smaller, asymmetry.

In addition the profiles of Ar II Mult 6, 4848 Å and 4806 Å, used as a density diagnostic in Chapter II are also strongly asymmetric with enhanced blue wings, as may be seen from Fig.6.3. These profiles are all given in the relevant preceding chapters, but they are repeated as Figs.6.1, 6.2 and 6.3 for convenient reference. In the following chapter some of the mechanisms that might give rise to asymmetries of this magnitude are considered.

6.2 Analysis of the Measured Asymmetries

Figs.6.4, 6.5 and 6.6 are plots of the asymmetry as a function of wavelength for Ar II Mult 1.U.V., Ar II Mult 6 4806 Å and 4848 Å, and Ar III Mult 1.U.V. respectively. The measured asymmetry, $A(\omega)$, is found from

$$A(\omega) = \frac{I(\lambda_o - \Delta\lambda) - I(\lambda_o + \Delta\lambda)}{\frac{1}{2} I(\lambda_o - \Delta\lambda) + I(\lambda_o + \Delta\lambda)} \qquad (6.1)$$

where $I(\lambda)$ is the intensity at a wavelength λ, and λ_o is the wavelength of the measured line centre.

Measurements of the asymmetry were made as far into the wings as possible (i.e. as far as the wavelength at which the wing intensity

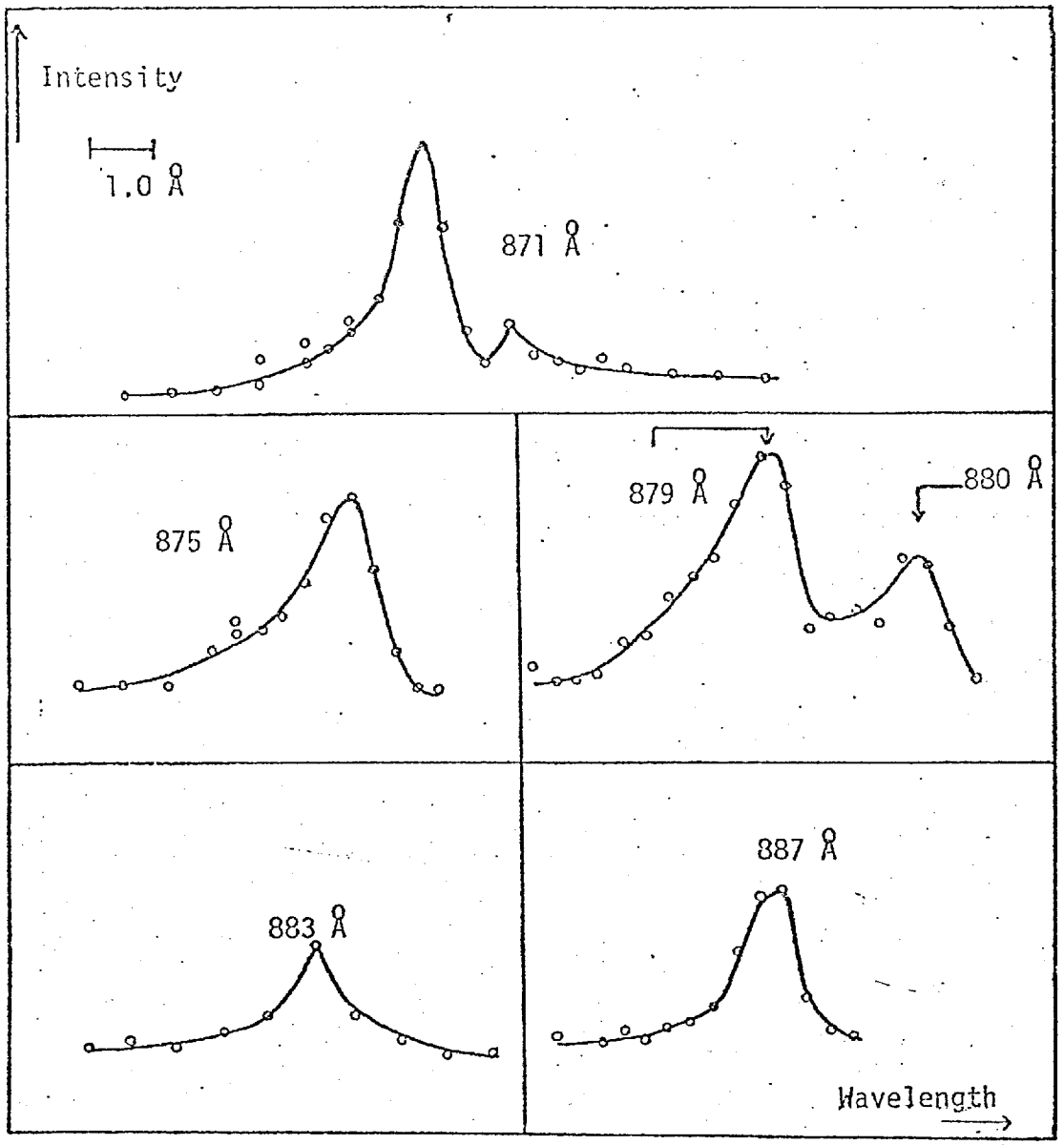

Fig 6.1 : ArIII Mult luv Profiles, for n_e= 1.3 x 10^{18} cm^{-3}, T_e= 27,000 K

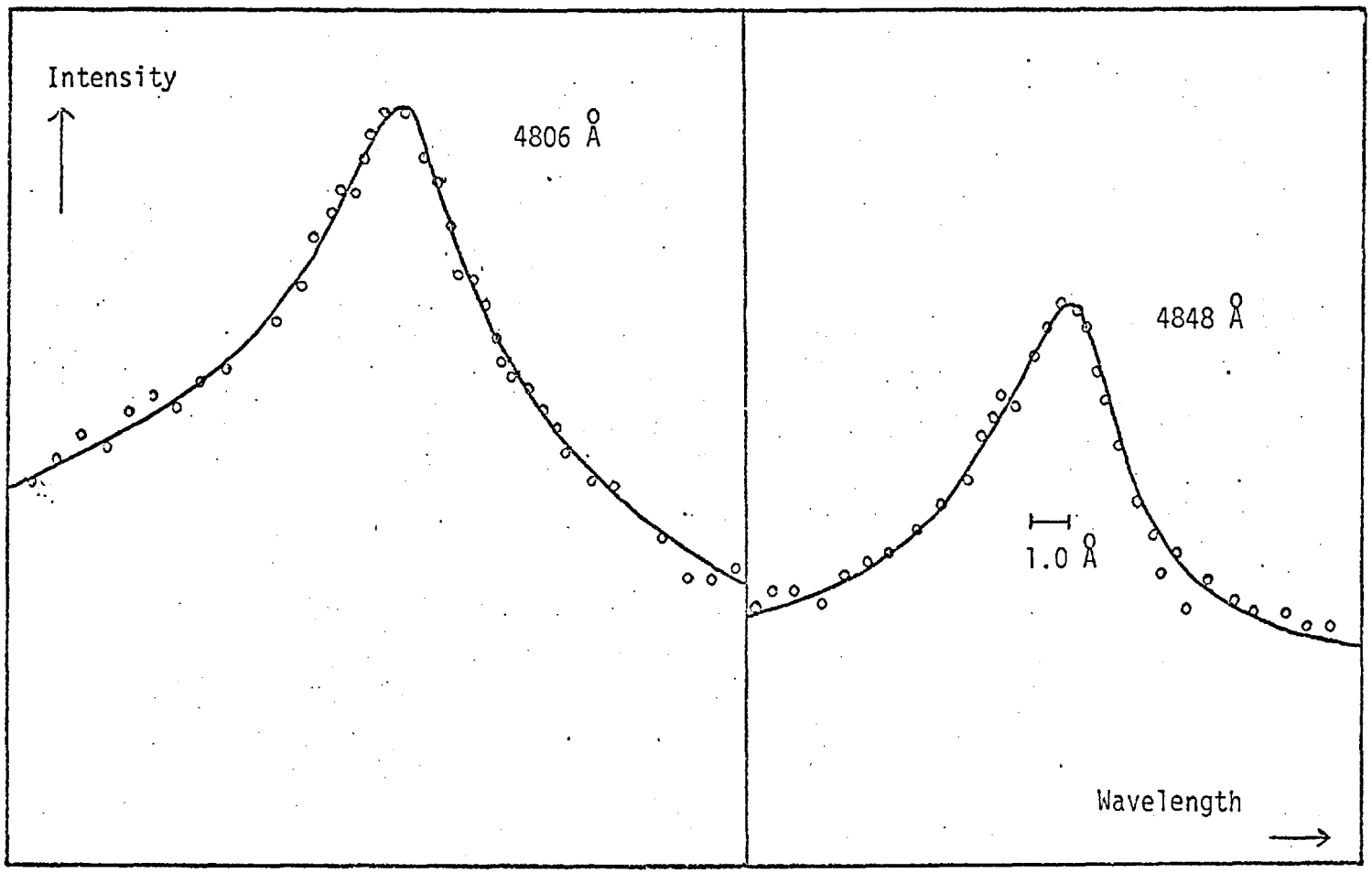

Fig 6.2 : Ar II Mult 6 Profiles for n_e = 2.0 x 10^{18} cm^{-3}, T_e = 24,5000 K.

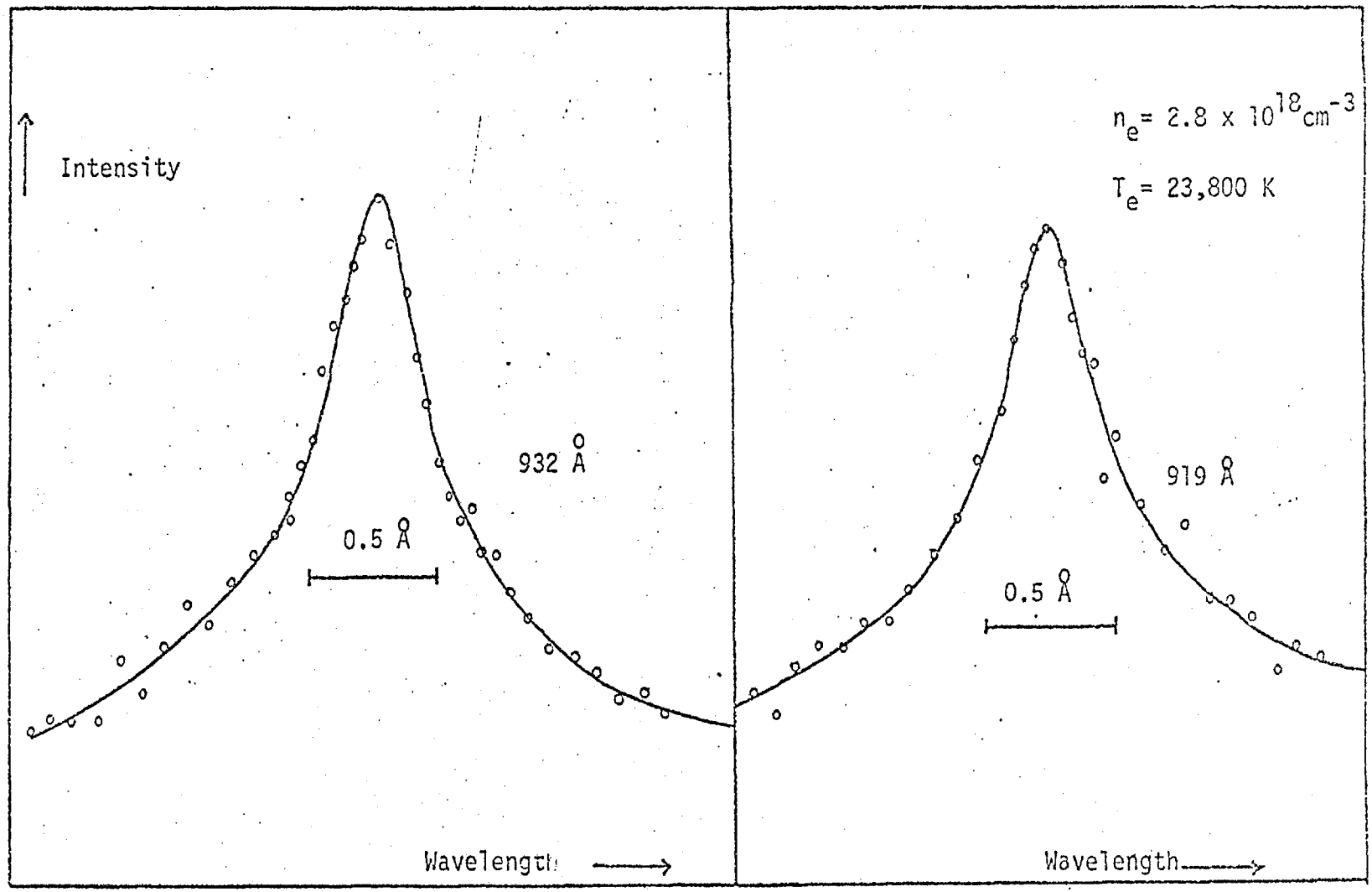

Fig 6.3 : Ar II Mult 1uv Profiles.

becomes comparable with the shot noise).

6.2.1 Ar II Mult 6

The asymmetry of the visible Ar II lines (Fig 6.5) can be fitted to a linear dependence on wavelength from line centre, the slope of the linear fit being approximately the same for both transitions. The measured asymmetry is about 100% when the wavelength separation is 7 Å.

6.2.2 Ar II Mult 1.U.V.

The measured asymmetries for the Ar II U.V. lines are shown in Fig.6.4. The asymmetry of 932 Å fits a linear variation with wavelength, the asymmetry being about 25% for a wavelength separation of 1 Å. However at wavelength separations greater than 0.2 Å, the asymmetry of 919 Å changes sign. The measured red asymmetry in the wings of this transition can be attributed to overlap with impurity nitrogen transitions, and will be shown (Section 6.4) to be in good agreement with the red asymmetry predicted by simple numerical modelling for the overlap of these lines.

6.2.3 Ar III Mult 1.U.V.

The Ar III lines all show large asymmetries for relatively small wavelength separations. Unfortunately the mutual overlap of the transitions within this multiplet precludes observations very far into the wings of these lines. In particular, the $J = 1 \longrightarrow 1$ transition lies wholly within the wing of $J = 2 \longrightarrow 2$, so no measurements of the asymmetry were possible. In cases where asymmetry measurements were possible Fig.6.6 shows that this asymmetry increases with wavelength, and apart from the $J = 0 \longrightarrow 2$ transitions, this variation can be fitted to a linear dependence on wavelength.

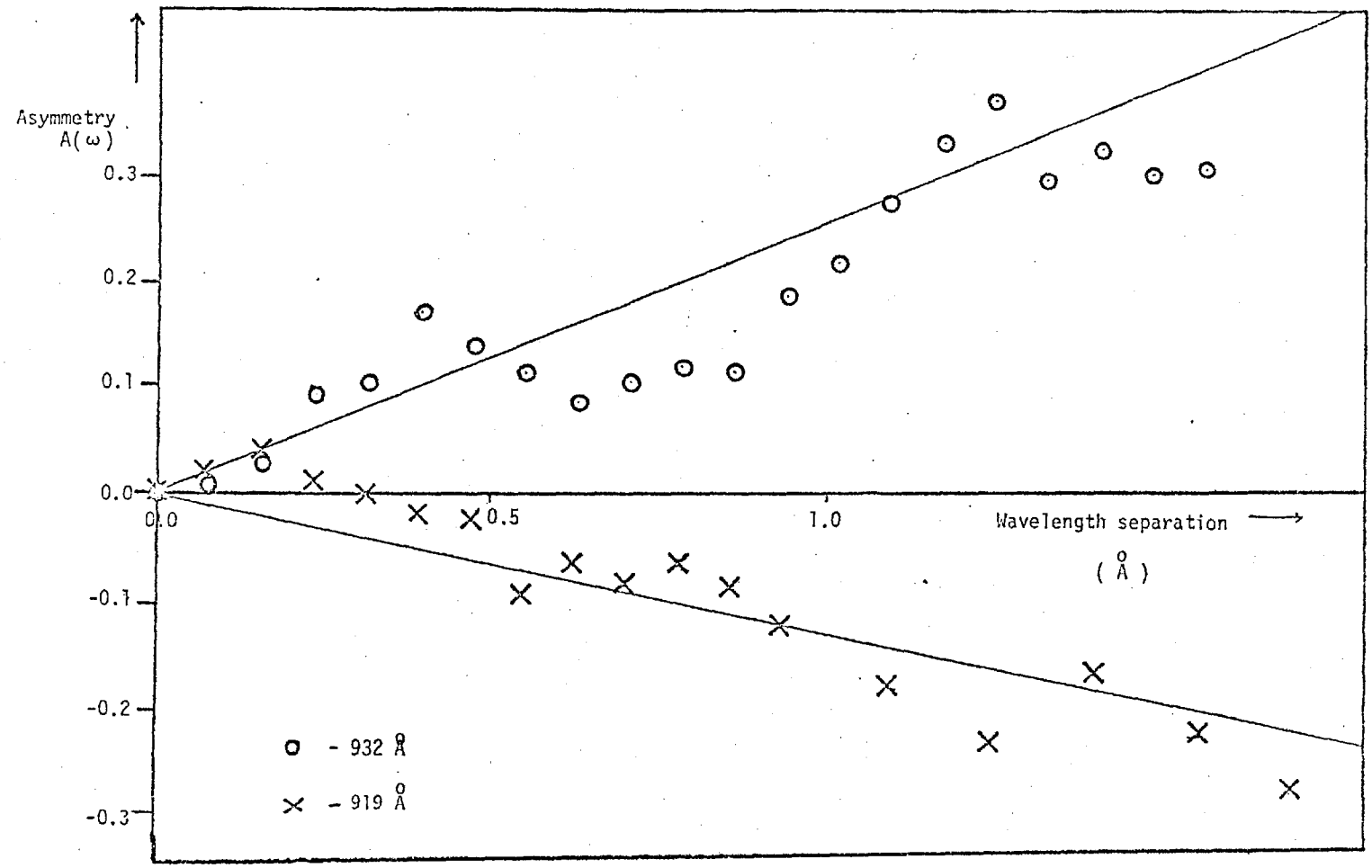

Fig 6.4 : Asymmetry, A(ω), versus wavelength separation for Ar II Mult luv.

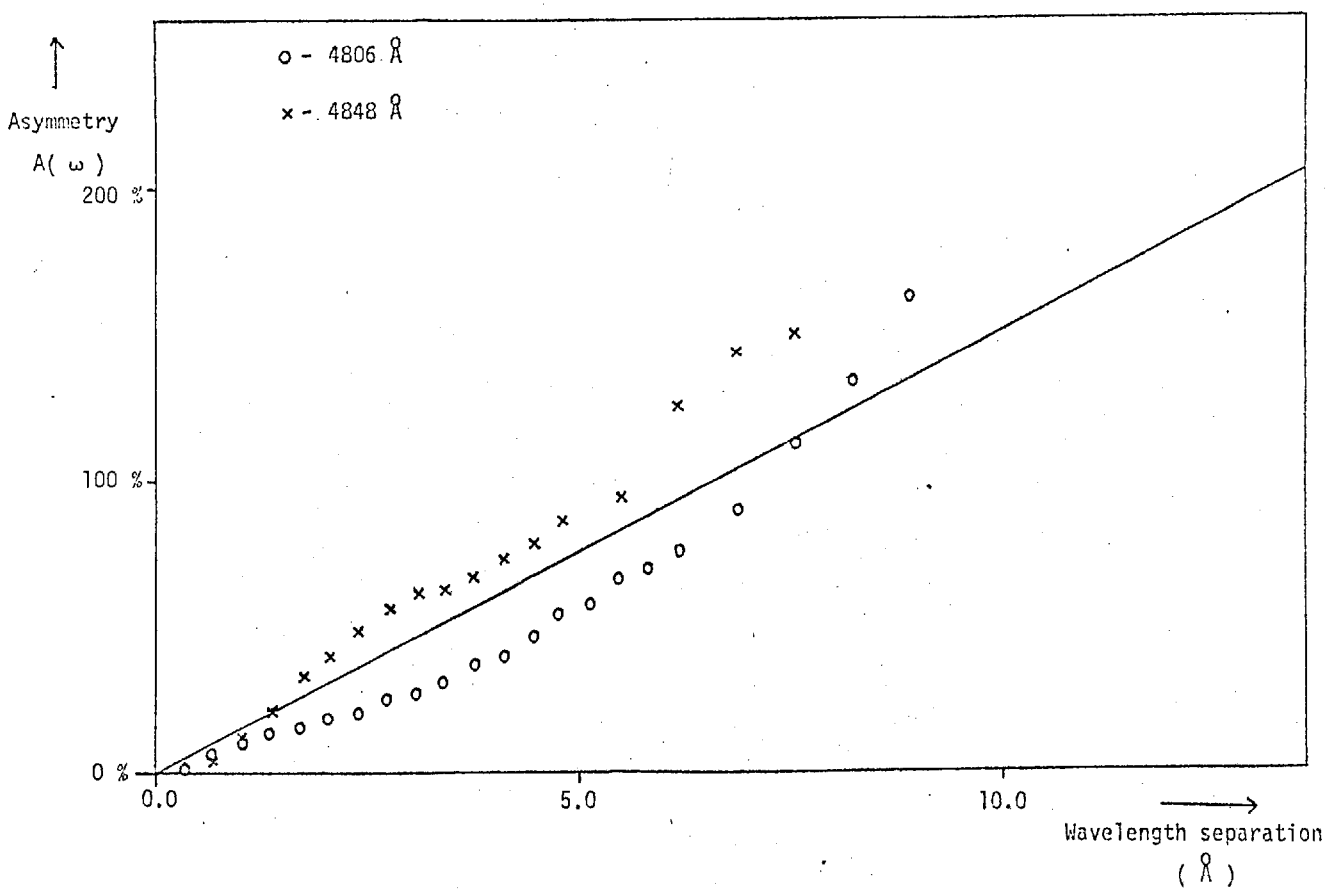

Fig 6.5 : Asymmetry A(ω) of Ar II Mult 6 as a function of wavelength separation.

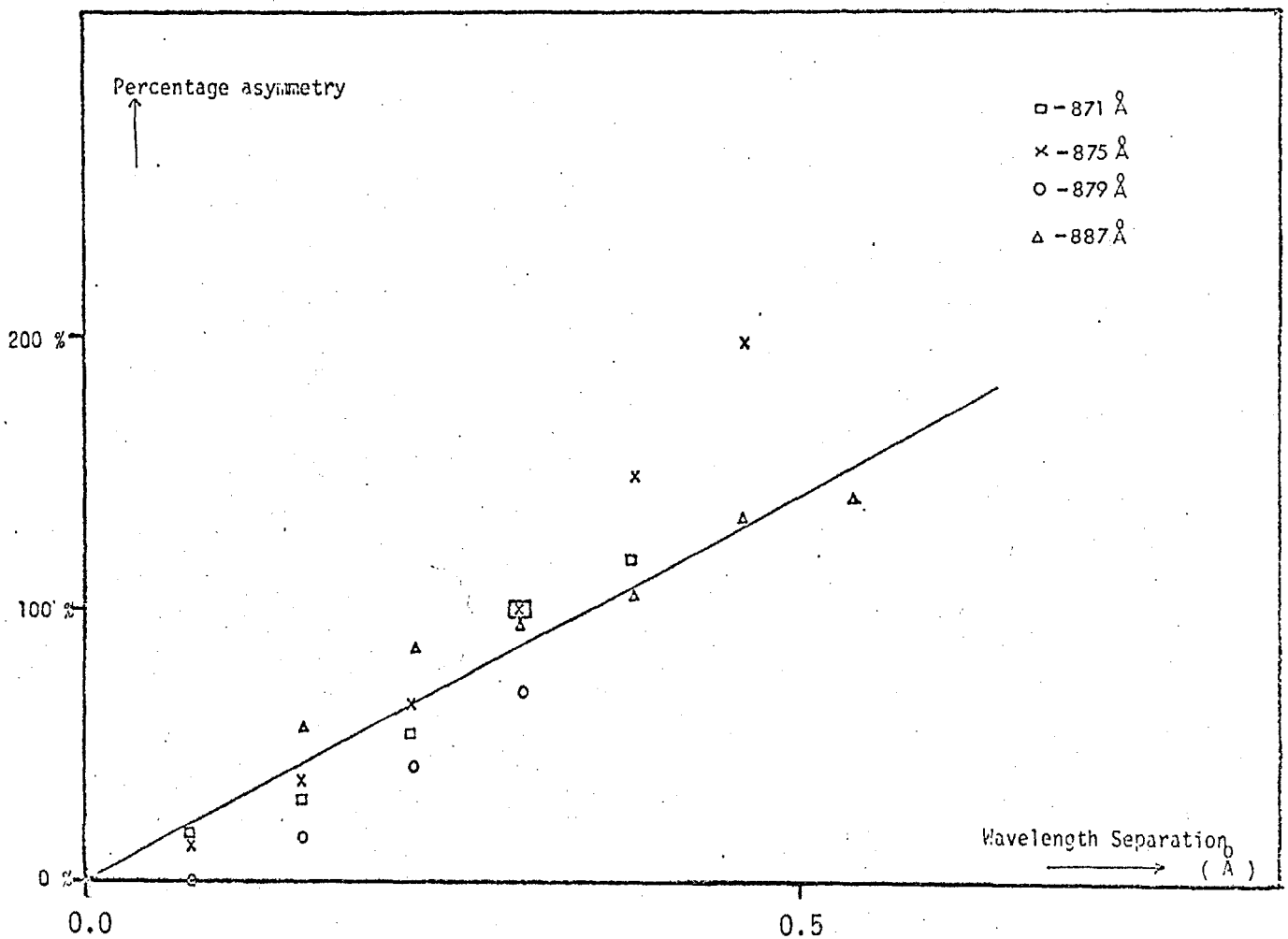

Fig 6.6 : Percentage Asymmetry versus wavelength separation for ArIII Mult 1uv

6.3 Trivial Causes of Asymmetry

6.3.1 Instrument Asymmetries

The measured asymmetries cannot be attributed to an instrument asymmetry, since the U.V. profiles and the visible profiles were taken on different spectrographs. Moreover for both spectrographs the instrument profile was extremely symmetric and showed no signs of any asymmetry of the magnitude required to explain the observed asymmetries of the emission profiles from the plasma.

6.3.2 Asymmetry due to Motion of Ions along the line of sight

Asymmetries due to the Doppler effect for emitters moving along the line of sight may be ruled out in this case. Observations are made at the time of peak compression, when the emitters are no longer collapsing into the centre of the pinch. Asymmetries due to the motion of emitters along the line of sight would be largest as the plasma is 'pinching', and at peak compression there would be no asymmetry due to emitter motion. By contrast, the asymmetries observed in the present work are most apparent at peak compression, when the line profiles are broadest. The asymmetries are undetectable at the lowest densities when the profiles are relatively narrow.

6.4 Asymmetries due to overlap with neighbouring lines

In all cases except Ar II 919 Å this source of asymmetry can be disregarded, on two counts. Firstly, as will be proved below, a consideration of the intensity produced by the overlap of two Lorentzians shows that this overlap will never result in an asymmetry which increases linearly with wavelength. Secondly, the measured asymmetries are always several orders of magnitude larger than those which would result from the overlap of neighbouring lines with the profiles concerned.

6.4.1 Frequency Dependence of the Asymmetry resulting from overlap with a nearby line.

The overlapping lines are assumed to be Stark-broadened Lorentzian profiles of the form

$$I(\omega_o + \Delta\omega) = I_o \frac{d}{\Delta\omega^2 + d^2}$$

where the peak intensity is I_o/d and the half-half width is d.

In the line wing this profile gives an intensity of approximately :-

$$I_A(\omega_o + \Delta\omega) = \frac{I_o\, d}{\Delta\omega^2} = \frac{A}{\Delta\omega^2} = I_A(\omega_o - \Delta\omega) \qquad (6.1B)$$

where $I_o\, d = A$.

Consider the overlap of the wing of this line with the wing of a second line at a frequency separation ω' from the original line. This second line contributes an intensity

$$I_B(\omega_o + \Delta\omega) = \frac{B}{(\omega' - \Delta\omega)^2}$$

$$I_B(\omega_o - \Delta\omega) = \frac{B}{(\omega' + \Delta\omega)^2}$$

Substituting into Eqn.6.1, the asymmetry produced by the overlapping line is :-

$$A(\omega) = \frac{\left[\frac{A}{(\Delta\omega)^2} + \frac{B}{(\omega'-\Delta\omega)^2}\right] - \left[\frac{A}{(\Delta\omega)^2} + \frac{B}{(\omega'+\Delta\omega)^2}\right]}{\frac{1}{2}\left[\left[\frac{A}{(\Delta\omega)^2} + \frac{B}{(\omega'-\Delta\omega)^2}\right] + \left[\frac{A}{(\Delta\omega)^2} + \frac{B}{(\omega'-\Delta\omega)^2}\right]\right]}$$

$$= \frac{\frac{B}{2}\left[\frac{1}{(\omega'-\Delta\omega)^2} - \frac{1}{(\omega+\Delta\omega)^2}\right]}{\frac{2A}{(\Delta\omega)^2} + B\left[\frac{1}{(\omega'-\Delta\omega)^2} + \frac{1}{(\omega'+\Delta\omega)^2}\right]}$$

$$\text{or} \qquad A(\omega) = \frac{\dfrac{\omega'\Delta\omega}{(\omega'^2 - \Delta\omega^2)^2}}{\dfrac{A}{B(\Delta\omega)^2} + \dfrac{\omega'^2 + \Delta\omega^2}{(\omega'^2 - \Delta\omega^2)^2}}$$

$$= \frac{\omega'\Delta\omega^3}{\frac{A}{B}(\omega'^2 - \Delta\omega^2)^2 + \omega'^2\Delta\omega^2 + \Delta\omega^4}$$

$$= \frac{\Delta\omega}{\frac{A}{B}\left[\frac{\omega'^3}{\Delta\omega^2} + \frac{\Delta\omega^2}{\omega'} - 2\omega'\right] + \omega' + \frac{\Delta\omega^2}{\omega'}}$$

Rearranging the above expression -

$$A(\omega) = \frac{\Delta\omega}{\omega'\left[(1 - \frac{2A}{B}) + \frac{\Delta\omega^2}{\omega'^2}(\frac{A}{B} + 1) + \frac{\omega'^2}{\Delta\omega^2}(\frac{A}{B})\right]} \qquad (6.2)$$

This may be written as

$$A(\omega) = \frac{\Delta\omega}{\omega'(X_1 + X_2 + X_3)}$$

where X_1, X_2 and X_3 refer to the first, second and third terms in the denominator of Eqn.6.2.

Clearly the Asymmetry $A(\omega)$ will only depend linearly on $\Delta\omega$ if X_2 and X_3 are both negligible. If $A \gg B$ or $A \sim B$ (if the perturbing lines is relatively weak) it is impossible that X_2 and X_3 should both be negligible, so that the resultant asymmetry will not fall off as a simple linear function of $\Delta\omega$. If $A \ll B$ (if the perturbing line is strong) the dominant term in the denominator is X_2 and the asymmetry will fall off as $\frac{1}{\Delta\omega}$.

6.4.2 Quantitative estimates of overlap asymmetries

Using Eqn.6.2 the wing asymmetry resulting from the nearest perturbing lines may be estimated. The nearest neighbouring transitions in both the red and blue wings are considered. The results are summarised in Table 6.1 below. It would be wrong to put too much stress on the actual numerical values of the predicted overlap asymmetries since uncertainties in estimating the relative intensities and widths of the Lorentzians might introduce errors of up to $\pm$ 50% in the resulting asymmetry. However, the asymmetries resulting from overlaps are typically between two and three orders of magnitude below those measured, which are included, for reference, in the same table. The only case where strong overlap asymmetries are predicted is that of the Ar II 919 Å transition - the only profile which shows a red asymmetry. This red asymmetry is adequately accounted for by overlap with N IV impurity lines which appear in the spectrum at 924 Å. These lines are predicted to produce a sizeable red asymmetry (about 8% at $\Delta\lambda = 1$ Å). Overlap with N II lines in the blue wing also produces a measurable asymmetry (about 3% at $\Delta\lambda = 1$ Å). The resultant overlap asymmetry is $\sim$ - 5% which is in rough agreement with the measured asymmetry of - 10%, thus accounting for the red asymmetry observed in this case.

In view of the approximate nature of the overlap asymmetry estimates, there would be little value in subtracting the predicted overlap asymmetries from the measured asymmetry, and attempting to draw any conclusions about the residual asymmetry, in this case, of Ar II 919 Å.

6.4.3 Some Comments on the Ar II Mult 6 Asymmetries with relation to Overlap Asymmetries

It should be emphasized that in the case of Ar II Mult 6 in particular the observed asymmetries are very different from the

TABLE 6.1

Calculated Overlap Asymmetries for Ar II Mult 6, Ar II Mult 1.U.V. and Ar III Mult 1.U.V. Lines Studied

Transition	Blue Wing				Red Wing				
	Nearest Line	$A/_B$	Resultant Asymmetry At a Typical $\Delta\lambda$		Nearest Line	$A/_B$	Resultant Asymmetry At a Typical $\Delta\lambda$		Measured Asymmetry At $\Delta\lambda$
			$\Delta\lambda$	$A(\Delta\lambda)$			$\Delta\lambda$	$A(\Delta\lambda)$	$A(\Delta\lambda)$
Ar II Mult 1.U.V. 919 Å	N II	2	1 Å	3%	N IV	.77	1 Å	- 8%	- 10%
Ar II Mult 1.U.V. 932 Å	N IV	.77	1 Å	0.5%	-	-	-	-	25%
Ar III Mult 1.U.V. 875.53 Å	Ar III 871.1Å	.84	0.32 Å	0.1%	Ar III 878.73 Å	.84	0.32 Å	-0.5%	100%
Ar II Mult 6 4848 Å	Ar II 4806 Å	.55	5.0 Å	1%	Ar II 4903 Å	.33	5.0 Å	-0.2%	58%
Ar II Mult 6 4806 Å	Ar II 4736 Å	2.1	5 Å	0.06%	Ar II 4848 Å	1.8	5 Å	-0.3%	88%

asymmetries expected due to overlap, since the overlap effects would be very different for the two lines. From Table 6.1 for a wavelength separation of 5 Å, 4848 Å is expected to show a blue overlap asymmetry of order + 0.8%, while 4806 Å is predicted to show a red asymmetry of order - 0.24%. This should be compared with measured asymmetries which are blue asymmetries in both cases and of order 75% at this wavelength separation, the measured asymmetries being the same to within an error of about ± 15%.

6.5 Other Non-Pressure-Broadening Causes of Asymmetry

In line broadening calculations the ω^4 factor in the quantum mechanical expression for the power radiated by an ion is assumed to be constant for each line. This is not justifiable for broad lines, and can give rise to measurable asymmetries. Partially compensating this ω^4 asymmetry is the consideration that all substates of the initial state were assumed to be equally populated whereas inclusion of a Boltzmann factor would introduce a red asymmetry. Further, the transformation from angular frequencies to reduced wavelengths, through $\Delta\omega = \frac{\Delta\lambda}{2\pi c \lambda_o^2}$, is only approximately valid since it assumes $\frac{\Delta\lambda}{2\pi c\,(\lambda_o + \Delta\lambda)^2} \approx \frac{\Delta\lambda}{2\pi c \lambda_o^2}$ and introduces errors of order $2\Delta\lambda / \lambda_o$, giving asymmetries which favour the blue wing.

The asymmetry due to these three causes may be written

$$\frac{I_R - I_B}{\frac{1}{2}(I_R + I_B)} = -A(\omega) \approx \left(-6 + \frac{hc}{\lambda_o kT}\right) \cdot \frac{2\Delta\lambda}{\lambda_o} \qquad (6.3)$$

(Griem 1964, p.94).

The asymmetries arising from non pressure-broadening causes, as calculated from Eqn.6.3 are compared with the measured asymmetries in Table 6.2 below.

TABLE 6.2

Calculated Asymmetries due to Non-Pressure Broadening Causes

	$\Delta\lambda$	$A(\Delta\lambda)$ Non-pressure Broadening	$A(\Delta\lambda)$ Measured
Ar II Mult 1.U.V. λ_o = 932 Å	1 Å	- 0.05% (red wing higher)	+ 25%
Ar III Mult 1.U.V. $\overline{\lambda_o}$ = 875 Å	0.32 Å	- 0.04%	+ 100%
Ar II Mult 6 λ_o = 4848 Å	5.0 Å	+ 0.35%	+ 58%

Except in the case of the visible Ar II lines, the asymmetry predicted by Eqn.6.3 produces enhanced red wings, as opposed to the enhanced blue wings observed. For Ar II Mult 6, the predicted asymmetry from this cause is too small to account for the observed asymmetry by two orders of magnitude.

6.6 Ion Broadening

Since the dominant broadening mechanism for these lines is electron impact broadening, the profiles are expected to be symmetrical Lorentzians. In the line wings, the impact approximation is valid for

the electrons to well beyond the wavelength separations of present interest (i.e. valid for Ar II Mult 6 to $\Delta\lambda \sim 1200$ Å, for Ar II Mult 1.U.V. to ~ 120 Å, and for Ar III Mult 1.U.V. to ~ 100 Å).

However the inclusion of corrections due to quasistatic ion broadening might be expected to introduce asymmetries into the otherwise symmetrical Lorentzian profiles. The quadratic Stark effect will become most important at high field strengths, i.e. at great distances from line centre. As discussed in Section 1.5.4, at large distances from line centre, corresponding to close perturbers, the inhomogeneity of the perturbing field will also become important, and quadrupole corrections should be included in the calculation of the line profile as well as corrections for the quadratic Stark effect.

According to Griem (1974), the ratio of the line wing intensities due to quasistatic ion broadening $I_i(\omega)$, and due to electron impact broadening $I_e(\omega)$ is

$$\frac{I_i(\omega)}{I_e(\omega)} \approx 0.7 \left(\frac{kT}{E_H}\right)^{\frac{1}{2}} \left(\frac{N_p \; n^{\frac{1}{2}} \; Z_p^{\,3/2}}{NZ}\right) \left(\frac{\hbar\omega}{E_H}\right)^{1/4} \tag{6.4}$$

where N_p is the ion number density, n is the effective principal quantum number of the upper state of the transition, Z_p is the perturber charge, and $Z = 1$ for neutrals, $Z = 2$ for singly-ionized emitters, etc.

Griem (1974) gives the correction due to quadrupole interactions, relative to the wing intensity due to ion broadening as :-

$$\frac{\Delta I}{I} \approx \left(\frac{Z^2}{20n\, Z_p}\right)\left(\frac{E_H}{\hbar\omega}\right)^{\frac{1}{2}} \quad \text{for} \quad \ell \geq 1$$

$$\frac{\Delta I}{I} = 0 \quad \text{for} \quad \ell = 0 \tag{6.5}$$

For all the asymmetric profiles under discussion in this chapter, the optical electrons are s-electrons, so from Eqn.6.5 $\Delta I/I = 0$. Thus quadrupole effects do not contribute to the ion broadening for these lines, the ion broadening correction to the Lorentzian wing intensity being due to quadratic Stark effects.

Table 6.3 compares the measured asymmetry $A(\Delta\lambda)$ at a wavelength separation $\Delta\lambda$ with percentage wing intensity due to ion broadening at this wavelength separation, calculated from Eqn.6.4.

TABLE 6.3

Ion Broadening Contribution to Wing Intensities for Ar II Mult 1.U.V., Ar II Mult 6 and Ar III Mult 1.U.V.

	$\Delta\lambda$	$A(\Delta\lambda)$ measured	% Wing contribution due to ion broadening at $\Delta\lambda$
Ar II Mult 1.U.V. 932 Å	1 Å	+ 25%	3.5%
Ar II Mult 6. 4848 Å	5.0 Å	58%	2.7%
Ar III Mult 1.U.V. 875 Å	0.32 Å	+100%	2.0%

Since at the frequency separation of interest, ion broadening contributes a negligible amount ($< 3.5\%$), asymmetries due to the quadratic Stark effect cannot account for the large asymmetries observed.

6.7 Asymmetries due to plasma inhomogeneity

It might be argued that the observed asymmetries are due to inhomogeneities in the plasma along the line of sight. The line from a dense part of the plasma will have width d_1 and shift s_1, while from a less dense region outside the core the width of the line will

be d_2 and the shift s_2, where $d_2 < d_1$, $s_2 < s_1$. Thus the superposition of the profiles will give a total profile which is asymmetric. However such arguments are not tenable in this case.

First, the predicted Stark shifts are small for these lines, even for the core densities of 2×10^{18} cm^{-3} (see Appendix 3). Thus the resulting asymmetries would be very small. Table 6.4 presents the results of a very approximate calculation of the resulting asymmetry. Equations 6.1B and 6.2 are used for the model for these calculations. The resulting asymmetry in the line wing is calculated for the superposition of two Lorentzians, one shifted by s_1 and of width d_1, corresponding to emission from an outer region of density 0.5×10^{18} cm^{-3} and one of the same intensity, and width d_2 shifted by an amount equal to the predicted Stark shift s_2 at a core density 2×10^{18} cm^{-3}. The assumption that the shifted and unshifted Lorentzians are of the same intensity is based on the hypothesis that the temperature of the plasma does not change too drastically from dense to less dense regions, since this intensity depends chiefly on the temperature and only weakly on the density. If this hypothesis is not true (i.e. if the temperature falls off rapidly outside the dense core) the intensity from the low density surrounding regions will be negligible, and the problem of spatial inhomogeneity asymmetries will not arise. Thus the assumption that the Lorentzians must be of roughly equal intensity if this asymmetry contribution is to be important may be justified on physical grounds. On the basis of this somewhat crude model, the percentage asymmetry $A(\Delta\lambda)$ at a wavelength separation $\Delta\lambda$ may be estimated, and compared with the measured asymmetry. (Table 6.4).

Although these calculations of the asymmetry due to plasma inhomogeneity are only approximate, they are unlikely to be in error by more than 100%. Even with an error of this magnitude the asymmetries could not be explained in these terms since the calculated asymmetries are smaller than the observed asymmetries by almost 2 orders of magnitude.

TABLE 6.4

Estimated Asymmetry due to Spatial Inhomogeneity

	Stark shift s for $n_e=2\times10^{18}cm^{-3}$	$\Delta\lambda$	Asymmetry due to spatial inhomogeneity	Measured Asymmetry
Ar II Mult 1.U.V.	- 0.013 Å	1 Å	0.3%	25%
Ar III Mult 1.U.V.	- 0.006 Å	.32 Å	0.4%	100%
Ar II Mult 6.	- 0.3 Å	5 Å	1.2%	~73%

Moreover, this source of asymmetry can also be dismissed on the grounds that it would produce asymmetries of a quite different nature from those observed. Asymmetries due to inhomogeneities will be most important nearer line centre. The intensity in the far wings is entirely due to emission from the densest part of the plasma. Thus the wing intensities will be symmetric about a wavelength which is shifted by an amount s from line centre. If the symmetry of the wings is considered with respect to the peak intensity of emission from a less dense region, this corresponds to introducing an error in the line centre position of size $\leq$ s. In the wings this will produce an asymmetry which does not depend strongly on the wavelength separation from line centre. By contrast, the observed asymmetries apparently increase rapidly with wavelength separation from line centre.

Thus the observed asymmetries cannot be attributed to plasma inhomogeneities along the line of sight.

6.8 Asymmetries due to the Contributions of Perturber Radiation

As demonstrated in previous sections, the observed asymmetries cannot be satisfactorily explained in terms of the usual asymmetry sources.

Instead alternative explanations must be considered.

In 1968, Burgess suggested that inclusion be made of the coupling of the perturbing electrons with the transverse radiation field, hitherto neglected in theories of electron-impact broadening. According to the treatment presented by Burgess in the same publication, the inclusion of the resulting interference terms leads to asymmetries of the lines of ionized emitters, with an enhanced blue wing, which might, under the special circumstances discussed in Section 6.8.2 below be observable for some spectral lines.

6.8.1 Some Comments on the Nature of the Asymmetry predicted by Burgess (1968).

Burgess (1968) proposed that the absorption profile $\sigma(\omega)$ should be calculated by summing three types of contribution; namely, the contribution σ_1 due to interactions of photons with bound electrons, contributions σ_2 due to interactions involving photons and free electrons, and contributions σ_3 due to interactions involving photons and bound and free electrons.

$$\sigma = \sigma_1 + \sigma_2 + \sigma_3$$

The term σ_1 corresponds to the usual electron-impact broadened Lorentzian profile, and σ_2 corresponds to the continuum radiation, practically constant over the profile. Contributions of the kind σ_3 have previously been neglected.

Consider the possible routes for photon absorption, assuming that the initial state comprises a ground state ion and a free electron.

The first route (a) involves Bremsstralung absorption, the free electron absorbing energy $h\nu$ from the field of the ionized species. The final state after this process is a ground state ion and an excited free electron.

Secondly, consider absorption in the wing of a pressure-broadened line (route (b)). Absorption of a photon causes excitation of the bound electron to an off-resonance virtual state of the ion. Then interaction with the free electron can cause a transition back to ground, so that the final state in this case is a ground state ion plus an excited free electron which has received energy $h\nu$.

The first route, (a), corresponds to the terms represented by σ_2, while the second (b) corresponds to terms represented by σ_1. The routes (a) and (b) have exactly the same initial and final states (ground state ion plus free electron plus photon $h\nu$ going to ground state ion plus excited free electron with energy $h\nu$). However in general the probability amplitude phase will be different for these two routes, giving rise to interference terms, σ_3. Asymmetries arise because the probability amplitude for route (b) goes as $\frac{1}{\omega - \omega_o}$.

The formal treatment is similar to that for profiles of transitions to autoionizing states in unperturbed atoms, and the asymmetries predicted are similar to the Fano shapes obtained in the autoionization process.

6.8.2. Conditions for Asymmetry to be large

Clearly photon absorption by route (b) only involves transitions between the upper and lower states of a transition, so contributions of these interference terms will be most important when the broadening by interaction between the upper and lower states of the line contributes a large part of the broadening of the line.

If the ground state is a multiplet with different j-values for each level, processes of type (b) can result in transitions back to different j-levels in the ground state. In this case, since the j-value of the ground state ion will be unaltered by Bremsstrahlung absorption, the lines of the multiplet most strongly affected by interference terms will be the $\Delta j = 0$ transitions.

6.8.3 Inclusion of Interference Terms in the Line Shape

The total line shape may be written :-

$$\sigma(\omega) = \sigma_1 + \sigma_2 + \sigma_3$$

$$= \frac{A}{(\omega-\omega_o)^2} + C(\omega) + \frac{B}{(\omega-\omega_o)} \qquad (6.6)$$

where $C(\omega)$ is essentially constant over the line. Burgess (1968) estimated the possible asymmetry due to the contributions of process (b) as :-

$$\frac{\sigma_3}{\sigma_1} = 2\sqrt{2}\,\frac{Z}{m\omega_o^2}\,\frac{2(\ell_b + 1)\,(E_a - E_b + h\nu)}{\left[I(a,b)\right]^2\,\max(\ell_a, \ell_b)} \qquad (6.7)$$

where subscripts a,b refer to the lower and upper states of the transition respectively. Z_e is the charge seen by the perturbing electron. $I(a,b)$ is the transition integral.

For a given wavelength separation from line centre, the percentage asymmetry is independent of perturber density. Thus as the density is raised a given percentage asymmetry will occur at a smaller number of half-widths from line centre, since the half-width of the Lorentzian component σ_1 is proportional to the perturber density. Hence at high densities the asymmetry becomes more noticeable.

The asymmetry is predicted to increase linearly with frequency separation. The shape of the profile (Eqn.6.6) is the same as the Fano profile for the case when $(\omega - \omega_o)$ is large compared with the half-width.

The theoretical treatment by Burgess, which leads to Eqn.6.7, predicts an enhanced blue wing, although it is not clear physically why the asymmetry should always be in this direction. Nor is it clear

why the asymmetry should depend on ℓ_b, the ℓ-value of the intermediate state for process (b), although an ℓ-dependence is predicted by Eqn.6.7.

6.8.4 Importance of Perturber Contribution Corrections to the profiles of Ar II and Ar III Studied

The Ar II ($3s^2\ 3p^5\ {}^2P^o \longrightarrow 3s\ 3p^6\ {}^2S$) and Ar III ($3s^2\ 3p^4\ {}^3P \longrightarrow 3s\ 3p^5\ {}^3P^o$) U.V. resonance lines both involve transitions of an inner shell electron. Thus the nearest interacting level to the upper state will lie very high in energy, and the broadening is due mainly to the interaction between the upper and lower states, with transitions from the lower state to other high lying levels contributing only a small amount of the width. Thus both these transitions will be very likely to show asymmetries of the type discussed above. On the basis of the somewhat crude semi-empirical calculations discussed in Appendix 3, broadening due to interactions between the upper and lower state account for 54% of the broadening for the Ar II U.V. resonance lines and 53% of the broadening for the Ar III U.V. resonance lines. Upper-lower state interaction is also the dominant mechanism in the broadening of the lines of Ar II Mult 6 ($4s\ {}^4P - 4p\ {}^4P$) since, purely accidentally, the lower state happens to be the closest interacting level to the upper state of the optical transition.

6.8.5 Estimates of these Asymmetries for the Ar II and Ar III Lines Studied

Using the line strengths quoted by Wiese (1966) and the usual relations for the line and multiplet factors (see, for example, Shore and Menzel 1968), the transition integral I(a,b) can be estimated. Hence the wavelength separation, $\Delta\lambda_c$, from line centre at which 10% asymmetry occurs between the blue and red wings can be estimated

from Eqn.6.7. In Table 6.5, the values of $\Delta\lambda_c$ calculated from Eqn.6.7 are compared with the wavelength separation $\Delta\lambda_M$ at which 10% measured asymmetry occurs.

TABLE 6.5

Calculated asymmetry due to coupling of perturbing electrons with the transverse radiation field

	Estimated Transition Integral $I(a,b)^2$	Calculated Wavelength separation for 10% asymmetry $\Delta\lambda_c$	Measured Wavelength separation for 10% asymmetry $\Delta\lambda_M$
Ar II Mult 1.U.V. $3s^2\ 3p^5\ 2p^o \rightarrow$ $3s\ 3p^6\ {}^2S$	.1215	0.336 Å	~ 0.4 Å
Ar III Mult 1.U.V. $3s^2\ 3p^4\ {}^3P \rightarrow$ $3s\ 3p^5\ {}^3p^o$	.0944	0.13 Å	~ 0.032 Å
Ar II Mult 6. $3p^4\ 4s\ {}^4P \rightarrow$ $3p^4\ 4p\ {}^4p^o$	17.3	32 Å	~ 1 Å

The calculated wavelength separations at which a given asymmetry occurs, $\Delta\lambda_c$, are only approximate because of uncertainties in the theory. To begin with, the treatment of Burgess (1968) is based on perturbation theory to second order.

Secondly, the treatment of the effect by Burgess (1968) depends on relating radial integrals dependent on $(1/r)$ and r through assuming a Coulomb approximation for the ion field seen by the perturber. While the Coulomb approximation is probably a good approximation for Ar II Mult 1.U.V. and Ar III Mult 1.U.V., since these transitions correspond

to inner shell transitions, when the optical electron lies within the 3p shell and so does not see much of $3p^6$ electrons, the Coulomb approximation will not be so good for Ar II Mult 6. In this latter case the transition is $3p^4\ 4s$ to $3p^4\ 4p$, so the field of the ion as seen by the optical electron will be perturbed by the 3p electrons. Thus in this case the Coulomb approximation will not be so good, and the treatment presented by Burgess (1968) will not be expected to yield good quantitative predictions for the asymmetry.

In view of these uncertainties it is the close quantitative agreement between $\Delta\lambda_C$ and $\Delta\lambda_M$ for Ar II Mult 1.U.V. and Ar III Mult 1.U.V. that is surprising, rather than the poor agreement in the case of Ar II Mult 6.

Moreover the approximate fit to a linear increase of asymmetry with wavelength separation (which is particularly well demonstrated for the Ar II Mult 6 lines) would agree with the predictions of Eqn. 6.7. The Ar III Mult 1.U.V. lines showed no evidence for the predicted Δj dependence of the asymmetry.

6.8.6 Conclusions

In view of the approximate nature of the theoretical calculations it would be wrong to put too much emphasis on quantitative agreement with theory. However all the other usual causes of asymmetry have been shown to be unimportant for these lines. Thus it is apparent from the above discussion that unless some quite unknown mechanism is involved, the only predicted effect which would yield asymmetries of the size observed is the effect predicted by Burgess (1968).

CHAPTER VII

An Experimental Study of Lyman$_\alpha$ at High Electron Densities

7.1 Introduction

A number of effects might be expected to affect the profile of Lyman$_\alpha$ at high densities, for a variety of reasons, as discussed below.

7.1.1 The influence of Quasimolecular States

As pointed out by Stewart, Peak and Cooper (1973), the influence of perturbing ions in the immediate vicinity of an emitter will affect the optical electron of the emitter. For the case of Lymanα perturbed by nearby protons H^+, Stewart et al predicted that the perturbation would give rise to satellite-like features in the wings of the transition.

Under the influence of a close perturbing ion, the optical electron is likely to spend an increasing amount of time "on" the perturbing ion, as opposed to the emitting ion, without actually becoming bound. The emitter, the perturbing ion and the electron can be considered to form a "quasi-molecule". When the interatomic potentials lie parallel for a range of different radii, this produces a satellite at the energy separation in question. Detailed calculations for this effect are difficult, since this is essentially a three-body problem, so at present little quantitative information is available for the satellite positions. However, as pointed out in Section 1.5.2, it is reasonable to expect that at high densities the probability of observing quasimolecular features will be greater, since the likelihood of an ion lying close enough to an emitter to affect the optical electron will be much greater.

Further calculations for proton perturbers were carried out by Le Quang Rang and Voslamber in 1975.

Previous experimental studies of Lyman α from low concentration hydrogen in plasmas which are predominantly singly-ionized argon show satellites similar to those predicted for proton perturbers, although these occur at different wavelengths from those theoretically predicted for proton perturbers. Both Quefflec and Girault (1973) and Preston (1977) observed such satellite-like features in the wings of Lyman α, emitted from argon-hydrogen mixture plasmas. There is some uncertainty about whether the satellites should in these cases be attributed to proton perturbers (after Stewart et al. 1973) or to Ar^+ perturbing ions.

Previous work on these features is summarised in Table 7.1 below.

TABLE 7.1

Lyman α Satellites previously predicted or Found Experimentally

Paper	Theory or Experimental	Satellite Positions	Attributed to
Stewart et al. 1973	Theory	+17.8Å, +24.8 Å, +189.2Å, -0.48Å -109.2Å, -197.7Å -250.7Å	Proton perturbers
Fussmann 1972	Experiment in Ar plasma	+ 38 Å	Not commented on at time of publication.
Quefflec and Girault 1974	Experiment in argon/hydrogen plasma	+ 16.5 Å	Proton perturbers
Le Quang Rang and Voslamber 1975	Theory	+ 18.6 Å + 25.6 Å - 108.7 Å	Possibly proton perturbers, although Ar^+ perturbers are not excluded.
Preston 1977	$n_e \sim 10^{17}$ Experiment in argon/hydrogen plasma	+ 37 Å + 190 Å	Ar^+ perturbers
This Work	$n_e \sim 3 \times 10^{18}$ Experiment in argon/hydrogen plasma	-31.5Å, -15.9Å +8.3 Å, +16.9Å + 40.1Å, +23.9Å	Ar^+ and Ar^{++} perturbers

7.1.2 Plasma Satellites

As discussed in Section 1.5.3, because of the high energy density in electrostatic waves in this plasma, it is possible that plasma frequency satellites may be excited by purely thermal fluctuations.

Ya'akobi and Bekefi (1969) reported a thermally-excited satellite near the 2P - 3P forbidden line of a lithium plasma. The density and temperature conditions in their experiment corresponded to a low number of particles per Debye sphere ($N_D \sim 1.7$), corresponding to nearly one percent of the total energy in electrostatic waves.

The density and temperature conditions in the lithium plasma discussed above are in some ways similar to those in the argon plasma of this experiment. The diagnostic measurements on the pinch indicate that similarly low concentrations of particles per Debye sphere can be achieved in this source, N_D(minimum) being ~ 3.0. In this case 0.5% of the total energy would be in the form of electrostatic waves, so that it is arguable that in this source plasma satellites could be similarly excited.

However, plasma satellites of the kind predicted by Baranger and Mozer (1961), would not be expected for Lyman α, strictly speaking, since this formalism requires the existence of a forbidden component in the wing of the allowed line. Thus the application of Baranger and Mozer's (1961) expression for the intensity of the satellites relative to the forbidden component would be of little relevance in this case.

7.1.3 Asymmetry due to Quadrupole Interactions

For reasons discussed in Section 1.5.4, the profile of Lyman α is predicted to show an asymmetry due to quadrupole interactions, the asymmetry becoming more important at higher densities.

To date, all the theoretical calculations of the asymmetry have been confined to the density and temperature conditions of an experiment by Boldt and Cooper (1964) in which the asymmetry of the wings of Lyman α was measured (i.e. $n_e = 8.4 \times 10^{16}$ cm^{-3}; $T_e = 12{,}200$K).

The asymmetry of Lyman α is usually discussed in terms of the parameters $(\Delta\lambda)_1$ and $(\Delta\lambda)_2$. If λ_1 and λ_2 are the red- and blue-wing wavelengths at which the specific intensity is identical, $(\Delta\lambda)_1$ and $(\Delta\lambda)_2$ are defined from :-

$$\begin{aligned} (\Delta\lambda)_1 &= \frac{1}{2}(\lambda_1 - \lambda_2) \\ (\Delta\lambda)_2 &= \frac{1}{2}(\lambda_1 + \lambda_2) - \lambda_o \end{aligned} \qquad (7.1)$$

where λ_o is the wavelength of line centre.

Sholin (1969) obtains an expression for $(\Delta\lambda)_2$ in terms of $(\Delta\lambda)_1$, applicable to the density and temperature of the Boldt and Cooper (1964) experiment :-

$$(\Delta\lambda)_2 = 1.58 \times 10^{-2} \; (\Delta\lambda)_1^{3/2}$$

More recent calculations by Bacon (1973) for the same density yield smaller asymmetry.

Sholin (1969) treats the electrons by the impact approximation and the ions by the quasi-static approximation. Fussmann (1973) observed an asymmetry in accordance with the calculations of Sholin (1969) up to $(\Delta\lambda)_1 \sim 5.0$ Å and then a gradual turn over to smaller asymmetry, this data crossing the predicted curve by Bacon (1973) at $(\Delta\lambda)_1 = 7$ Å. This turn-over to smaller asymmetry was attributed to the change from impact to quasistatic approximations for the electrons. According to Griem (1964) the turn-over occurs at a much larger wavelength separation, namely:-

$$\Delta\lambda = \frac{\lambda_o^2 \, kT}{c \, h \, n^2} \qquad (7.2)$$

which corresponds to $\Delta\lambda = 31$ Å in the Fussmann experiment.

The other chief cause of asymmetry is the "trivial asymmetry" discussed by Griem (1964). This arises from the assumption that the spectral line broadening is considerably smaller than the line wavelength, so that the effective transition probability is constant throughout the line profile. This results in an asymmetry which is small compared with the asymmetry predicted by Sholin (1969) and by Bacon (1973) for the particular conditions of the experiment of Boldt and Cooper (1964).

7.2 This Experiment

The profile of Lyman α has been studied in the high density plasma of this experiment by introducing into the pinch a small amount (1%) of hydrogen. The presence of hydrogen in this concentration did not disturb the pinch characteristics. The profile of Lyman α was studied in emission. Studies in the region of line centre are not possible because the line is self-reversed by cold hydrogen outside the pinch. Problems of optical thickness would thus preclude any studies of the line in this region. The usual rule of thumb requires that for a resonance line ($f \sim 1$) of a gas at a pressure 1 milli-torr, the geometric depth of plasma must be of order 1 micrometer for the transition to be optically thin at line centre. For the case of Lyman α in this plasma, this corresponds to the requirement that the geometric depth be of order 3×10^{-5} mm or less for the line centre to be optically thin, which should be compared with the measured geometric depth of about 1.0 mm.

However, the features of interest at these densities are all

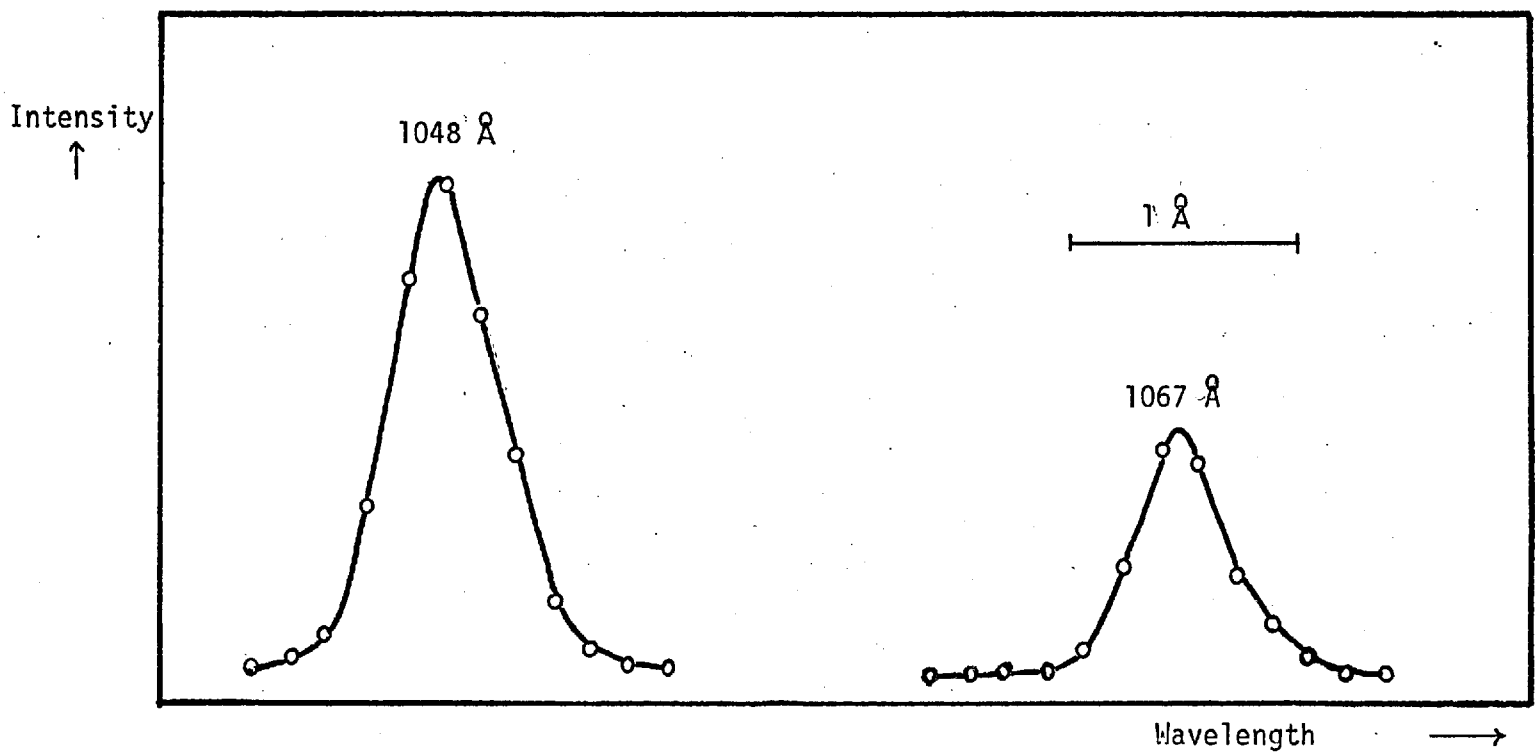

Fig 7.1 : Instrument Profile : Ar I Mult 1u.v. lines emitted from a cooled-cathode discharge.

concerned with the line wings, rather than the region near line centre. In these experiments, measurements were made from line centre to 40 Å in the wings, the measured (apparent) half-half width of Lyman α being about 2.5 Å in this experiment.

7.3 Apparatus

The measurements were made on the 1 metre scanning vacuum monochromator (discussed in Chapter IV) fitted with a 1200 lines/mm, 1200 Å - blazed grating.

The signal was detected using an R.C.A. 1P21 photomultiplier, coated with a scintillating compound, sodium salicylate, in order to make the photomultiplier sensitive to U.V. radiation.

The instrument profile was found by running a cooled-cathode discharge in argon and measuring the profiles of Ar I 1048 Å and 1067 Å. The profiles gave an instrumental full-half width of about 1/2 Å. The instrument profile showed no signs of asymmetry, nor of any grating ghosts. Fig.7.1 shows a typical instrument profile. The profile of Ly_α was scanned from shot to shot. The monochromator could be advanced in steps of $\sim$ 1/6 Å. It was usually more practical to scan in steps of 1/2 Å, except on occasions where the exact wavelengths of Ly_α and associated features were needed, when the profile was scanned in steps of 1/6 Å. The profile was scanned from the line centre to about $\pm$ 40 Å in the wings. Scans were made for a variety of density and temperature conditions.

7.4 Results

A typical scan is shown in Fig.7.2 for a bank voltage 5 KV and filling pressure 0.55 Torr. The profile is self-reversed, and slightly asymmetric, with an enhanced red wing. In addition, the profile shows a number of satellite-like features in both the red and blue wings. Of these features, S_{5-}, S_{4-} and S_{2-} in the blue wing,

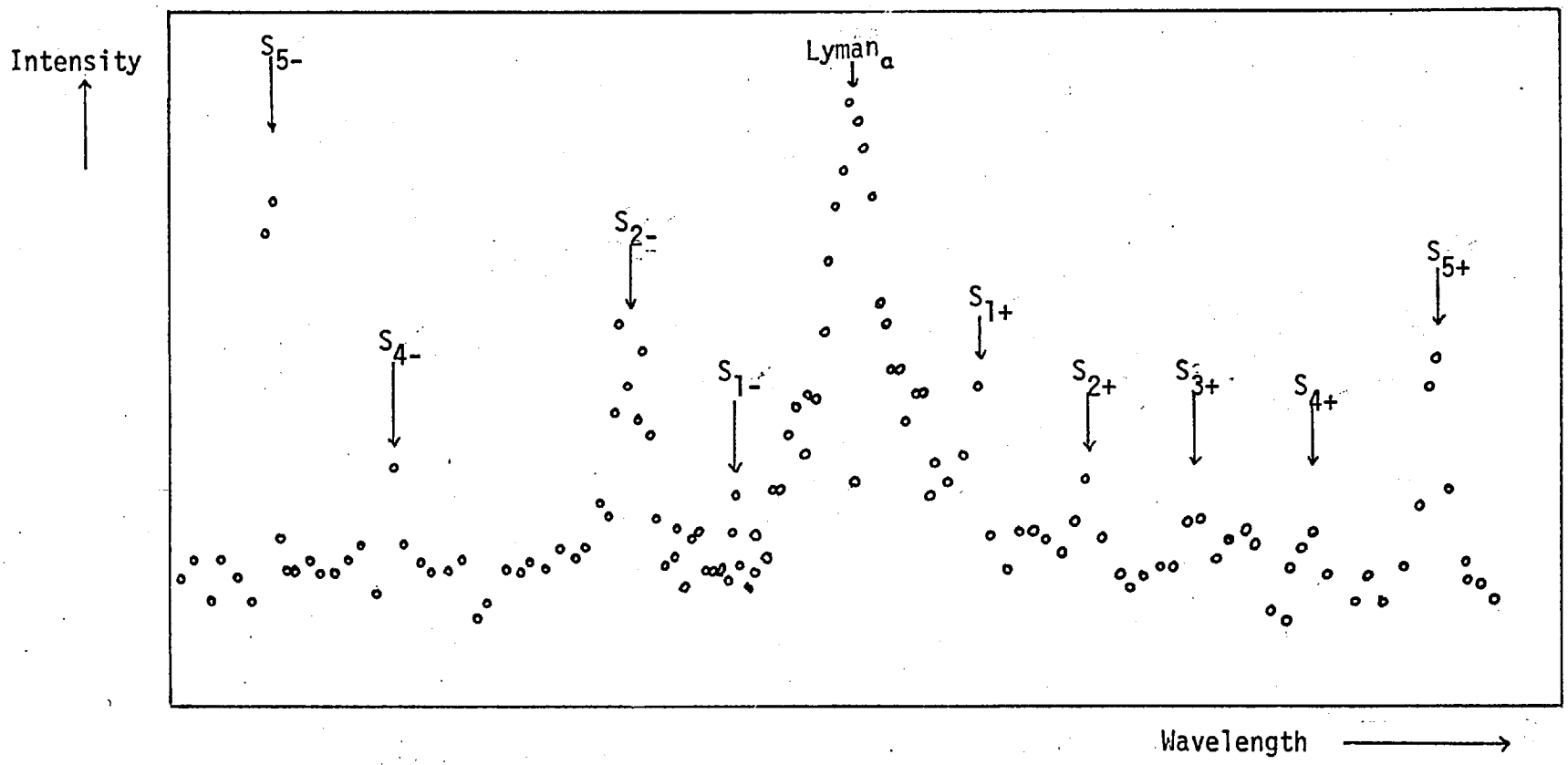

Fig 7.2 : A scan of Lyman$_\alpha$ showing satellite-like features in the wing.
Bank Voltage 5kV, filling pressure 0.55 Torr.

and S_{1+}, S_{2+} and S_{5+} in the red wing are most intense. There are also fainter features, S_{3-}, S_{1-} in the blue wing and S_{3+}, S_{4+} in the red wing.

7.5 Possible Origins of the Satellite-like Features in the Wings of Lyman α

7.5.1 Grating Ghosts

Since the instrument profile shows no evidence of any grating ghosts to a relative intensity of 1 in 10^3, the possibility that these features in the wing of Lyman α are grating ghosts can be discounted.

7.5.2 Impurity Lines

Table 7.2 lists the wavelengths of the satellite-like features, together with the possible impurity lines to which these features might correspond.

Many of the impurity lines can be discounted, since they arise from species which would not be compatible with the temperature in the source. For example, the plasma consists of Ar II (ionization potential 27.63 eV) and Ar III (ionization potential 40.91 eV), no Ar I emission is observed. Thus any species with an ionization potential lower than that of Ar I (15.76 eV) is expected to be completely "burnt through" to higher ionization stages.

Other impurity lines can be discounted since they would require unreasonably large errors in the measured wavelengths of the features (the measured wavelengths are expected to be good to $\pm$ 0.2 Å).

Moreover, as discussed in Section 1.4.4, the middle of the plasma column is expected to be completely free from electrode impurities, so these impurity lines may also be ruled out.

Some of the impurity lines are also very weak, and therefore unlikely to correspond to the intense satellite features observed.

TABLE 7.2

Wavelengths of the Lyman α Satellite Features and Possible Corresponding Impurity Lines

Satellite Feature Observed			Nearest Possible Impurity Lines			
	λ (Å)	Δλ (Å) From line centre	Impurity	λ (Å)	* Intensity	Comments
S_{5-}	1175.8	-39.9	C III	1175.7	1000	Cannot be ruled out at this stage.
S_{4-}	1184.1	-31.5	N III	1184.5	400	Unlikely, requires error of 0.4Å in measured wavelength.
S_{3-}	1192.0	-23.7	C I	1192.2	70	Unlikely, pinch too hot for C I.
			Al II	1191.8	100	Electrode impurity, thus unlikely at pinch stage.
			Si III	1192.3	-	Cannot be ruled out at this stage.
S_{2-}	1199.8	-15.9	N I	1199.5	1000	Unlikely, pinch too hot for N I.
S_{1-}	1207.4	- 8.3	Si III	1207.5	180	Cannot be ruled out at this stage.
(Ly α)	1215.7	0			1000	- -
S_{1+}	1224.0	+ 8.3	Si II	1223.9	20	Unlikely, pinch too hot for Si II, also weak impurity line.
S_{2+}	1232.6	+16.9	N I	1231.6	5	Unlikely, pinch too hot for N I, also weak impurity line.
S_{3+}	1239.6	+23.9	Al IV	1240.2	100	Unlikely, requires error of 0.8Å in measured wavelengths, also this is an electrode impurity.
			Mg II	1239.9	-	Unlikely, pinch too hot for Mg II, also this is an electrode impurity.
S_{4+}	1244.3	28.6	N IV	1244.9	50	Unlikely, requires error of 0.6Å in measured wavelength
S_{5+}	1255.8	40.1	Si I	1255.3	10	Unlikely, requires error of 0.5Å in measured wavelength, also weak impurity line.
			Si I	1256.5	40	Unlikely, requires error of 0.7Å in measured wavelength.

* As quoted by K.L.Kelly "Atomic Emission Lines Below 2000 Å" N.R.L.Report

As may be seen from Table 7.2, there are no possible impurity lines that would correspond to the observed features at S_{4-}, S_{2-}, S_{1+}, S_{2+}, S_{3+}, S_{4+} and S_{5+} in this pinch. The possibility that S_{5-}, S_{3-} and S_{1-} are impurity lines cannot be ruled out at this stage.

7.5.3 The Dependence of the Satellite Features on the Hydrogen Concentration in the Pinch

Fig.7.3 shows on the same intensity scale two scans of Lyman α with identical firing conditions (5 KV bank voltage, and 0.1 Torr filling pressure), but with different hydrogen concentrations. For Scan (1) the hydrogen concentration is 1% hydrogen in argon, and for Scan (2) the pinch was run in pure (99.99%) argon, the Lyman α emission arising from the very small concentration of residual hydrogen in the pinch.

With the exception of S_{5-} and S_{3-}, the satellite features all become less intense when the hydrogen concentration is reduced. The intensity of Lyman α also falls with the hydrogen concentration. The continuum intensity appears to be lower when the hydrogen concentration is smaller, although this apparent reduction is probably simply due to the reduction in the Lyman α wing intensity.

Table 7.3 compares the intensities of the satellite for the two different hydrogen concentrations. The clear dependence of the intensity of these features on the hydrogen concentration and on the Lyman α intensity indicates that these features cannot be simply impurity lines, but that their origin must be linked with the pressure of hydrogen in the plasma.

Because the features designated S_{5-} and S_{3-} show no dependence on the hydrogen concentration, these features have been attributed to impurity lines. This is not inconsistent with the

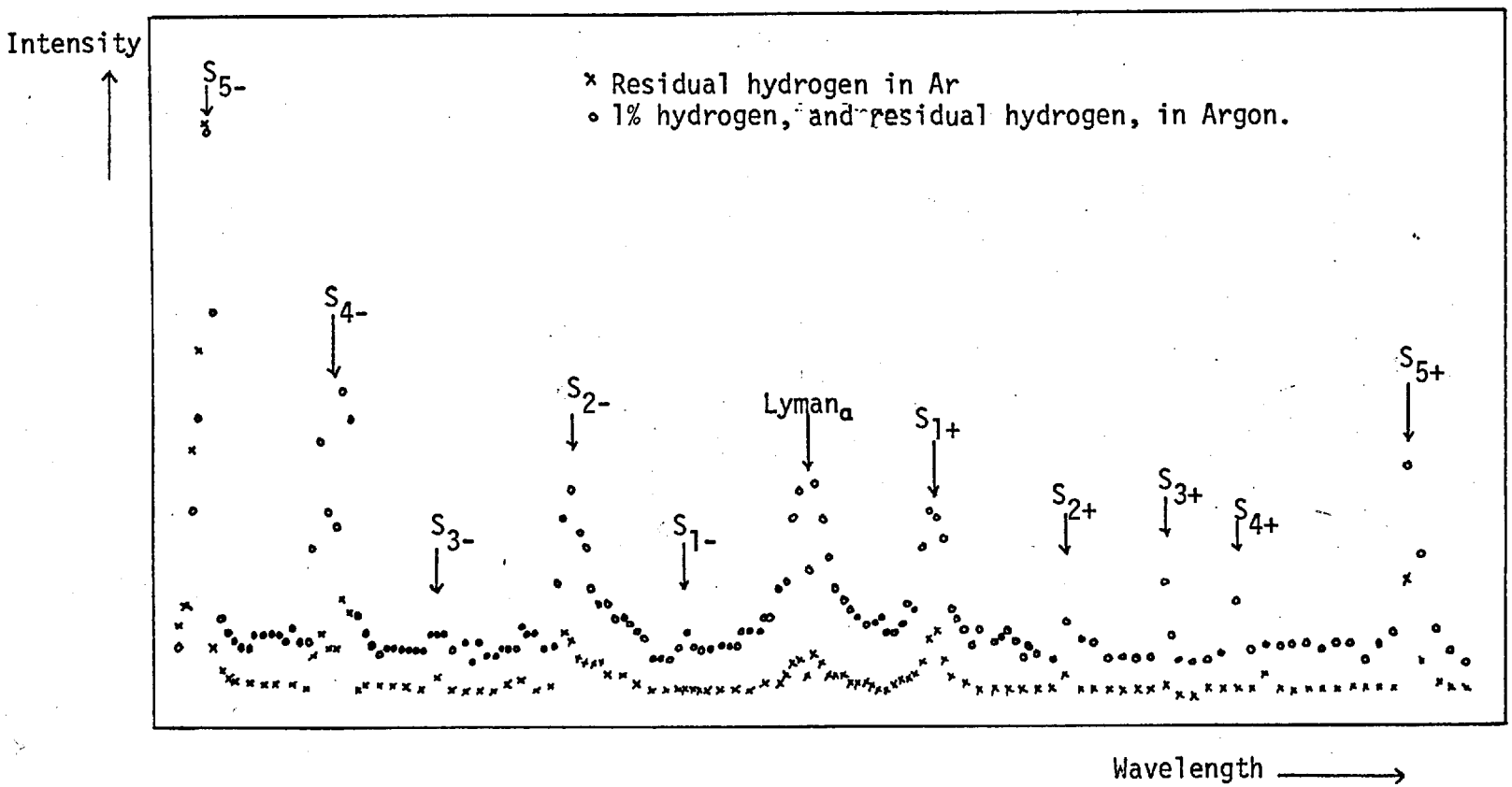

Fig 7.3 : Two scans of Lyman$_\alpha$ and satellite features for different hydrogen concentrations.

Bank voltage 5kV, filling pressure 0.1 Torr in both cases.

discussion in Section 7.5.2, and reference to Table 7.2 shows that S_{5-} may be attributed to C III 1175.7Å, while S_{3-} is probably Si III 1192.3Å.

TABLE 7.3

Satellite Intensities (arbitrary units) for two different hydrogen concentrations

	0% Hydrogen	1% Hydrogen
Lyman α	0.25	1.40
S_{5-}	4.0	3.7
S_{4-}	0.65	2.5
S_{3-}	0.1	0.1
S_{2-}	0.4	1.2
S_{1-}	0.0	0.2
S_{1+}	0.4	1.0
S_{2+}	0.1	0.25
S_{3+}	0.03	0.25
S_{4+}	0.1	0.4
S_{5+}	0.75	1.25

7.5.4 Plasma Satellites

The approximate periodicity of the wavelength spacings of the satellite features (at wavelength intervals which correspond very roughly to multiples of the plasma frequency from line centre) suggests at first sight that the features might be plasma frequency satellites.

As discussed in Sections 1.5.3 and 7.1.2, it is not unlikely that plasma satellites might be observed, because of the special conditions in this plasma. However a closer consideration shows that this cannot be the origin of the satellites in the Lyman α wing.

Firstly, the apparent periodicity of the observed of the observed features is rather misleading since the features S_{5-} and S_{3-} are almost certainly attributable to some impurity, and are in no way connected with the hydrogen emission.

Moreover, if the features are assumed to lie at multiples of the plasma frequency on either side of the Lyman α frequency, this requires that the plasma frequency be about 1.6×10^{13} /s, corresponding to an electron density of 3.4×10^{18} cm^{-3}. This is considerably higher than any of the electron density measurements discussed in Chapter II. Although such a density would be arguably consistent with the highest Abel-inverted interferometric density determinations (which predict maximum densities of 2.8×10^{18} $\pm$ 20%), the lowest Abel-inverted interferometric densities ($\sim$ 1.0×10^{18} cm^{-3} $\pm$ 20%) would have to be in error by $\sim$ 250%. Moreover the electron densities determined from the Ar II half widths would have to be in error by 75% - an error which would be totally inconsistent with the quoted error of $\pm$ 30%. In view of the excellent agreement between these two independent diagnostic measurements, and, indeed, between all the other diagnostic experiments performed on the source, it seems extremely unlikely that such large errors in all the diagnostic experiments could be involved.

Finally, the wavelengths of the features shown no apparent change (to within $\pm$ 1/6 Å) when the electron density is varied from 0.5×10^{18} cm^{-3} to 2.8×10^{18} cm^{-3}. The measured wavelength separations from line centre are plotted as a function of electron density in Fig.7.4.

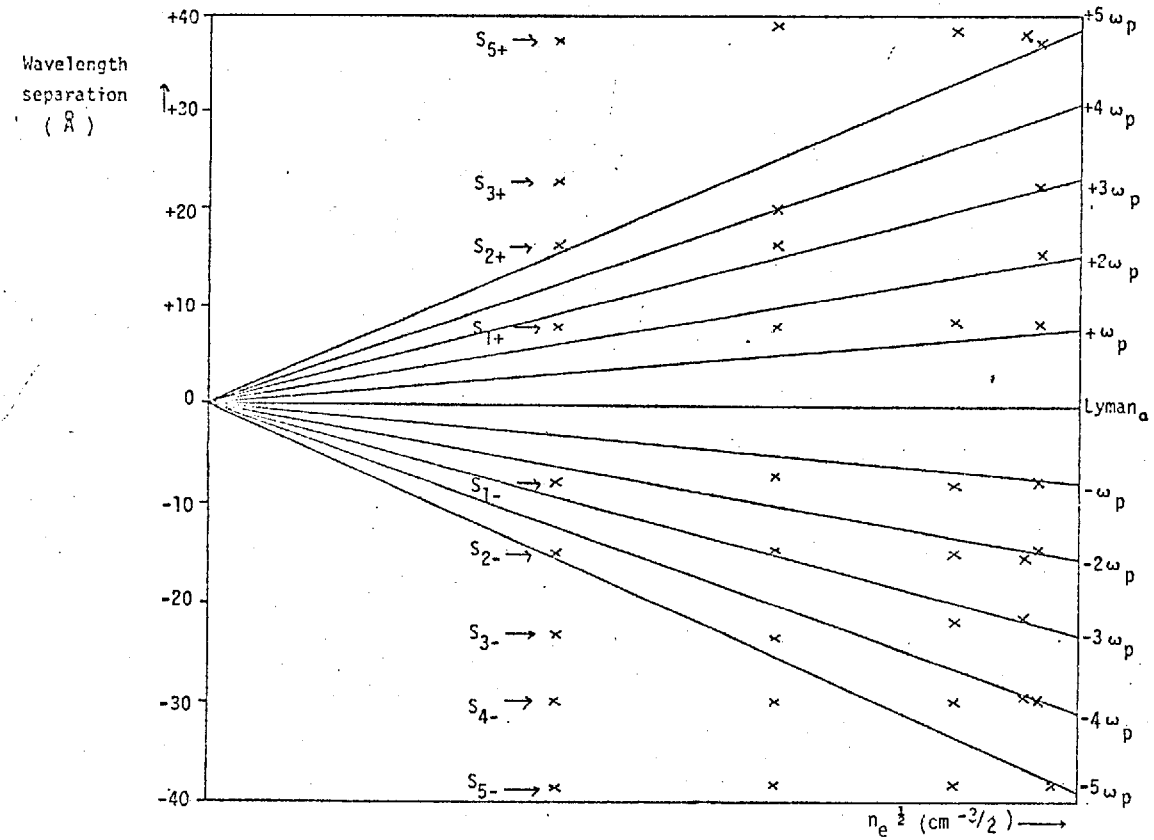

Fig 7.4 : Satellite positions as a function of the square root of the electron density, $n_e^{\frac{1}{2}}$.

The wavelength separations are measured from the self-reversed centre of Lyman α. The predicted $n_e^{\frac{1}{2}}$ dependence which would be expected for plasma frequency satellites is shown on the same graph for comparison. The wavelength separations of the satellite show no detectable density scaling.

In view of these findings it would clearly be incorrect to interpret these features as plasma frequency satellites.

7.5.5 Quasi-molecular Features

It is possible that the observed features may be quasi-molecular satellites of the kind discussed in Section 7.1.1. Since the concentration of Ar III is of the same order as the Ar II concentration in this plasma, it is possible that quasi-molecules of the form H Ar^{++} will be as important as those of the form H Ar^{+}.

In order to test the hypothesis that the satellites arise because of perturbation of the hydrogen emitter by Ar^{+} and Ar^{++} ions, it is necessary to investigate the scaling of the satellite intensities with the relevant ion concentrations. It is also possible that some of the satellites might be due to the influence of proton perturbers as predicted by Stewart, Peak and Cooper (1973).

7.5.5.1 Calculation of the Ion Concentrations

As the pinch density and temperature are changed, the intensity of the satellites alters. It is necessary to correlate changes in electron density and temperature with changes in ionic concentrations.

Using Burgess' tables of argon plasma composition (Burgess 1965) the concentration of Ar II ($N^{Ar^{+}}$) and of Ar III ($N^{Ar^{++}}$) was found for the different densities and temperatures at which the profile was scanned.

The variation of the proton concentration $N^{H^{+}}$ with density and temperature was calculated using the Saha equation.

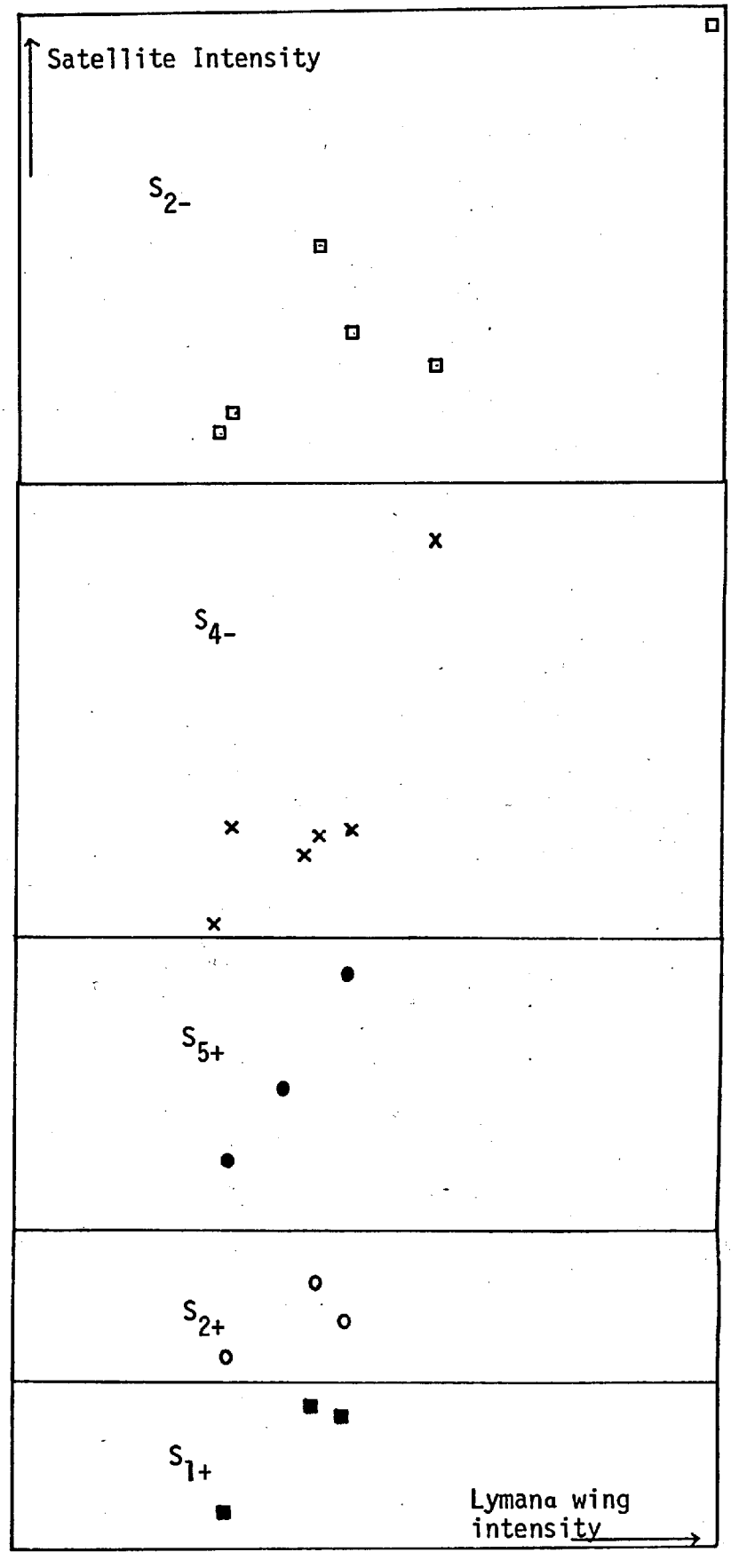

Fig 7.5 : Satellite Intensities versus Lymana Wing Intensity, ($N^{H(2)} \times N_e$).

Since the intensity of the satellites will depend not only on the ion concentration, but also on the number of electrons in the n = 2 (upper) state of Lyman α (N_2^H), the variation of N_2^H was also found, using a Boltzmann factor ($N_2^H \propto e^{-\Delta E/kT}$).

7.5.5.2 Scaling of the Satellite Intensities with the Lyman α wing intensities

The Lyman α wing intensity scales as $N_2^H n_e$ for a given wavelength. In Fig.7.5 the intensity of the satellites is plotted as a function of $N_2^H n_e$. It may be seen that the satellite intensities increase with the Lyman α wing intensity, suggesting that the satellites are connected specifically with the Lyman α transition.

7.5.5.3 Scaling of the Satellite Intensities with the proton concentration

There was no apparent correlation between the satellite intensities and the product ($N_2^H \times N^{H+}$), suggesting that the satellites did not arise because of proton perturbers.

Stewart et al (1973) predicted that, for proton perturbers, the satellite width should vary as $T_e^{\frac{1}{2}}$, while the peak intensity should scale as $T_e^{-1/4}$. However, over the range of temperatures used in this experiment, no convincing agreement with these temperature dependences could be found.

7.5.5.4 Scaling of the Satellite Intensities with the Ar^+ and Ar^{++} concentrations

The intensities of S_{2-}, S_{1+}, S_{2+}, S_{3+} and S_{5+} scaled with the product of the Ar^+ concentration and the population of the upper state of Lyman α ($N_2^H \times N^{Ar^+}$). The intensity of S_{4-}, on the other hand, seemed to depend rather on the concentration of Ar^{++}, fitting better to a linear scaling with ($N_2^H \times N^{Ar^{++}}$). This is illustrated in Figs.7.6 and 7.7.

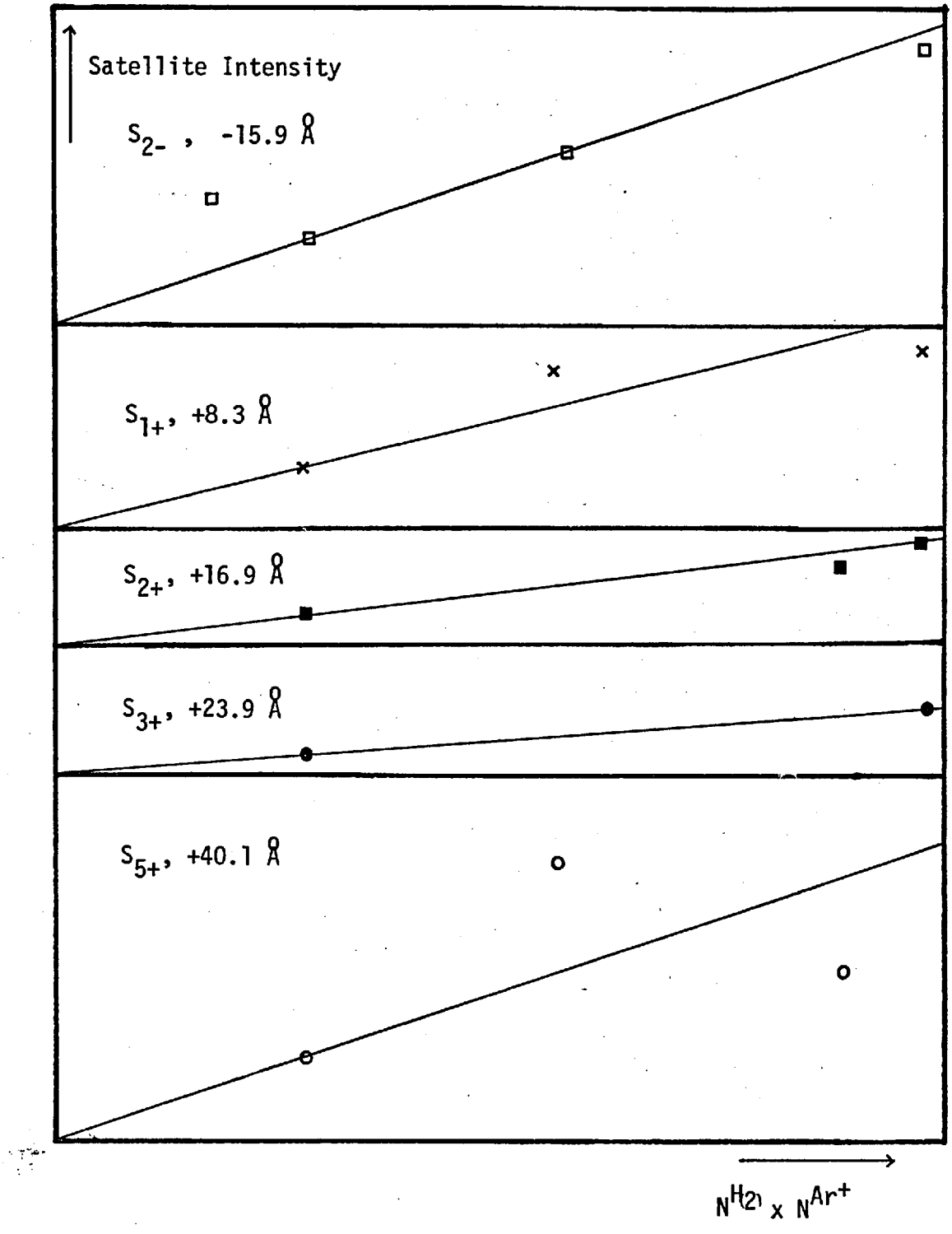

Fig 7.6 : Satellite Intensities as a function of $N^{H2)} \times N^{Ar+}$.

$N^{H2)}$ is the number of hydrogen atoms in n=2

N^{Ar+} is the number of Ar^+ ions.

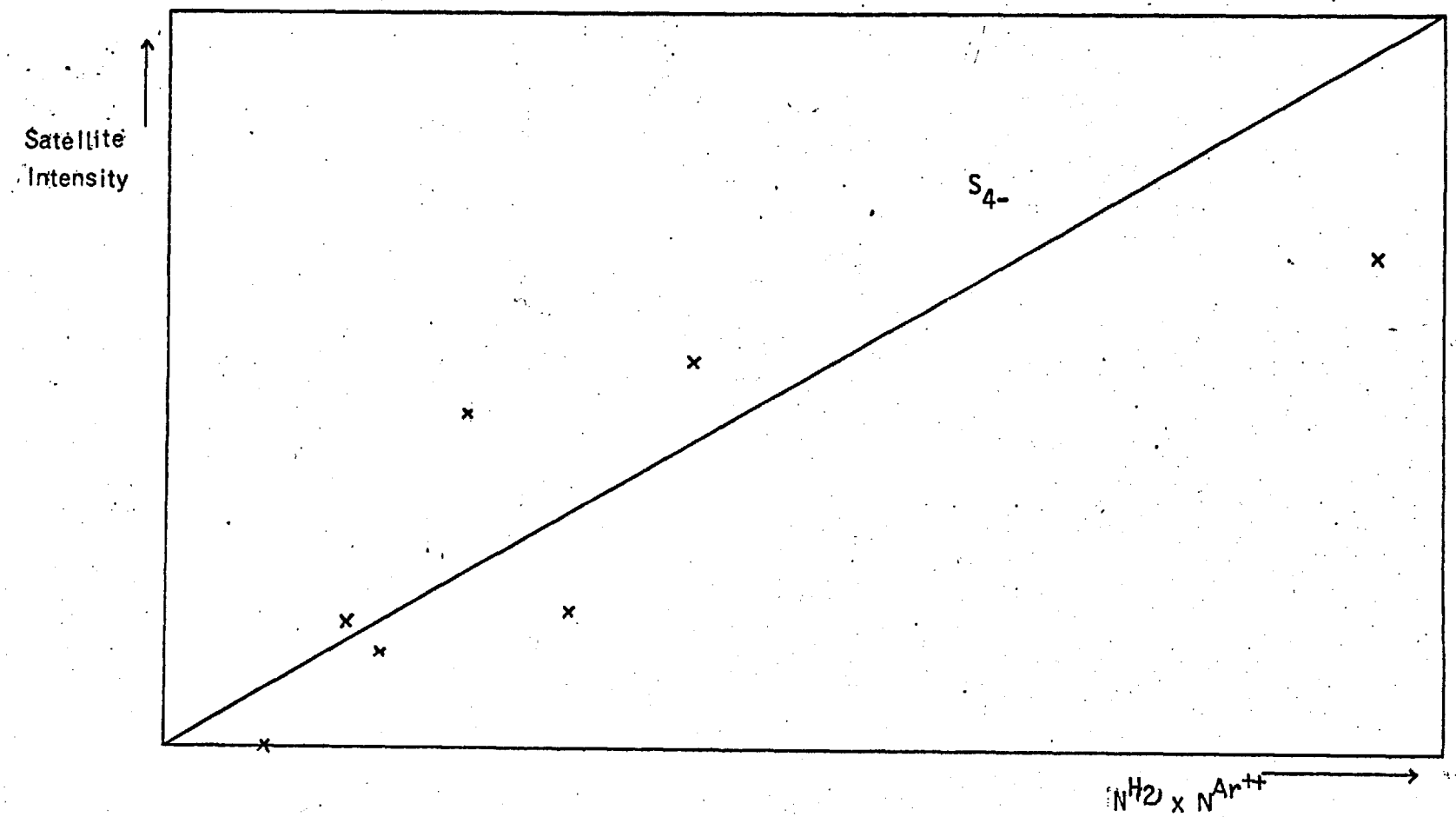

Fig 7.7 : Intensity of satellite S_{4-} as a function of $N^{H_2)} \times N^{Ar^{++}}$.

The intensity of S_{1-} did not appear to scale with either concentration.

7.5.5.5 Conclusions

It seems likely that the satellite features observed in the wing of Lyman α should be attributed to the formation of quasi-molecular states of excited (n = 2) hydrogen atoms with the argon ions in the plasma. The satellites at -15.9Å, +8.3Å, +16.9Å, +23.9Å and +40.1Å are attributed to quasi-molecules of the form $H\,Ar^+$. It also seems possible that the satellite at -31.5Å might be due to the formation of a quasi-molecule between excited (n = 2) hydrogen and Ar^{++}.

7.5.5.6 Relation to Previous Work

The wavelengths of S_{2+} and S_{3+} (+16.9Å and 23.9Å respectively) are quite close to those predicted for satellites by Le Quang Rang and Voslamber (1975) (+18.6Å and 25.6Å). The satellite S_{5+} at 40.1Å is quite close in wavelength to the satellite observed by Preston (1977) which was similarly attributed to quasi-molecules of the form $H\,Ar^+$.

The satellites at -31.5Å, -15.9Å and +8.3Å do not correspond to any satellite features previously observed or predicted.

7.6 The Asymmetry of the Lyman α Profile

The asymmetry of three of the Lyman α profiles taken at different densities and temperatures was studied. Two of the profiles used were taken at relatively low temperatures when the satellite intensities drop dramatically. In these cases it is then possible to make measurements of the asymmetry out to $\sim$ 30 Å in the wings.

The third profile considered was taken at a higher temperature when the satellite intensities were at least an order of magnitude

higher. Because of this it was only possible to make measurements on the asymmetry out to $\sim \pm 5$ Å into the wing, before the satellites began to perturb the wing intensities seriously.

Fig.7.8 shows a plot of $(\Delta\lambda)_2$ against $(\Delta\lambda)_1$ for the three Ly_α profiles considered. Since there are currently no theoretical calculations available for these densities, only a qualitative comparison with theory is possible. The asymmetry is considerably greater than that predicted for "trivial" causes (Griem 1964) and also greater than that predicted by Sholin (1969) and by Bacon (1973) for a density 8×10^{16} cm^{-3}.

7.6.1 The Observed Turn-Over to Smaller Asymmetry

There is also evidence for a gradual turn-over to smaller asymmetry at about $\Delta\lambda \sim 5$ Å (corresponding to the wavelength at which Fussmann (1975) observed a similar fall-off), although according to Eqn.7.2 the transition to less asymmetry because of the breakdown of the impact approximation for electrons should not occur till wavelengths $\sim$ 70.0Å. The similarity between this result and the result of Fussmann, obtained for different plasma conditions, is rather suspicious. The assumption that this turn-over is a result of the onset of the quasi-static behaviour of the electrons is thus questionable. Although the onset wavelength may not be in quantitative agreement with Eqn.7.2, yet it should nevertheless be dependent on the plasma conditions. It thus seems possible that the observed turn-over may be due to some other reason. The turn-over measured in this experiment would correspond to a feature at ω_p ($\sim$ 6.5Å), in the red wing. However, the turn-over observed by Fussmann (1975) cannot be explained in these terms, since in his experiment a plasma frequency feature in the red wing would occur at $\sim$1.2 Å.

7.6.2 Errors

The chief source of error in these measurements is the uncertainty in the position of the unshifted line centre. The error bars in Fig.7.8

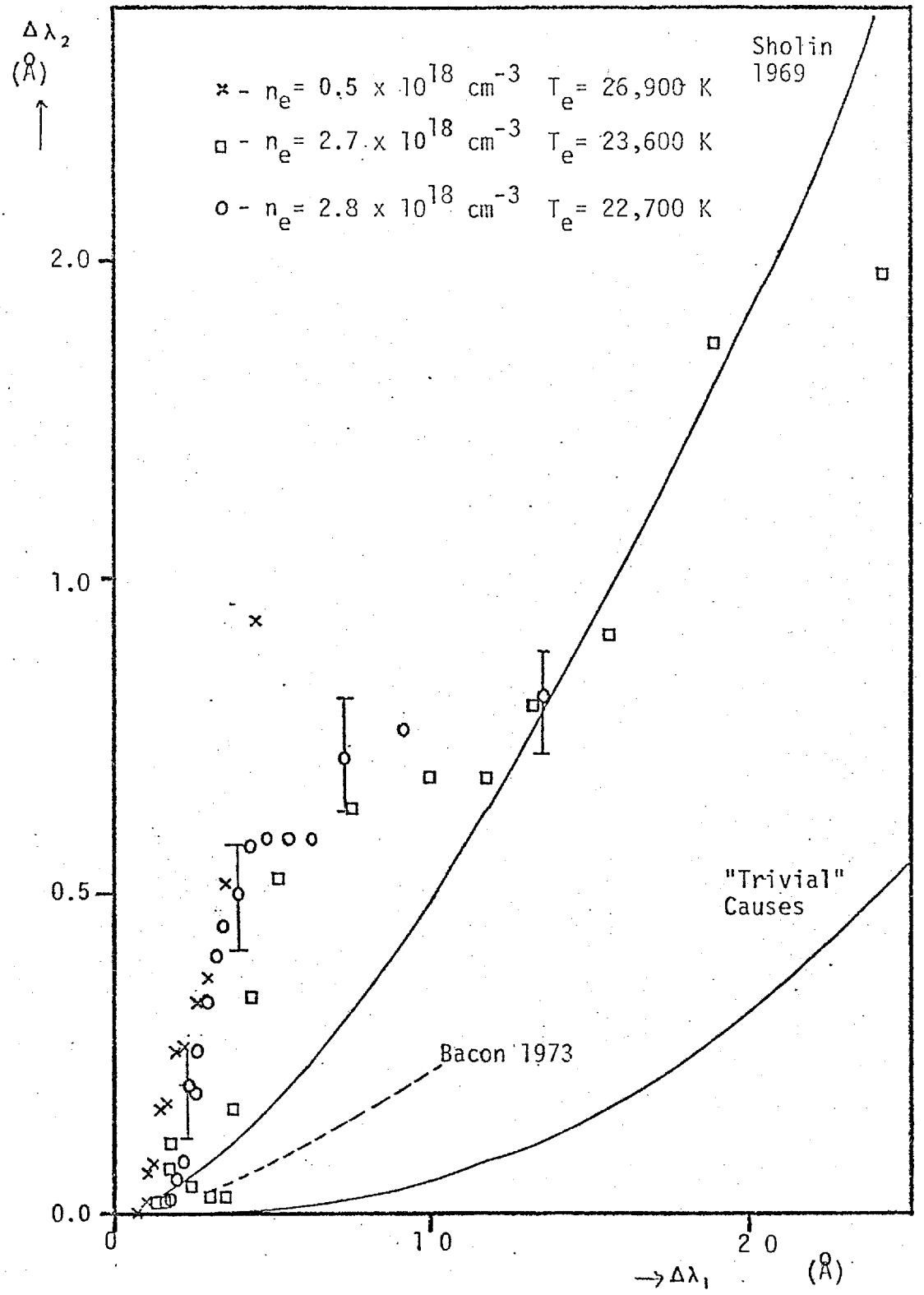

Fig 7.8 : Asymmetry of Lyman$_\alpha$ in terms of the usual parameters $\Delta\lambda_1$ and $\Delta\lambda_2$ (see Equation 7.1).

Theoretical curves given are all for a density $n_e = 8 \times 10^{16}$ cm^{-3}.

represent an estimated error of ± 0.1 Å in the position of line centre.

7.6.3 Conclusions

This data confirms that at higher electron densities the asymmetry due to quadrupole interactions becomes much more pronounced, although in the absence of any theoretical calculations for these densities it is not possible to make a choice between the Bacon (1973) and Sholin (1969) treatments of the quadrupole interaction.

CHAPTER VIII

Conclusions

In spite of the many difficulties associated with extending diagnostic methods and line profile studies to denser sources, the electron density and temperature of the source used in the present investigation were determined to within acceptable limits by a careful choice of diagnostic techniques.

The experimental studies described in this thesis indicate some of the shortcomings of existing theories when applied to the high density régime.

No evidence was found of the large polarization shifts predicted for these densities by many theoretical estimates of the effect. Instead the dominant effect at high densities was found to be a marked asymmetry, observed for all the transitions for which detailed line profile studies were possible.

For the electron-impact broadened lines studied the profiles showed enhanced blue wings. The asymmetry in this case has been attributed to the coupling of perturbing electrons with the transverse radiation field, as predicted by Burgess (1968).

For the quasi-statistically broadened profile of Lyman α , the intensity in the red wing was enhanced, the asymmetry in this case being due to quadrupole interactions, as predicted by Sholin (1969).

In addition, the wings of Lyman α show a number of satellite-like features which have been attributed to the formation of quasimolecular states with perturbing ions close to the emitter.

Since both the asymmetries and the quasimolecular features observed are predicted to become increasingly important at higher

densities, an investigation of these kinds of effect on even denser sources would provide a valuable extension to the work presented in this thesis.

APPENDIX 1

Abel Inversion Routine.

```
      DIMENSION A(20,20),F(20,10),DENSIT(20),RADIAL(20),AXIS(2,39)
     1,R(10),PRES(10)
      READ(5,200) ((A(J,K),J=1,20),K=1,20)
  200 FORMAT(57(7F10.6/),F10.6)
      DO 88 K=1,20
      WRITE(6,550) (A(J,K),J=1,20)
  550 FORMAT(7(4X,F10.6)/7(4X,F10.6)/6(4X,F10.6))
   88 CONTINUE
      READ(5,990) (PRES(N),N=1,10)
      WRITE(6,990) (PRES(N),N=1,10)
  990 FORMAT(9(F6.1/),F6.1)
      READ(5,993) (R(N),N=1,10)
      WRITE(6,993) (R(N),N=1,10)
  993 FORMAT(9(F6.2/),F6.2)
      READ(5,994) ((F(J,N),J=1,20),N=1,10)
      WRITE(6,994) ((F(J,N),J=1,20),N=1,10)
  994 FORMAT(19(10F5.2/),10F5.2)
      READ(5,995) LIMIT
  995 FORMAT(I2)
      N=0
  124 N=N+1
      IF(N.GT.LIMIT) GO TO 125
      WRITE(6,980) PRES(N)
  980 FORMAT(//18H FILLING PRESSURE=,F6.1,8H MICRONS//)
      WRITE(6,985) R(N)
  985 FORMAT(//23H ASSUMED PLASMA RADIUS=,F6.2,4H MMS//)
      WRITE(6,986)
  986 FORMAT(10X,20H INPUT FRINGE SHIFTS)
      WRITE(6,987) (F(J,N),J=1,20)
  987 FORMAT(10(4X,F5.2)/10(4X,F5.2)//)
      J=21

  160 J=J-1
      DENSIT(J)=0.0
      RADIAL(J)=FLOAT(J-1)*R(N)/20.0
      DO 89 K=1,20
      HEIGHT=FLOAT(K-1)*R(N)/20.0
      VAR2=F(K,N)*1.77E19
      DENSIT(J)=DENSIT(J)+VAR2*A(J,K)/R(N)
   89 CONTINUE
      WRITE(6,560) J,RADIAL(J),DENSIT(J)
  560 FORMAT(4X,I3,4X,F1).6,4X,1PE20.7)
      IF(J.GT.1) GO TO 160
      DO 99 J=2,20
      II=21-J
      AXIS(2,II)=DENSIT(J)
      AXIS(1,II)=-RADIAL(J)
   99 CONTINUE
      DO 97 J=1,20
      II=40-J
      AXIS(2,II)=DENSIT(J)
      AXIS(1,II)=RADIAL(J)
   97 CONTINUE
      GO TO 124
  125 STOP
      END
```

Input

Filling Pressure (PRES)

Plasma Radius (R)

20 Fringe Shifts measured as a function of radius. (Mach Zender interferometer with a He-Ne laser source).

Matrix of fitting coefficients A(J,K).

Output

20 Electron Density Readings as a function of radius.

Data for A(J,K)

```
 15.251944     .926330          -0          -0          -0          -0          -0
        -0          -0          -0          -0          -0          -0          -0
        -0          -0          -0          -0          -0          -0          -0
-11.601925    7.212600     .647988          -0          -0          -0          -0
        -0          -0          -0          -0          -0          -0          -0
        -0          -0          -0          -0          -0          -0          -0
 -1.169395   -5.902555    5.307693     .526364          -0          -0          -0
        -0          -0          -0          -0          -0          -0          -0
        -0          -0          -0          -0          -0          -0          -0
  -.673948    -.364801   -4.116741    4.397163     .454572          -0          -0
        -0          -0          -0          -0          -0          -0          -0
        -0          -0          -0          -0          -0          -0          -0
  -.394076    -.429782    -.277457   -3.332457    3.836836     .405558          -0
        -0          -0          -0          -0          -0          -0          -0
        -0          -0          -0          -0          -0          -0          -0
  -.253755    -.269299    -.324996    -.224644   -2.869807    3.447613     .370040
        -0          -0          -0          -0          -0          -0          -0
        -0          -0          -0          -0          -0          -0          -0
  -.176556    -.184085    -.210052    -.267629    -.191252   -2.557173    3.157023
   .342232          -0          -0          -0          -0          -0          -0
        -0          -0          -0          -0          -0          -0          -0
  -.129814    -.133868    -.147364    -.175382    -.231096    -.168301   -2.328017
 2.929337     .319955          -0          -0          -0          -0          -0
        -0          -0          -0          -0          -0          -0          -0
  -.099424    -.101793    -.109490    -.124654    -.152493    -.205566    -.151499
 -2.150895    2.744824     .301492          -0          -0          -0          -0
        -0          -0          -0          -0          -0          -0          -0
  -.078572    -.080047    -.084759    -.093710    -.109157    -.136142    -.186578
  -.138610   -2.008747    2.591264     .285895          -0          -0          -0
        -0          -0          -0          -0          -0          -0          -0
  -.063650    -.064615    -.067663    -.073305    -.082629    -.097858    -.123912
  -.171513          -0          -0          -0     .272491          -0          -0
        -0          -0          -0          -0          -0          -0          -0
  -.052606    -.053265    -.055325    -.059066    -.065060    -.074395    -.089219
  -.114137    -.159944    -.119998   -1.792466    2.348415     .260810          -0
        -0          -0          -0          -0          -0          -0          -0
  -.044206    -.044670    -.046112    -.048696    -.052740    -.058826    -.068015
  -.082374    -.106310    -.150153    -.113010   -1.707542    2.250070     .250513
        -0          -0          -0          -0          -0          -0          -0
  -.037667    -.038004    -.039045    -.040288    -.043724    -.047883    -.053935
  -.062912    -.076793    -.099826    -.141909    -.107070   -1.633625    2.163130
   .241347          -0          -0          -0          -0          -0          -0
  -.032479    -.032729    -.033499    -.034851    -.036903    -.039852    -.044028
  -.049989    -.058726    -.072156    -.094349    -.134852    -.181947   -1.568530
 2.985548     .233115          -0          -0          -0          -0          -0
  -.028293    -.028483    -.029065    -.030079    -.031603    -.033759    -.036747
  -.040889    -.046727    -.055222    -.068221    -.089651    -.128726    -.097472
-1.510633    2.015756     .225677          -0          -0          -0          -0
  -.024867    -.025014    -.025462    -.026238    -.027394    -.029010    -.031212
  -.030197    -.030278    -.031928    -.052239    -.064835    -.085566    -.123347
  -.090522   -1.458699    1.952933     .218905          -0          -0          -0

  -.022028    -.022143    -.022493    -.023098    -.023922    -.025229    -.026992
  -.029106    -.030062    -.031669    -.041636    -.049365    -.061855    -.081975
  -.118576    -.000603   -1.411772    1.894909     .212709          -0          -0
  -.019953    -.019041    -.019311    -.019776    -.020457    -.021393    -.022638
  -.024271    -.026415    -.029252    -.033075    -.038371    -.045999    -.057612
  -.076732    -.111652    -.083135   -1.363193    1.854467     .345124          -0
  -.020355    -.020439    -.020694    -.021132    -.021772    -.022643    -.023790
  -.025276    -.027192    -.029675    -.032930    -.037283    -.043270    -.051835
  -.064781    -.085922    -.124215    -.105395   -1.373121    1.366258
```

APPENDIX 2

Radial Variation of Electron Density

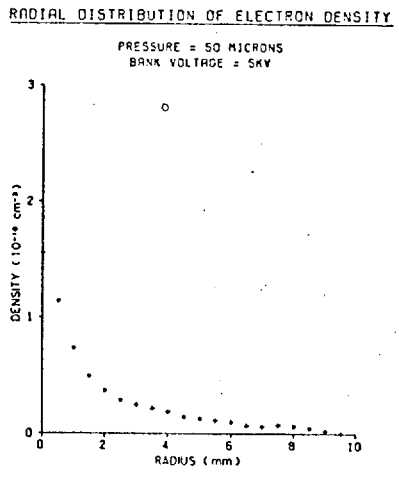

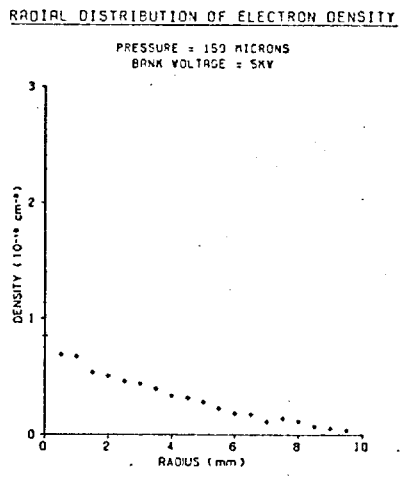

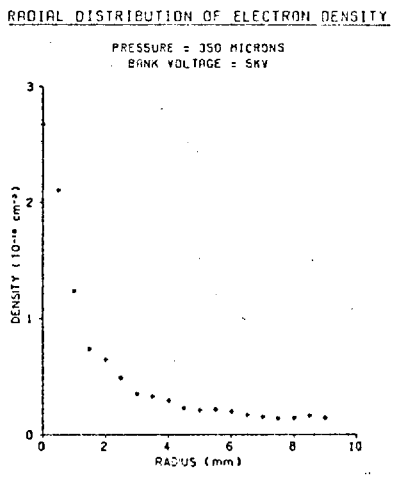

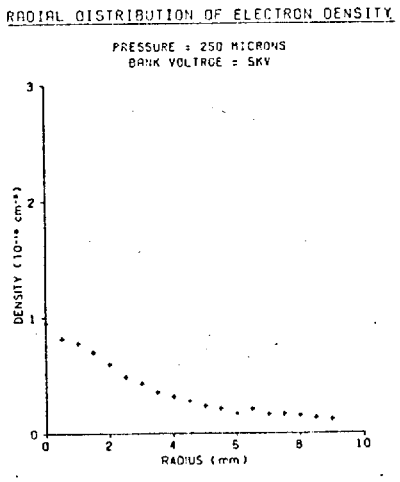

Filling Pressures in microns .

100 microns = 10^{-1} Torr

RADIAL DISTRIBUTION OF ELECTRON DENSITY

PRESSURE = 400 MICRONS
BANK VOLTAGE = 5KV

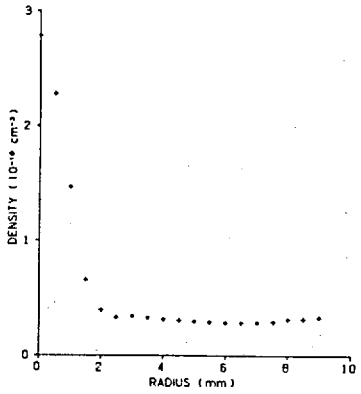

RADIAL DISTRIBUTION OF ELECTRON DENSITY

PRESSURE = 500 MICRONS
BANK VOLTAGE = 5KV

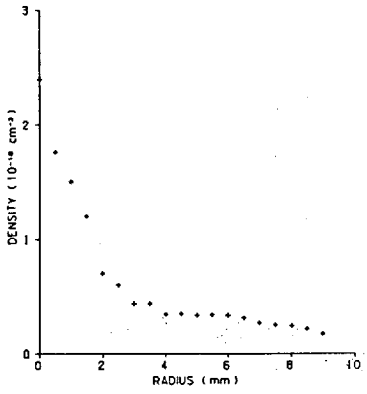

RADIAL DISTRIBUTION OF ELECTRON DENSITY

PRESSURE = 600 MICRONS
BANK VOLTAGE = 5KV

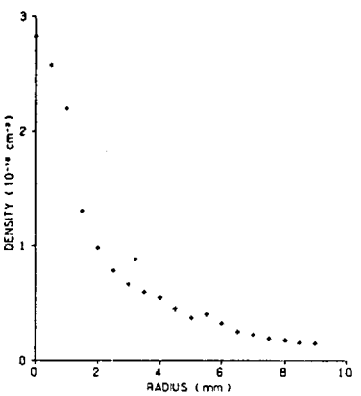

RADIAL DISTRIBUTION OF ELECTRON DENSITY

PRESSURE = 700 MICRONS
BANK VOLTAGE = 5KV

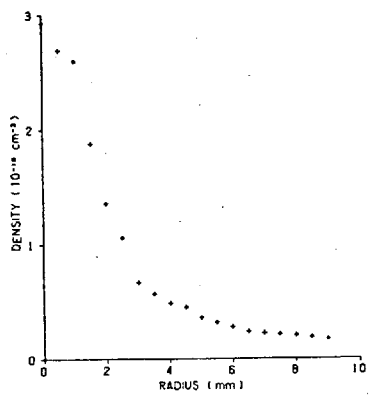

RADIAL DISTRIBUTION OF ELECTRON DENSITY

PRESSURE = 800 MICRONS
BANK VOLTAGE = 5KV

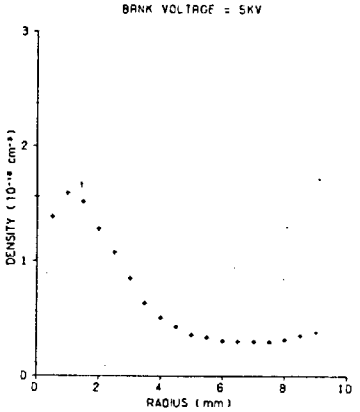

RADIAL DISTRIBUTION OF ELECTRON DENSITY

PRESSURE = 900 MICRONS
BANK VOLTAGE = 5KV

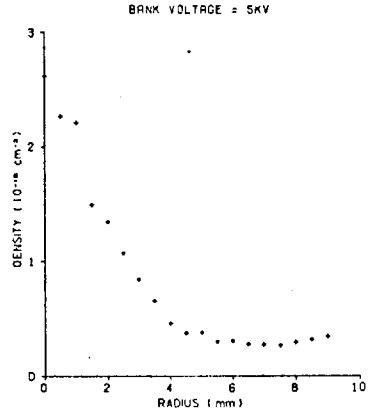

RADIAL DISTRIBUTION OF ELECTRON DENSITY

PRESSURE = 1000 MICRONS
BANK VOLTAGE = 5KV

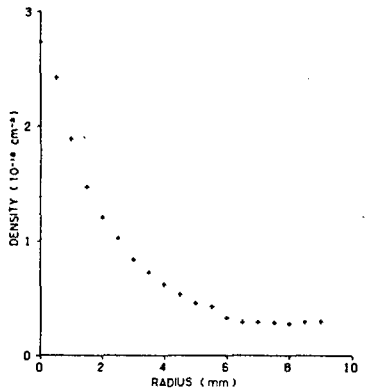

RADIAL DISTRIBUTION OF ELECTRON DENSITY

PRESSURE = 1200 MICRONS
BANK VOLTAGE = 5KV

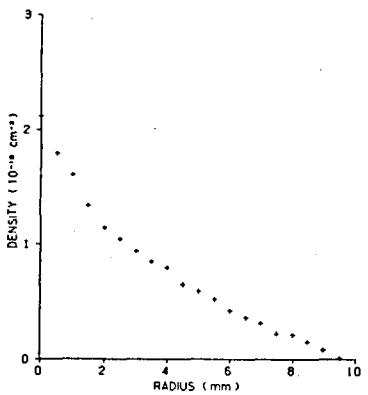

RADIAL DISTRIBUTION OF ELECTRON DENSITY

PRESSURE = 1400 MICRONS
BANK VOLTAGE = 5KV

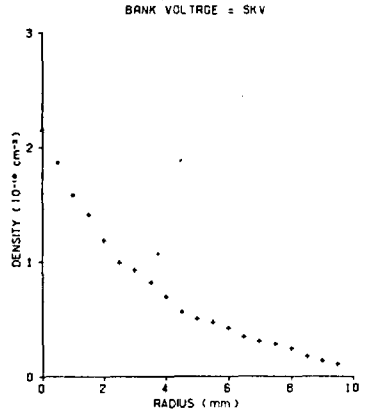

RADIAL DISTRIBUTION OF ELECTRON DENSITY

PRESSURE = 1500 MICRONS
BANK VOLTAGE = 5KV

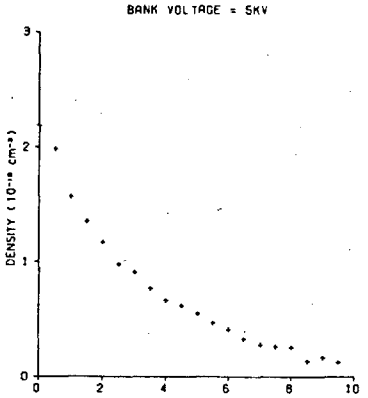

RADIAL DISTRIBUTION OF ELECTRON DENSITY

PRESSURE = 1700 MICRONS
BANK VOLTAGE = 5KV

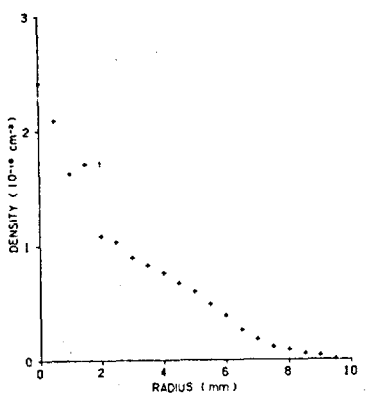

RADIAL DISTRIBUTION OF ELECTRON DENSITY

PRESSURE = 1900 MICRONS
BANK VOLTAGE = 5KV

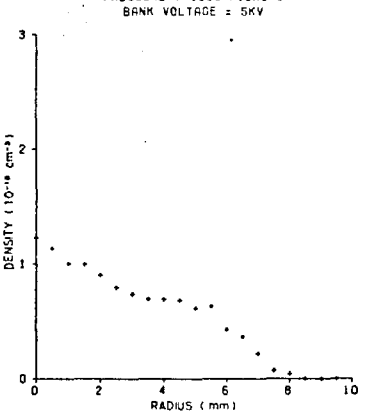

RADIAL DISTRIBUTION OF ELECTRON DENSITY

PRESSURE = 180 MICRONS
BANK VOLTAGE = 6KV

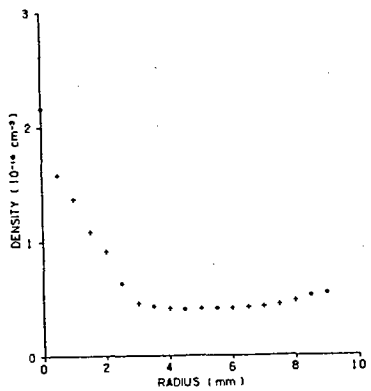

RADIAL DISTRIBUTION OF ELECTRON DENSITY

PRESSURE = 250 MICRONS
BANK VOLTAGE = 6KV

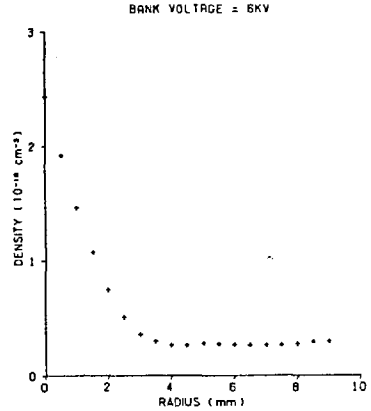

RADIAL DISTRIBUTION OF ELECTRON DENSITY

PRESSURE = 400 MICRONS
BANK VOLTAGE = 6KV

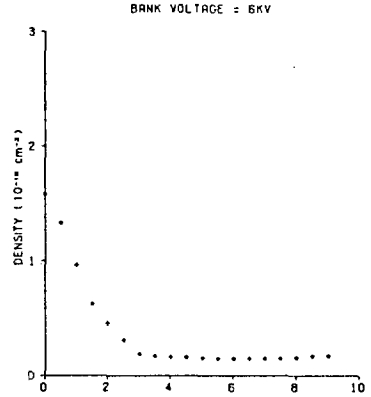

APPENDIX 3

Calculation of Electron-Impact Broadened Stark Widths and Shifts by Semiempirical Estimates

The Stark widths and shifts of the lines of Ar II Mult 1.U.V., Ar III Mult 1.U.V., and N II Mult 2.U.V. studied in Chapters IV and V were calculated using the semiempirical formulae of Griem (1968).

A.3.1 Width Calculations

The width is given by :-

$$w \approx 8\left[\frac{\pi}{3}\right]^{3/2} \frac{\hbar}{m a_0} N \left[\frac{E_H}{kT}\right]^{1/2} \sum_{i'f'} \left[|\langle i'|r|i\rangle|^2 . \bar{g}\left(\frac{\bar{E}}{|\Delta E_{ii'}|}\right) + |\langle f'|r|f\rangle|^2 . \bar{g}\left(\frac{\bar{E}}{|\Delta E_{ff'}|}\right) \right] \qquad (A.3.1)$$

where the summation is performed over interacting states i' and f'. $\bar{g}(\ )$ is the effective Gaunt factor, which is taken to have the threshold value ($g = 0.2$) in these calculations since $\frac{\bar{E}}{|\Delta E|}$ is < 1 for all perturbing levels studied.

As pointed out by Griem, the summation is often dominated by the nearest perturbing levels, in which case the width is given by replacing the actual $|\Delta E|$ by those corresponding to these levels, $|\Delta E_i|$ and $|\Delta E_f|$ say.

The expression for the width then becomes -

$$w = 8\left[\frac{\pi}{3}\right]^{3/2} \frac{\hbar}{m a_0} N \left[\frac{E_H}{kT}\right]^{1/2} \left\{ \langle i|r^2|i\rangle . \bar{g}\left(\frac{3kT}{2|\Delta E_i|}\right) + \langle f|r^2|f\rangle . \bar{g}\left(\frac{3kT}{|2\Delta E_f|}\right) \right\} \qquad (A.3.2)$$

where the hydrogenic ion value may be taken for the matrix elements of r^2 :-

$$\langle i|\, r^2 \,|i\rangle = \frac{n_i^2}{2Z^2}\left[5n_i + 1 - 3\ell_i(\ell_i+1)\right] a_o^2 \qquad \text{(A.3.3)}$$

n_i is the effective principle quantum number of E_i.

A.3.2 Shift Calculations

The shifts may be calculated from a formula similar to Eqn.A.3.1:-

$$d \approx -8\left[\frac{\pi}{3}\right]^{3/2} \frac{\hbar}{m a_o} N\left[\frac{E_H}{kT}\right]^{1/2} \sum_{i'f'} \left\{ \frac{\Delta E_{ii'}}{|\Delta E_{ii'}|} |\langle i'|r|i\rangle|^2 \bar{g}\left(\frac{3kT}{|2\Delta E_{i'i}|}\right) - \frac{\Delta E_{f'f}}{|\Delta E_{f'f}|} |\langle f'|r|f\rangle|^2 \bar{g}\left(\frac{3kT}{|2\Delta E_{f'f}|}\right)\right\} \qquad \text{(A.3.4)}$$

A simplification to an equation of the form of Eqn.A.3.2 will not usually be justified unless the summation is dominated by a single term, or at least all contributions have the same sign. The atomic matrix elements may be estimated from :-

$$|\langle i'|r|i\rangle|^2 \approx \frac{1}{\{2\ell_i+1\}} \cdot \left\{\frac{3n_\ell}{2Z}\right\}^2 \cdot \left(n_\ell^2 - \ell^2\right) \times \Phi^2(n_{\ell-1}, n_\ell, \ell)\, a_o^2 \qquad \text{(A.3.5)}$$

where $\Phi^2(\ )$ is a correction factor tabulated by Bates and Damgaard (1949).

A.3.3 Calculation of Stark Widths and Shifts for Ar II Mult 1.U.V., Ar III Mult 1.U.V. and N II Mult 2.U.V.

The application of Eqns.A.3.2, A.3.3 to find the widths of these lines was appropriate since in all cases, detailed calculation of terms in the summations over all interacting states revealed that

the broadening was dominated by interactions between the upper and lower states of the transition (See Fig.3.1).

The shifts were calculated from Eqns.A.3.4 and A.3.5.

The shifts and widths calculated for a density $N = 2 \times 10^{18}$ cm^{-3} are given in Table A.3.1. below.

TABLE A.3.1

Semiempirical estimates for Shifts and Widths at an electron density 2×10^{18}

	Half-Half Width	Shift
Ar II Mult 1.U.V.	0.023 Å	-0.0133 Å
Ar III Mult 1.U.V.	0.0227 Å	-0.0058 Å
N II Mult 2.U.V.	0.0175 Å	-0.0014 Å

The minus signs indicate blue shifts.

The chief source of error in these estimates arises from uncertainties in the value of the effective Gaunt factor. This is unlikely to produce errors of greater than ±50%.

APPENDIX 4

The Cooled Cathode Discharge as a V.U.V. Wavelength Standard

The cooled cathode discharge is a source designed to produce a discharge in a region of low temperature, so that the lines emitted will be negligibly Doppler broadened. The cooled cathode discharge is sketched in Fig.A.4.1. The high voltage electrode is constructed of brass and lined with aluminium in the region of the discharge, to prevent sputtering, and is water-cooled. The vacuum port connector farthest from the spectrograph was used at the earthy electrode.

The "domes" on either side of the high voltage electrode are constructed of pyrex.

The whole tube is evacuated to a filling pressure of about 0.2 Torr.

The high voltage electrode is raised to about 600 V by a D.C. power source, which supplies about 200 mA.

By adjusting the voltage on the high voltage electrode and the filling pressure in the tube, the discharge can be confined to the region inside the cathode. Because the cathode is water-cooled the temperature in this region is relatively low, and the emitted lines are not significantly Doppler broadened or shifted. Thus the hollow cathode discharge provides an excellent wavelength standard for use in the V.U.V. region.

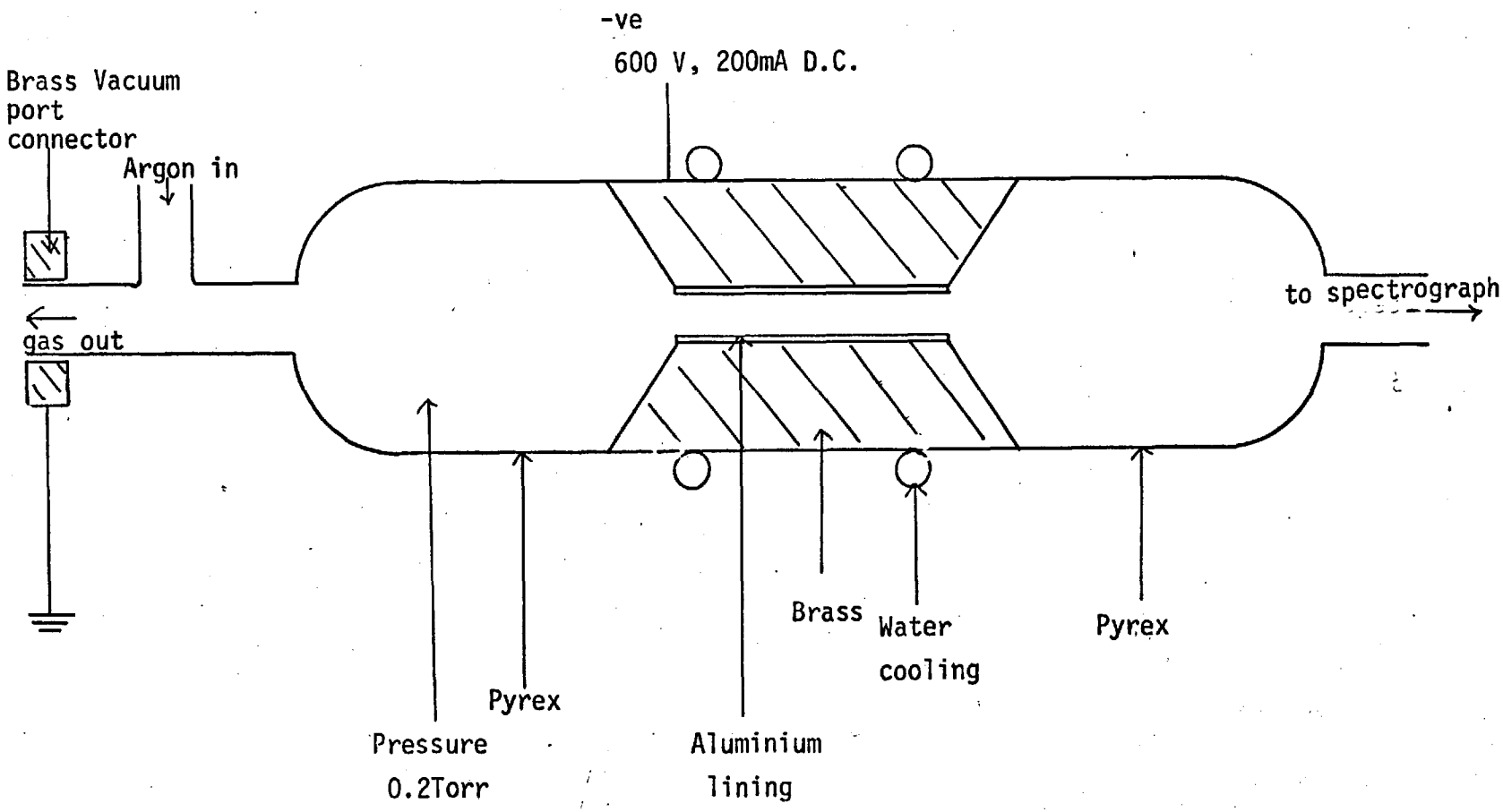

Fig A4.1 : Cooled-Cathode Discharge.

APPENDIX 5

Reprint of Paper published in Journal of Physics B,
Atomic and Molecular Physics, Volume 10, No.5,
L177, 1977.

"Observations of quantum mechanical interference effects in the wings of electron-impact broadened lines of ionized emitters"

by

E.A.M. Baker and D.D. Burgess

J. Phys. B: Atom. Molec. Phys., Vol. 10, No. 5, 1977. Printed in Great Britain. © 1977

LETTER TO THE EDITOR

Observations of quantum-mechanical interference effects in the wings of electron-impact-broadened lines of ionized emitters

E A M Baker and D D Burgess
Physics Department, Imperial College of Science and Technology, London SW7 2BZ, England

Received 11 January 1977

Abstract. We report observations of asymmetric non-Lorentzian wings of impact-broadened lines of ionized emitters in a high-density plasma. The only explanation appears to be a quantum-mechanical interference effect. The effect may be of consequence in opacity calculations in dense plasmas.

In this letter we report the first observation of an effect previously predicted (Burgess 1968) that modifies the otherwise Lorentzian wings of electron-impact-broadened lines of ionized emitters at high densities.

Quantum-mechanical interference effects for systems undergoing radiative transitions between specific upper and lower states connected by two or more separate channels are well known in the study of autoionizing transitions, e.g. by optical spectroscopy. The characteristic resultant asymmetric profiles consisting of combined Lorentz and dispersive terms, usually referred to as Fano profiles in the case of autoionization, have been much studied experimentally and theoretically. On the other hand the line profiles occurring in the simplest possible case of pressure broadening in a plasma, namely the impact broadening of an isolated line, are usually predicted to be of pure Lorentzian form, and this prediction has of course been confirmed many times in observations of lines of both neutral and ionized emitters.

However, Burgess (1968) pointed out that an approximation made in almost all pressure-broadening theories, namely that the perturbing particles do not couple to the radiation field, may fail significantly in the line wings in some cases, in particular for resonance lines of ionized emitters. Allowance for the coupling of the perturbing electron to the radiation field results in an asymmetric contribution to the total pressure-broadened profile (in addition of course to the usual bremsstrahlung background continuum). The interference effect yielding the extra non-Lorentzian contribution can be understood as follows. Consider absorption in the wing of a pressure-broadened line. In the impact approximation the role of the perturbing free particle is to remove or provide excess energy, ΔE, such that a bound electron ends in some energy eigenstate, 3, (which may or may not be either of the states of the optical transition of interest). This process is shown schematically in figure 1. If no account is taken of the coupling between the perturber and the radiation field, the usual Lorentzian profile of the Baranger theory (Baranger 1962) results. However, now consider the special case (which is actually quite common for resonance lines)

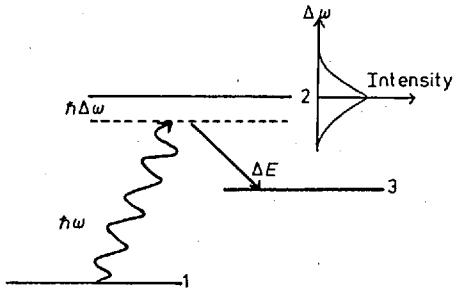

Figure 1. Schematic diagram of impact-broadening processes.

where the state 3 is identical with the initial state 1. There are now *two* routes for the absorption of a photon $\hbar\omega$. In one, the photon initially interacts with the ground-state ion, the free electron then interacts with the consequent excited optical electron and removes energy $\Delta E = \hbar\omega = E_2 - E_1 - \hbar\Delta\omega$ ($\Delta\omega$ being the frequency separation from the line centre). In the second case the photon interacts directly with the free electron (in the field of the ion). The initial and final states of the complete system are *identical* in the two separate absorption channels (line broadening and inverse bremsstrahlung) and they cannot simply be treated independently as assumed in the usual theories.

In Burgess (1968) estimates were given for the magnitude of corrections due to this effect. The integrated strength of the pressure-broadened transition remains unaltered, but an extra term has to be added to the usual Lorentzian shape, this extra contribution being of dispersive form. In the line wing this extra contribution scales as $1/\Delta\omega$ and one wing is enhanced and the other diminished. (At least within the limits of the treatment in Burgess (1968) it is always the high-frequency (blue) wing which is enhanced.) The consequent asymmetry

$$A(\omega) = \frac{I(+\Delta\omega) - I(-\Delta\omega)}{I(+\Delta\omega) + I(-\Delta\omega)}$$

is a linear function of $\Delta\omega$ and at given $\Delta\omega$ is independent of density. Consequently the effect becomes more significant with increasing density as the wing intensity, $I(\Delta\omega)$, at given $\Delta\omega$, increases. Clearly, the extra contribution will be negligible where collision-induced transitions to states other than to the states of the transition itself dominate the usual pressure-broadening processes. However for certain resonance lines and some excited transitions the most important broadening mechanism may indeed be transitions between the states of the line itself. In the case of pressure-broadened resonance lines the modified wing shape may then be of more than academic interest, since it may control opacities, e.g. in stellar interiors, in line-blanketing effects in stellar atmospheres, and in other dense energetic plasmas.

We have now made observations in which we appear to have observed this effect. Specifically, we have observed the resonance lines in the VUV of Ar II (919 and 932 Å) ($3s^23p^5\ ^2P^o$–$3s3p^6\ ^2S$) and Ar III (887, 883, 878, 879, 875 and 871 Å) ($3s^23p^4\ ^3P$–$3s3p^5\ ^3P^o$), and also the excited visible $4s\ ^4P$–$4p\ ^4P^o$ Ar II transitions (4806 and 4848 Å), all in a dense ($3 \times 10^{18}\,cm^{-3}$) argon Z-pinch. For all of these transitions the usual pressure broadening is dominated by interactions involving the upper and lower states of the line alone. All these multiplets show characteristic blue asymmetries at high electron densities despite the fact that at lower densities in this and other sources the profiles are excellent Lorentzians. The asymmetries (which are of varying magnitude, dependent

on the particular transition, being particularly marked for the Ar III resonance line) all show the predicted linearity with $\Delta\omega$. The numerical estimates in Burgess (1968) are subject to two limitations. A Born expansion was used for the usual pressure-broadening and extra (interference) contribution to the total line profile (although if some assumptions about convergence are valid, the result is independent of this expansion, since the term-by-term expansions are in constant ratio). Also, to allow analytic evaluation a Coulomb approximation was made for relevant matrix elements, and particularly in order to relate radial integrals depending on r to those involving $1/r^2$. Nevertheless for the Ar II and Ar III resonance lines where observations could be made out to about 1·5 Å in the line wings, the magnitudes of the asymmetry are in good agreement with the simple analytic estimate given in Burgess (1968), being 1·68 and 1·30 times the predicted values respectively. For the visible Ar II 4806 and 4848 Å lines the observed asymmetry could be measured out to about 10 Å from the line centre and is larger than predicted throughout by about a factor of 30, (however some assumptions of the theory might be expected to be poor for these transitions). Typical profiles and the scaling of $A(\omega)$ with $\Delta\omega$ are shown in figures 2 and 3.

We believe all other known potential causes of these asymmetries can be ruled out. On the purely experimental side, diagnostic measurements on the plasma are of good accuracy. Fully spatially resolved measurements of electron density have been made by two separate laser techniques (continuous absorption and refractive index) using He–Ne and cw dye lasers. Similarly, the electron temperature is known accurately from resonant absorption measurements made using an argon-ion laser. These techniques have been complemented by independent spectroscopic observations based, e.g., on pressure-broadening of lines of established halfwidth. Details will not be presented here, since the exact plasma parameters are irrelevant to the effect under discussion (the asymmetry at given $\Delta\omega$ depending only on the atomic transition), but will be deferred to a subsequent paper on argon, nitrogen and hydrogen resonance profiles in this plasma. Suffice it to say that ample information on, e.g., n_e and Ar^+ distributions in the plasma is available to allow modelling of the effect of density gradients on the observed profile; see below and Baker (1977).

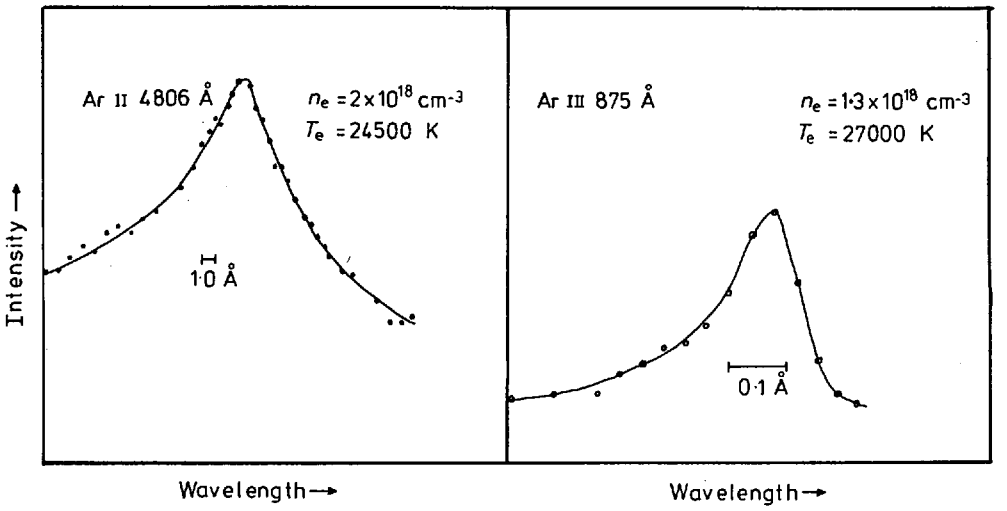

Figure 2. Profiles of Ar II 4806 Å and Ar III 875 Å.

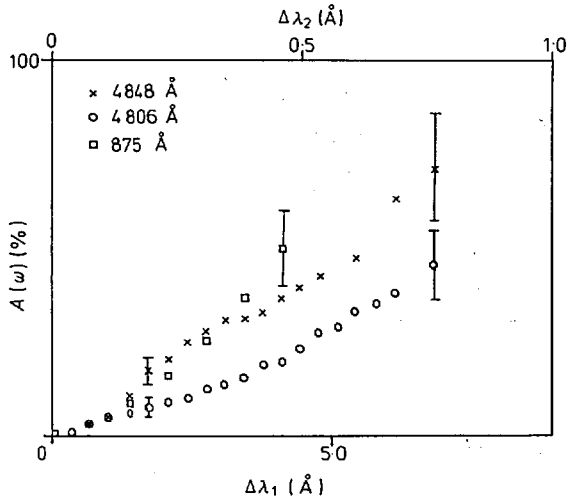

Figure 3. Percentage asymmetry $A(\omega)$ as a function of wavelength separation from the line centre for Ar II 4806 Å and 4848 Å ($\Delta\lambda_1$), and for Ar III 875 Å ($\Delta\lambda_2$).

Instrumental effects can be ruled out. The instrument profiles for the spectrometers used (a Monospek 1000 Czerny–Turner with a 1200 line/mm grating for the visible lines, and a 1-metre normal-incidence Eagle vacuum spectrograph with a 3600 line/mm platinized grating for the VUV lines) are well known from observations of cooled-cathode and microwave sources and are entirely symmetric. In addition observations of other transitions in the plasma itself show normal symmetric profiles, and on those lines for which asymmetries *are* observed, there are marked differences in magnitude from transition to transition, inexplicable by instrumental effects.

Other experimental effects capable of causing apparent asymmetries are overlap from other neighbouring lines (impurity or otherwise), superposition of slightly shifted profiles of the line itself emitted in regions of differing density, and self-absorption effects. All can be ruled out by detailed numerical modelling (Baker 1977). In addition in almost no case can the observed linear scaling of the asymmetry with $\Delta\omega$ be produced over the requisite wavelength range. Line overlap effects cannot produce asymmetries of the requisite magnitude, let alone $\Delta\omega$ variation, unless the overlapping line is immediately detectable. In only one case—the Ar II 919 Å line whose red wing is contaminated by N IV 923 Å—is an impurity line of sufficient strength present. In this case the resultant asymmetry is indeed reversed at large distances from the line centre and agrees excellently with numerical modelling of the overlap. Particularly significant is the behaviour of the observed blue asymmetries within a multiplet, since overlapping lines would affect components at different wavelengths quite differently. (An excellent example is the Ar II 4806, 4848 Å pair where the only possible overlap effect would cause opposite effects on the two lines, contrary to observations.) Similarly, effects of varying density regions contributing to the profile have been modelled. Such effects cannot yield the observed form of the profiles in any case—the far wings are always weighted to high-density regions and become increasingly symmetric (even if relatively shifted by a constant small amount). Numerically, given the known spatial n_e variation, such effects cannot account for the observed asymmetries. In no case can density gradient effects cause more than 2% of the observed wing asymmetry. Very similar considerations apply to the possibility of self-absorption with relative wavelength shifts

between emitting and absorbing regions. Such effects cannot account for the observed form of the wing asymmetry, and are further ruled out by the small magnitude of observed wavelength shifts. Also, the line-centre optical depths vary widely between the observed transitions, the visible 4806 and 4848 Å lines being optically thin in contrast to the VUV resonance lines. The optical depths within a multiplet also vary significantly, again ruling out any possibility that the observed asymmetries are due to reabsorption effects.

The remaining consideration is then other pressure-broadening mechanisms capable of causing asymmetries. Four effects need mention, all of which can be ruled out by simple numerical estimates, e.g. as given by Griem (1964). So-called 'trivial' causes—for instance the ω^4 weighting of the power spectrum—cannot account for more than 0·35% of the observed asymmetry in any instance. Ion quasi-static broadening, another possible cause of asymmetry, is very small for the transitions of interest accounting for at most 5% of the total wing intensity at the largest $\Delta\omega$ values of interest whereas observed asymmetries exceed 20%. Moreover, ion broadening would not produce the observed $\Delta\omega$ scaling of $A(\omega)$. The transition to electron quasi-static broadening does not occur until at least two orders of magnitude further into the line wings than relevant to the observations, so that the impact approximation is truly valid. Finally, quadrupole contributions to the wing profile are always less than 1% of the total ion static broadening, and hence are quite negligible.

In conclusion, a marked asymmetry has been observed at high density for a number of transitions which cannot be accounted for by any obvious established experimental or theoretical reason. The transitions for which the asymmetry occurs are precisely those for which the effect discussed by Burgess (1968) should operate, the asymmetry is of the correct functional form, and for two of the multiplets concerned the agreement with numerical estimates is surprisingly good. At the present time, the interference mechanism, involving the perturber–radiation-field interaction, appears the most likely explanation.

References

Baker E A M 1977 *PhD Thesis* University of London
Baranger M 1962 *Atomic and Molecular Processes* ed D R Bates (New York: Academic Press)
Burgess D D 1968 *Phys. Rev.* **176** 150–60
Griem H R 1964 *Plasma Spectroscopy* (New York: McGraw-Hill)

REFERENCES

Allen, C.W. "Astrophysical Quantities", Athlone Press (London) 1955.

Bacon, M.E. J.Q.S.R.T. 1973, 13, pp.1161-70.

Baranger, M., Mozer, B. Phys.Rev. 1961, 123, p.25.

Bates, D.R., Damgaard, A. Phy.Trans.R.Soc.A, 1949, 242, pp.101-21.

Berg, H.F., Ali, A.W., Lincke, R., Griem, H.R. Phys.Rev. 1962, 125, pp.199-206.

Berg, H.F. Z.Phys. 1966, 191, pp.503-7.

Bockasten, K. J.Opt.Soc.Amer. 1961, 51, p.943.

Boldt, G., Cooper, W.S. Z.Naturforsch. 1964, 19A, pp.968-78.

Burgess, D.D. Phys.Lett. 1964, 10, p.286.

Burgess, D.D., Cooper, J. Proc.Phys.Soc. 1965, 85, p.1261.

Burgess, D.D. Ph.D. Thesis, 1965, Univ. of London.

Burgess, D.D., Fawcett, B.C., Peacock, N.J. Proc.Phys.Soc. 1967, 92, pp.805-816.

Burgess, D.D. Phys.Rev. 1968, 176, pp.150-160.

Burgess, D.D., Peacock, N.J. J.Phys.B., 1971, 4, L94-7.

Burgess, D.D. Space Sci.Rev. 1972, 13, 493-527.

Cairns, C. Ph.D. Thesis, 1971, Univ. of London.

Chowdhury, S.S. J.Phys.B., 1969, 2, pp.1090-3.

Day, R.A., Griem, H.R. Phys.Rev.A., 1965, 140, pp.1129-32.

Driver, R. Ph.D. Thesis, 1974, Univ. of London.

Fortna, J.D.E., Elton, R.C., Griem, H.R. Phys.Rev.A., 1970, 2, p.1150.

Fussmann, G. Phys.Lett. 1972, 41A, pp.155-6.

Fussmann, G. J.Q.S.R.T., 1975, 15, pp.791-809.

Gabriel, A.H., Jordan, C. Nature, Lond. 1969, 221, 947-949.

Gabriel, A.H., Volonté, S. Phys.Lett., 1973a, 43A, pp.372-4.

Gabriel, A.H., Volonté, S. J.Phys.B., 1973b, 6, pp.2684-700.

Goto, T., Burgess, D.D. J.Phys.B., 1974, 7, pp.857-64.

Greig, J.R., Griem. H.R., Jones, L.A., Oda, T. Phys.Rev.Lett. 1970, 24, pp.3-5.

References (Continued)

Griem, H.R. "Plasma Spectroscopy", McGraw Hill, New York 1964.

Griem, H.R. Phys.Rev.Lett., 1966, 17, pp.509-13.

Griem, H.R. Proc. 7th Int.Conf. on Phenomena in Ionized Gases 1966. (Belgrade: Gradevinska Knjiga).

Griem, H.R. Phys.Rev., 1968, 165, pp.258-266.

Griem, H.R. 1973. See Gabriel and Volonté 1973b.

Griem, H.R. "Spectral Line Broadening by Plasmas" (New York: Academic) 1974.

Jones, L.A., Kallne, E., Thomson, D.B. J.Q.R.S.T. 1977, 17, pp.175-180.

Kelly, R.L. N.R.L. Report, "Atomic Emission Lines Below 2,000Å", 1968.

Le Quang Rang, Voslamber, D. J.Phys.B. 1975, 8, pp.331-6.

Mahon, R. Ph.D. Thesis, 1973, Univ. of London.

Nation, I. Ph.D. Thesis, 1960, Univ. of London.

Neiger, M.. Griem, H.R. Phys.Rev.A, 1976, 14, p.291.

Preston, R.C. J.Phys.B. 1977, 10, pp.523-539.

Quefflec, J.L., Girault, M. Comptes Rendues, 1974, 279, B649-52.

Roberts, D.E. Ph.D. Thesis, 1967, Univ. of London.

Roberts, D.E. Proc.Phys.Soc., 1968, 98, pp.1-9.

Sholin, G.V. Optics and Spectroscopy, 1969, 26, 275-82.

Shore, B.W., Menzel, D.H. "Principles of Atomic Spectra" (Wiley & Sons Ltd., New York) 1968.

Smith, C. Ph.D. Thesis, 1977, Univ. of London.

Spitzer, L. "Physics of Fully Ionized Gases" (New York: Interscience) 1956.

Stewart, J.C., Peak, J.M., Cooper, J. Astrophys.J., 1973, 179, 983-6.

Volonté, S. J.Phys.B., 1975, 8, pp.1170-6.

Wheeler, C., Troughton, J. Plasma Physics, 1969, 11, pp.391-6.

Wiese, W.L., Smith, M.W., Glennon, B.M. "Atomic Transition Probabilities", National Standards Reference Data Series, NBS No.4, (U.S. Government Printing Office, Washington, D.C.) 1966.

Ya'akobi, B., Bekefi, G. Phys.Lett., 1969, 30A, p.539.

ACKNOWLEDGEMENTS

I would like to express my gratitude to all those people who have helped me during the course of this work.

To Dr. D.D. Burgess, my supervisor, I offer my deepest gratitude for his guidance and encouragement at all times. His advice, and his lively interest in all aspects of this work have been of the greatest help.

My thanks are also due to Professor W.R.S. Garton for making available to me the use of his laboratory.

I would like to thank all the members of the Spectroscopy Group, past and present, for their kindness, assistance, and for many fruitful discussions. In particular, I would like to express my appreciation of the patient technical assistance of Mr. J.E.G. Wheaton. I would also like to thank Dr. R.W. Lee for reading part of the rough draft of this thesis, and for making a number of helpful comments.

My thanks also go to Dr. S. Volonté (Mons) for theoretical calculations of the polarization shifts measured in this experiment.

I am grateful to Mr. S.J. Fielding (Culham) for supplying me with an Abel inversion routine.

Thanks are due to Mrs. T. Wright for her care and attention in typing this thesis.

I would also like to thank Culham Laboratories for financial support in the form of a Research Studentship.

Finally, I would like to thank my parents. Without their support and encouragement over the years, this work would not have been started or completed.